

Optical devices and subsystems for few- and multi-mode fiber based networks

Citation for published version (APA):

Chen, H. (2014). *Optical devices and subsystems for few- and multi-mode fiber based networks*. [Phd Thesis 1 (Research TU/e / Graduation TU/e), Electrical Engineering]. Technische Universiteit Eindhoven.
<https://doi.org/10.6100/IR773124>

DOI:

[10.6100/IR773124](https://doi.org/10.6100/IR773124)

Document status and date:

Published: 01/01/2014

Document Version:

Publisher's PDF, also known as Version of Record (includes final page, issue and volume numbers)

Please check the document version of this publication:

- A submitted manuscript is the version of the article upon submission and before peer-review. There can be important differences between the submitted version and the official published version of record. People interested in the research are advised to contact the author for the final version of the publication, or visit the DOI to the publisher's website.
- The final author version and the galley proof are versions of the publication after peer review.
- The final published version features the final layout of the paper including the volume, issue and page numbers.

[Link to publication](#)

General rights

Copyright and moral rights for the publications made accessible in the public portal are retained by the authors and/or other copyright owners and it is a condition of accessing publications that users recognise and abide by the legal requirements associated with these rights.

- Users may download and print one copy of any publication from the public portal for the purpose of private study or research.
- You may not further distribute the material or use it for any profit-making activity or commercial gain
- You may freely distribute the URL identifying the publication in the public portal.

If the publication is distributed under the terms of Article 25fa of the Dutch Copyright Act, indicated by the "Taverne" license above, please follow below link for the End User Agreement:

www.tue.nl/taverne

Take down policy

If you believe that this document breaches copyright please contact us at:

openaccess@tue.nl

providing details and we will investigate your claim.

Optical Devices and Subsystems for Few- and Multi-mode Fiber based Networks

PROEFSCHRIFT

ter verkrijging van de graad van doctor aan de
Technische Universiteit Eindhoven, op gezag van de
rector magnificus, prof.dr.ir. C.J. van Duijn, voor een
commissie aangewezen door het College voor
Promoties in het openbaar te verdedigen
op donderdag 8 mei 2014 om 16.00 uur

door

Haoshuo Chen

geboren te Shanghai, China

Dit proefschrift is goedgekeurd door de promotiecommissie:

voorzitter:	prof.dr.ir. A.C.P.M. Backx
promotor:	prof.ir. A.M.J. Koonen
copromotor:	dr. C.M. Okonkwo
leden:	prof.dr. A.D. Ellis (Aston University)
	prof.dr. P. Bayvel (University College London)
	dr. R. Ryf (Bell Laboratories)
	dr. J.J.G.M. van der Tol
	prof.dr. K.A. Williams

A catalogue record is available from the Eindhoven University of Technology Library

Optical Devices and Subsystems for Few- and Multi-mode Fiber based Networks

Author: Haoshuo Chen
Eindhoven University of Technology, 2014
ISBN: 978-90-386-3618-4
NUR 959

Keywords: Optical fiber communication / Mode division multiplexing / Wavelength division multiplexing / Photonic integrated circuits / Optical switch

The work described in this thesis was performed in the Faculty of Electrical Engineering of the Eindhoven University of Technology and was financially supported by the European Commission (EC) funded 7th framework project MODE-GAP.

Copyright © 2014 by Haoshuo Chen

All rights reserved. No part of this publication may be reproduced, stored in a retrieval system, or transmitted in any form or any means without the prior written consent of the author.

Summary

Optical Devices and Subsystems for Few- and Multi-mode Fiber based Networks

Due to the exponential growth of the required capacity of optical networks, it is foreseen that future bandwidth demands will exceed the maximum achievable capacity of single-mode fiber (SMF) based networks, limited by fiber nonlinearities. In the past few years, after a series of successful spatial division multiplexing (SDM) and wavelength division multiplexing (WDM) transmission demonstrations over few-mode fibers (FMFs), multi-mode fibers (MMFs) and multi-core fibers (MCFs), SDM has been regarded as a promising candidate to avert this optical network bottleneck. This thesis focuses on the investigation and comparison between different mode multiplexing approaches for mode division multiplexing (MDM) over FMFs and MMFs. The aim of the thesis is to find compact and scalable mode multiplexing approaches with low coupler insertion loss (CIL) and mode dependent loss (MDL).

In the first part of the thesis, approaches for enhancing the capacity of heavy-mode MMFs are discussed. The bandwidth of MMF is mainly limited by modal dispersion, which is caused by non-identical propagation constants of the modes and results in a frequency-selective fading channel with transmission nulls at some frequencies. Due to the fast-growing capacity requirements driven by the ubiquitous video and cloud computing applications, mode group control for mode group division multiplexing (MGDM) is investigated in detail with the aim of enhancing link capacity to 10Gb/s and above using already-installed MMFs. MGDM utilizes different subsets of guided modes as separate transmission channels, as a subset of modes exhibits less modal dispersion than the complete set of fiber modes. Therefore, the bandwidth of a subset can be larger than that of the entire set. Mode-selective spatial filtering (MSSF) utilizing the numerical aperture of optical fibers is proposed, which enables an MGDM receiver to separate different mode groups. Employing the MSSF-based MGDM receivers, 30Gbit/s 3×3 optical MGDM transmission is experimentally demonstrated to achieve signal recovery with a low computation complexity. A photonic integrated mode group coupler and optical multiple-

input and multiple-output (MIMO) demultiplexing are both discussed. Simulation results show that under -10dB mode group crosstalk, optical MIMO demultiplexing still works properly.

Free space selective mode excitation, which excites one pure fiber mode through spatially tailoring the input light field to match the field of the desired mode is investigated through a developed simulation model. It is verified that binary phase masks are able to generate suitable fields for selective mode excitation and the influence of mode rotations on detecting degenerate circularly-asymmetric modes is negligible. Compared to the widely-used phase-plate based mode demultiplexers, which need beam splitters to split light beams and binary phase masks to separate modes, a multi-mode phase mask (MMPM) that is able to demultiplex all mode channels simultaneously with a single multi-level mask is proposed. The MMPM is composed of mode-related masks, each of which is a summation of a binary phase mask and a blazed grating. Moreover, a LP_{01} and LP_{11} mode crossbar switch is experimentally demonstrated, in which a spatial light modulator (SLM) is used as a bar and cross state switch controller. A phase plate-based mode multiplexer and demultiplexer are used to offer a high mode extinction ratio.

Photonic integration allows more compact optical devices and facilitates the integration of multiple photonic functions together with electronic circuits. Therefore, there is a high interest in exploring photonic functions for mode (de)multiplexing. 2-dimensional (2D) top coupling with vertical emitters offers an interface between planar integrated circuits and FMFs. A push-pull scheme is proposed for LP_{11} mode excitation. Through extending the push-pull scheme, a Silicon-on-Insulator (SOI)-based integrated mode coupler, composed of five small vertical grating couplers is introduced and analyzed to support the LP_{01} and degenerate LP_{11} modes. Employing the proposed SOI mode coupler, 3.072Tb/s (6 spatial and polarization modes \times 4 WDM \times 128Gb/s 16QAM) transmission over 30km FMF is demonstrated with >20 dB mode extinction ratio between LP_{01} and LP_{11} modes. Small vertical emitters for the Indium Phosphide (InP) integration platform where mature active optical elements such as lasers and photo-detectors are available, are exploited to realize MDM compatible transceivers. Based on the total internal reflection, InP-based 45° vertical mirrors are designed and fabricated. Less than 9dB mirror-to-SMF coupling loss is achieved.

Spot-based mode couplers, which excite a linear combination of modes instead of one pure fiber mode, is more scalable to a larger mode number compared to the approaches based on selective mode excitation. A free space prism-based 3-spot coupler is proposed to support LP_{01} and LP_{11} modes. Three surfaces of the customized prism are used to combine three collimated light

beams and a telecentric lens setup is utilized for optimizing the coupling efficiency into an FMF. Low (<4dB) CIL is achieved whilst maintaining a low MDL of approximately 2dB. 7.68Tbit/s transmission of 6 spatial and polarization modes \times 8 WDM \times 160Gb/s 32QAM over a 120km differential group delay-compensated FMF span is demonstrated based on the proposed 3-spot couplers. A femto-second laser inscribed 3D Waveguide (3DW) based 3-spot coupler with weakly-coupled waveguides is thoroughly characterized and experimentally verified with 576Gb/s of 6 spatial and polarization modes \times 96Gb/s 8QAM over 480km FMF. The transmission distance is achieved by using an all few-mode re-circulating loop consisting of a 60km FMF span, a chopper as a loop switch and two few-mode erbium-doped fiber amplifiers. Besides 3DW technology, a fiber lantern is also able to merge a bundle of SMFs into a few-mode front-end, where supermodes can match the modes guided by an FMF. Therefore, it can be spliced directly to FMFs and potentially becomes a loss-less mode multiplexing approach. Low-loss fiber lanterns supporting 6 spatial and polarization modes are demonstrated in high capacity MDM transmission over a record distance of 1500km FMF with a spectral efficiency of 3.0bit/s/Hz. This is a highly promising solution for future ultra-long haul MDM/WDM transmission systems.

Contents

Summary.....	i
Contents.....	I
Chapter 1 Introduction.....	1
1.1 Spatial Division Multiplexing	1
1.2 State-of-the-art	3
1.3 Mode Division Multiplexing.....	7
1.3.1 Fiber optics	8
1.3.2 Mode (de)multiplexer	11
1.3.3 Digital signal processing	20
1.4 Preview of the Thesis	21
Chapter 2 Mode Group Control for Mode Group Division Multiplexing.....	23
2.1 Multi-mode Fiber	23
2.1.1 Modal dispersion	23
2.1.2 Proposed techniques	24
2.2 Mode Group Division Multiplexing.....	25
2.2.1 Mode-selective spatial filtering	25
2.2.2 Modal noise	28
2.2.3 MGDM transmission	29
2.3 Optical MIMO Tracking	31
2.3.1 Integrated MGDM (de)multiplexer	31
2.3.2 Optical MIMO demultiplexing.....	32
2.3.3 Simulation results	34
2.4 Summary	36
Chapter 3 Selective Mode Excitation.....	37
3.1 Selective Mode Excitation	37

3.2	Mode Detection	40
3.3	Multi-mode Phase Mask	41
3.4	Mode Crossbar Switch.....	46
3.5	Summary.....	50
Chapter 4	Photonic Integrated Mode Coupler	53
4.1	Silicon-on-Insulator Mode Coupler.....	53
4.1.1	Push-pull and push-push scheme	54
4.1.2	Vertical coupler.....	56
4.1.3	Circuit design	59
4.1.4	Thermo-optic phase tuning	60
4.1.5	Circuit characterization	61
4.1.6	High-order mode excitation	63
4.1.7	3-mode FMF	64
4.1.8	PBGF.....	67
4.2	InP-based 45° Vertical Mirror.....	69
4.3	Summary.....	74
Chapter 5	Spot-based Mode Coupler	77
5.1	Prism-based Spot Coupler	77
5.1.1	3-spot mode coupler.....	77
5.1.2	Coupler design	78
5.1.3	Transmission measurements	82
5.2	3D waveguide (3DW) Spot Coupler.....	86
5.2.1	3DW device.....	86
5.2.2	Transmission measurements	88
5.3	Multi-segment Phase Mask.....	91
5.3.1	MSPM functions	92
5.3.2	Simulations.....	93
5.3.3	Experimental results.....	95
5.4	Summary.....	96

Chapter 6	Photonic Lantern Mode Coupler.....	99
6.1	Photonic Lantern Schemes.....	99
6.2	Fiber Lantern.....	100
6.2.1	3-core fiber lantern.....	100
6.2.2	Transmission results.....	101
6.3	Summary.....	103
Chapter 7	Conclusions and Outlook.....	105
7.1	Conclusions.....	105
7.2	Outlook.....	107
References	109
Acronyms.....	125
Acknowledgments.....	129
List of Publications.....	131
Curriculum Vitae.....	137

Chapter 1 Introduction

1.1 Spatial Division Multiplexing

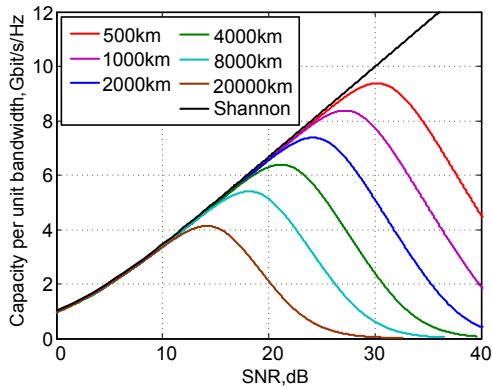


Figure 1-1 Spectral efficiency of SMF link versus SNR for various distances. [1]

C-band (1540-1565nm) and L-band (1565-1625nm) are the two optical wavelength bands used by high performance transmission systems, especially for long haul links. A combination of low loss in optical fibers and efficient optical amplification by Erbium-doped fiber amplifiers (EDFAs) or Raman amplification can be realized within the two bands, which provide a huge bandwidth around 8.75THz (70nm) [2]. In the linear region, fiber link capacity increases logarithmically with signal power according to Shannon's law. However, the capacity of the optical channel cannot be indefinitely enhanced since SNR is bounded by a maximum limit which is a function of the nonlinearity threshold [3]–[5]. The SMF nonlinear capacity limit is shown in Figure 1-1 with spectral efficiency versus SNR for various distances. Moreover, the capacity limit of the existing single-mode fiber (SMF) based optical networks has been forecasted by researchers [6]–[11].

Spatial division multiplexing (SDM), which utilizes the last unexplored physical dimension, space, to avert the network bottleneck looming in the SMF networks [12] and aims to achieve extra high spectral efficiency per fiber. Compared to simply adding parallel SMFs, SDM can be more cost- and energy-efficient through densely integrating transponders, optical amplifiers and other network elements [13], [14]. Both mode division multiplexing (MDM) deploying transverse modes guided in few-mode fiber (FMF) and the use of uncoupled fundamental modes or coupled supermodes in multi-core fiber (MCF) are labeled as SDM solutions, which are capable to expand optical fiber capacity by opening the spatial domain next to the wavelength and time domain. Compared to SMF, which only guides the fundamental mode as operating below the cut off frequency, FMFs generally have a slightly bigger core, as shown in Figure 1-2 (b) and are able to guide more modes. But the number of the guided modes of an FMF is much smaller than that of an MMF, which normally has more than 100 spatial and polarization modes propagating in a core diameter of $50\mu\text{m}$ or $62.5\mu\text{m}$. Figure 1-2 (d) shows an MCF, which consists of 7 single-mode cores. In Figure 1-2 (e), a multi-core FMF is given, which can be regarded as a combination of MDM and MCF [15].

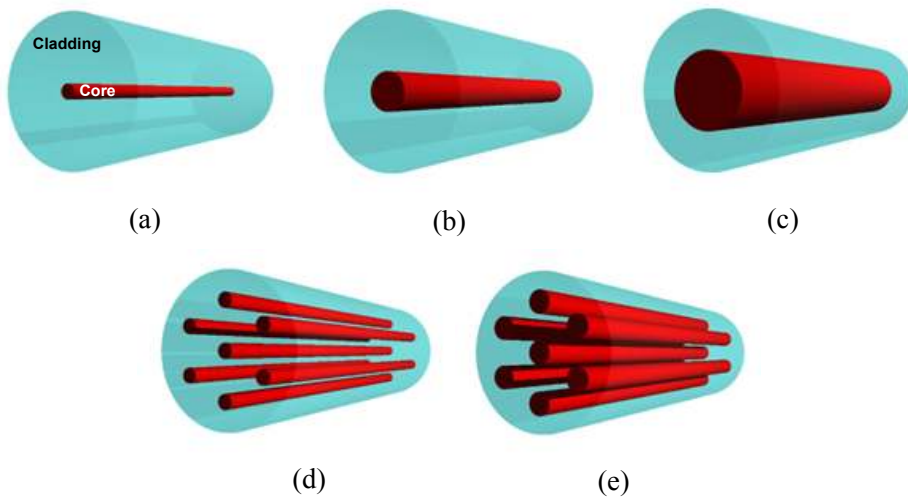


Figure 1-2 Structures for different types of optical fibers: (a) single-mode fiber (SMF); (b) few-mode fiber (FMF); (c) multi-mode fiber (MMF); (d) multi-core fiber (MCF) and (e) multi-core FMF.

1.2 State-of-the-art

To illustrate the breakthroughs in SDM long-distance transmission, Figure 1-3 gives the achieved spectral efficiencies per fiber for MDM and MCF experimental trials with transmission distances longer than 100km. As a comparison, the maximum spectral efficiencies attainable in an SMF in theory with 5 and 96 WDM channels as a function of transmission distance L are plotted within the same figure, where 50Gbaud symbol rate and 50GHz WDM channel spacing are assumed [1].

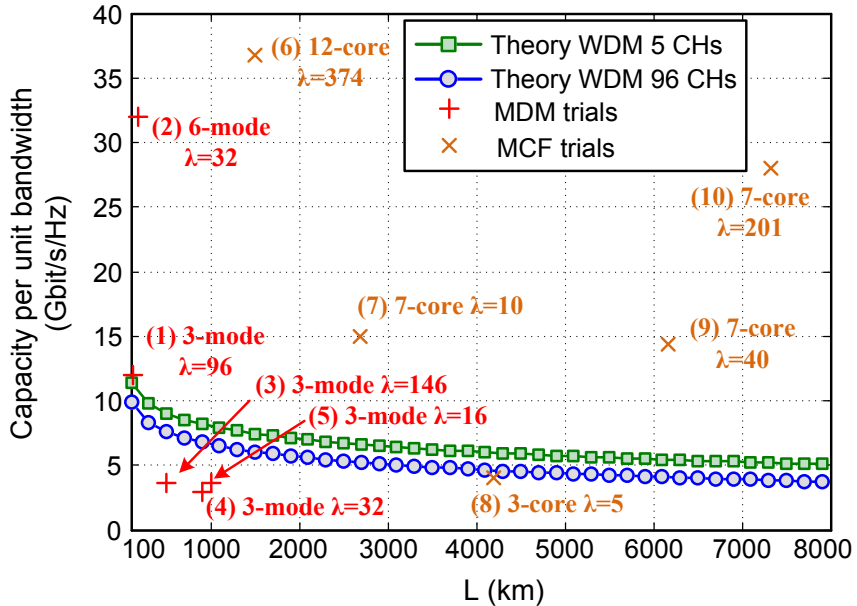


Figure 1-3 Comparison between achievable capacity (Gbit/s/Hz) for an SMF link in theory and experimentally achieved capacity by SDM/WDM transmission trials.

High capacity SDM, combined with WDM transmission trials plotted in Figure 1-3 are further compared in Table 1-1, denoted as number (1) to (10) with an increasing transmission distance. In the top half of Table 1-1, all state-of-the-art SDM system trials are realized by MDM. The highest achieved spectral efficiency per fiber core for MDM is 32 bit/s/Hz (the 2nd reference in Table 1-1) [16], almost 3 times larger than the maximum capacity that can be offered by an SMF in the same distance (Figure 1-3). At the end of March 2014, combined SDM and WDM trials with a transmission distance longer than 1000km were only demonstrated with MCFs, listed as number (6) to (10) in Table 1-1. Components for MCF based network such as multi-core EDFA [17],

MCF compatible reconfigurable optical add/drop (ROADM) [18] and MCF loop [19] were demonstrated through directly upgrading the existing SMF based ones. On the contrary to the MCF trials, although few-mode EDFA [20]–[22], few-mode re-circulation loop [23], [24] and low-loss mode coupler [25] were verified successfully, non-negligible mode-dependent loss (MDL) and coupling loss still exist in these components, which limit the distance, especially in an accumulated case such as loop measurements. Therefore, these MDM fields are still under active research to increase performance.

Table 1-1 High capacity SDM transmission trials

	Reference	Distance (km)	Capacity	Fiber type	SDM coupler solution	Loop	Highlight
(1)	Sleiffer [20]	119	73.7 Tb/s	3-mode	Phase plate		Few-mode EDFA
(2)	Ryf [16]	177	24.6 Tb/s	6-mode	3D waveguide	✓	High spectral efficiency: 32 bit/s/Hz
(3)	Ip [23]	500	30 Tb/s	3-mode	Phase plate	✓	Few-mode re-circulation loop
(4)	Ryf [25]	900	9.6 Tb/s	3-mode	Fiber lantern	✓	Low-loss fiber lantern coupler
(5)	Ip [23]	1000	3.5 Tb/s	3-mode	Phase plate	✓	Record MDM/WDM transmission distance
(6)	Kobayashi [26]	1500	2×344Tb/s	12-core	Fiber bundle [27]	✓	Nonlinear compensation
(7)	Chandrasekhar [28]	2688	7.5 Tb/s	7-core	Fiber bundle	✓	Core-to-core signal rotation
(8)	Ryf [29]	4200	1.2 Tb/s	3-core	Spot coupler	✓	3 coupled-core micro-structured fiber
(9)	Takahashi [17]	6160	28.8Tb/s	7-core	Fiber bundle	✓	Multi-core EDFA
(10)	Igarashi [19]	7326	140.7Tb/s	7-core	Fiber bundle	✓	Super-Nyquist WDM [30], [31]
(11)	Mizuno [32]	40.4	61.97Tb/s	MC-FMF	Planar lightwave circuit + Fiber bundle		Record spectral efficiency
(12)	Ryf [33]	17	23Tb/s	MMF	Fiber lantern		MDM over conventional MMF

1.3 Mode Division Multiplexing

From the state-of-the-art high capacity SDM transmission trials, as shown in the previous section, it may seem that MCF is more promising than MDM in terms of transmission distance. However, MDM has several advantages with respect to MCF such as:

¹⁾ Efficient fiber cross-section utilization: high mode scalability when using standard 125 μ m fiber diameter.

²⁾ Efficient pumping for optical amplification: strong modal overlap helps pump light to be shared by all the modes.

³⁾ Easy installation: compatible with conventional splicers.

From these points of view, MDM is more advantageous than MCF. Due to the consideration of fiber cross-section utilization, dense SDM (DSDM) was introduced in [32] employing an MC-FMF. A record spectral efficiency of 247.9-b/s/Hz was demonstrated over a 12-core \times 3-mode fiber with a distance of 40km, listed as the 11th reference in Table 1-1. Moreover, the 12th reference in Table 1-1 [33] shows successful 6-mode MDM transmission over a 17km conventional MMF. This result illustrates the possibility of enhancing the capacity of already-installed MMFs significantly with the MDM solution.

MDM research can be traced back to 1982, when two modes were excited over a 10m long MMF with -20dB crosstalk [34]. The first transmission experiment utilizing the diversity of fiber modes was demonstrated over a 1km long MMF in 2000 [35], shortly after multi-element array technology was announced in wireless communication [36], [37]. Thereafter, more and more research was presented in this area [38]–[42]. For most of this work, which was named as mode group division multiplexing (MGDM), MMFs were treated as a multi-path medium to offer spatial diversity. Instead of mapping different signals to different modes in MDM, MGDM used subsets of guided modes as mode groups to provide parallel transmission channels.

Therefore, research covering MGDM over MMF carried out during this Ph.D project is presented primarily for applications in short-reach networks such as in-building networks and data centers. Afterwards, this thesis focuses on solutions for realizing reliable and efficient mode multiplexing for MDM over FMF and investigates optical devices and subsystems for FMF-based long-haul networks.

In the following sections, three essential building blocks for MDM: FMF, mode (de)multiplexer and digital signal processing (DSP) will be briefly introduced. Chapter 1.3.1 presents the basics of fiber optics and gives the

relations between different fiber mode sets in order to clarify the consistent mode definitions used in the thesis.

1.3.1 Fiber optics

An optical fiber, typically made of high quality silica glass, acts as a waveguide to guide light. Mode theory, along with ray theory, is used to describe the propagation of light in an optical fiber. The former uses the electromagnetic behavior of light. Like all electromagnetic phenomena, propagation of optical fields in fibers is governed by Maxwell's equations. The propagation constant β of each mode can be found by numerically solving the eigenvalue equation derived from Maxwell's equations for a cylindrical dielectric waveguide [43]–[45]. The definition of β is:

$$\beta = n_{eff} * \frac{2\pi}{\lambda} \quad (\text{Eq. 1-1})$$

where λ is the wavelength in vacuum and n_{eff} is the effective index of each mode. The corresponding transverse mode field distribution can be calculated analytically using the value of β . An important parameter for optical fiber is the V number, also called the normalized frequency, represented as:

$$V = \frac{\pi d}{2\lambda} \sqrt{n_1^2 - n_2^2} \quad (\text{Eq. 1-2})$$

where d is the diameter of fiber core, and n_1 and n_2 are the refractive indices of the core and cladding, respectively. Figure 1-4 shows the effective index n_{eff} of lower order vector modes as a function of d (bottom axis) and V number (top horizontal axis) in a step-index (SI) fiber with $n_1 = 1.444$ and $n_2 = 1.439$. As shown in Figure 1-4, some vector modes have similar n_{eff} , due to the small index difference $\Delta = n_1 - n_2 = 0.005$, in the so-called weakly guiding case. Therefore, linearly polarized (LP) modes, which are called scalar modes, are usually used to represent fiber modes as an approximation of the vector modes. The relation between vector and scalar modes is shown in Figure 1-4.

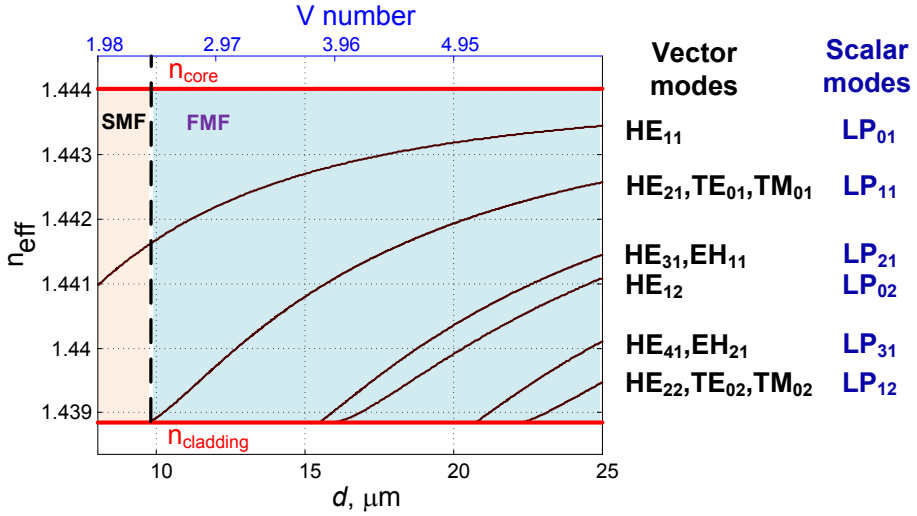


Figure 1-4 The effective index n_{eff} of lower order vector modes as a function of d (bottom axis) and V number (top axis) in an SI fiber.

In Table 1-2, definitions of modes used in this thesis and their relations are shown.

Table 1-2 Vector modes, LP modes and spatial modes

Vector modes	LP modes	Spatial modes	Spatial and polarization modes
HE_{1m}	LP_{0m}	LP_{0m}	$LP_{0m(x,y)}$
$HE_{2m} + TE_{0m} + TM_{0m}$	LP_{1m}	$LP_{1m(a,b)}$	$LP_{1m(a,b)(x,y)}$
$HE_{l+1,m} + EH_{l-1,m}$ ($l > 1$)	LP_{lm} ($l > 1$)	$LP_{lm(a,b)}$ ($l > 1$)	$LP_{lm(a,b)(x,y)}$ ($l > 1$)

Vector modes are the solutions of the vector wave equation and normally regarded as real fiber modes (l and m are azimuthal and radial order, respectively). *LP modes* are solved from scalar wave equations, which are linear combinations of the vector modes. *Spatial modes* recognizes the degenerate LP modes, where one mode rotates a certain degree with respect to the other, as two different modes. These modes are distinguished by subscripts a and b . *Spatial and polarization modes*: these modes can be further separated by

polarization, where subscripts x and y denote two polarizations of each spatial mode.

Given a fiber that supports LP_{01} and LP_{11} modes, this fiber can be seen as a two-mode fiber, counting only the LP modes, or it can also be seen as a three-mode fiber, where the different spatial modes are considered. In the thesis, the differentiation of spatial modes is used.

Figure 1-5 gives the mode profile of the fundamental mode of a fiber and shows the relationship between different mode definitions, where the arrows represent orientation and sign of the electric field.

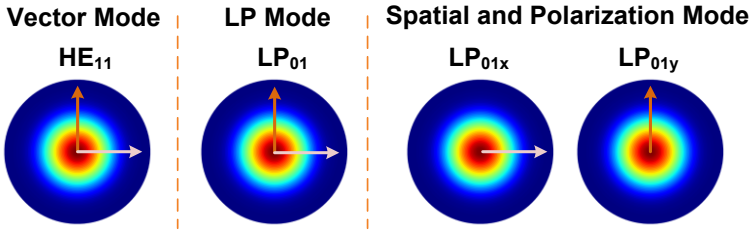


Figure 1-5 Fiber fundamental mode.

Compared to LP_{01} mode, the relationship for LP_{11} modes between spatial and polarization modes and vector modes is not very straightforward. The spatial modes are formed by a linear combination of vector modes as shown in Figure 1-6 [46]. The power normalization constant of $\frac{\sqrt{2}}{2}$ is omitted in Figure 1-6. This relation can be represented in a unitary transformation as:

$$\begin{bmatrix} LP_{11ax} \\ LP_{11ay} \\ LP_{11bx} \\ LP_{11by} \end{bmatrix} = \underbrace{\begin{bmatrix} \frac{\sqrt{2}}{2} & -\frac{\sqrt{2}}{2} & 0 & 0 \\ 0 & 0 & -\frac{\sqrt{2}}{2} & \frac{\sqrt{2}}{2} \\ 0 & 0 & \frac{\sqrt{2}}{2} & \frac{\sqrt{2}}{2} \\ \frac{\sqrt{2}}{2} & \frac{\sqrt{2}}{2} & 0 & 0 \end{bmatrix}}_T \begin{bmatrix} TM_{01} \\ HE_{21a} \\ HE_{21b} \\ TE_{01} \end{bmatrix} \quad (\text{Eq. 1-3})$$

where T is the unitary transfer matrix with $TT^* = I$. I is the 4×4 identity matrix.

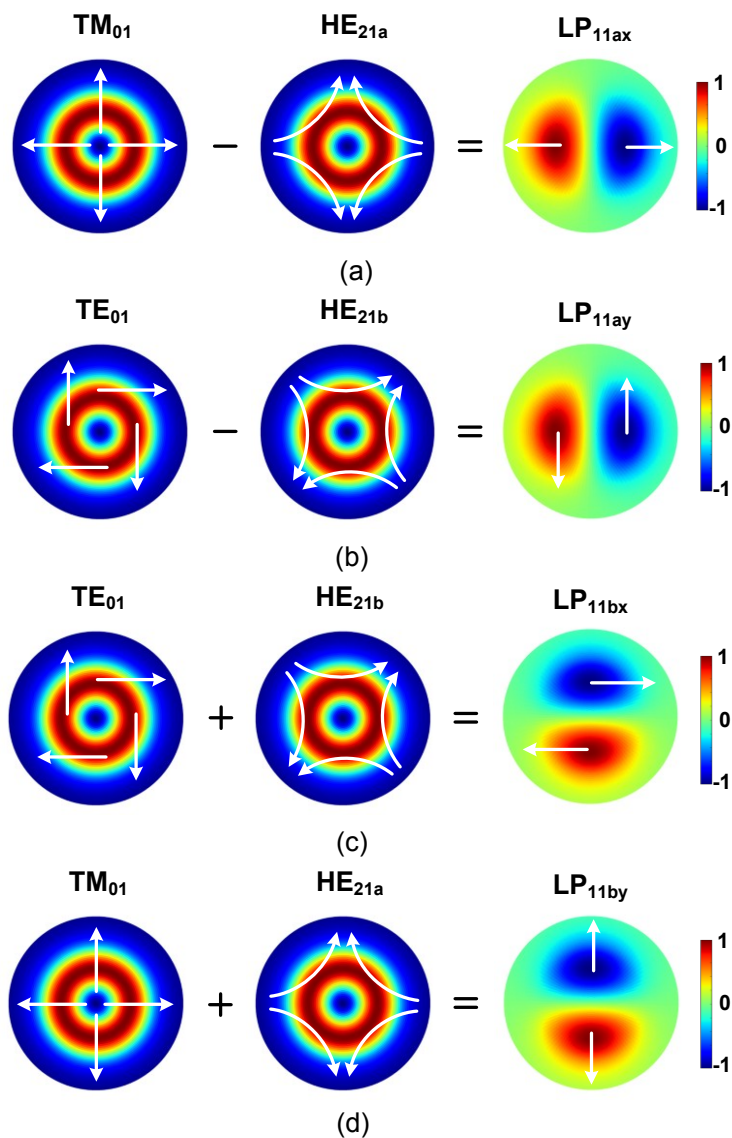


Figure 1-6 The relation between vector mode and spatial and polarization mode for LP₁₁ modes .

1.3.2 Mode (de)multiplexer

Since high capacity MDM demonstration systems based on 3-mode FMFs were first announced in 2011 [47], [48], the solutions for coupling the data

streams onto the different modes supported by the FMF, as manifested in a mode multiplexer (MUX) and demultiplexer (DEMUX) have evolved from the bulky phase-plate based mode coupler with high insertion loss to the recent demonstrated photonic lantern, which is compact, scalable and potentially lossless. In principle, these solutions can be categorized under two groups: mode selective excitation by matching the FMF mode profile [20], [47], [49]–[51] and mixed-mode excitation by arranging launch spots [52]–[54] or coupled waveguides [55], [56] in a particular structure [57] to launch the appropriate orthogonal mixtures of fiber modes.

The first group can be realized by using phase plates [20], [47], spatial light modulators [58] and a push-pull scheme [49], [59]. High mode extinction ratio can be achieved through closely matching the modulated optical signal beam profile with the FMF mode profile attributed to the orthogonality of fiber modes. However, mode mixing is inevitable in practical fiber links, and can be easily induced by bends, twists and structural defects randomly occurring along the fiber, which is similar to the coupling between two orthogonal polarizations in SMFs. Moreover, in the mode combination stage of the mode-selective (de)multiplexers, insertion loss or design complexity is proportional to the number of supported modes [47], [49], which limits their application for MDM with a large volume of modes.

The second group scheme, which is referred to as spot-based couplers [57], excites a set of linear combinations of modes instead of pure fiber modes. It has better scalability to support more modes with lower coupler insertion loss whilst maintaining low mode dependent loss (MDL). Spot-based mode couplers have been realized by bulky optics [52], [53], laser inscribed 3D waveguide devices [16], [56] and optical fiber lanterns.

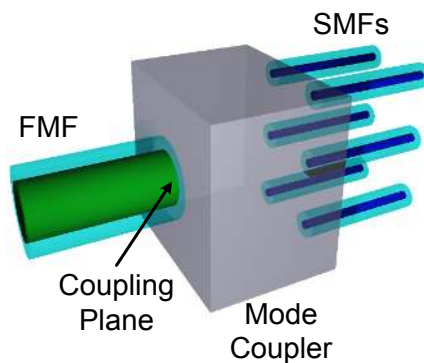


Figure 1-7 Schematic diagram of mode coupler

Figure 1-7 shows the schematic diagram of the mode coupler, whose basic functionality is to convert optical powers from a bundle of SMFs into guided

modes of an FMF. To discuss and compare the different mode coupler solutions, matrices are utilized to represent the mode coupler, as shown below:

$$\underbrace{\begin{bmatrix} \gamma_{1,1} & \gamma_{1,2} & \cdots & \gamma_{1,N} \\ \gamma_{2,1} & \gamma_{2,2} & \cdots & \gamma_{2,N} \\ \vdots & & \ddots & \vdots \\ \gamma_{N,1} & \gamma_{N,2} & \cdots & \gamma_{N,N} \end{bmatrix}}_{\substack{\Gamma: \text{mode conversion} \\ \text{efficiency}}} \underbrace{\begin{bmatrix} \alpha_1 & 0 & \cdots & 0 \\ 0 & \alpha_2 & \cdots & 0 \\ \vdots & \vdots & \ddots & \vdots \\ 0 & 0 & \cdots & \alpha_N \end{bmatrix}}_{\substack{A: \text{coupler} \\ \text{internal attenuation}}} \underbrace{\begin{bmatrix} I_1 \\ I_2 \\ \vdots \\ I_N \end{bmatrix}}_{\substack{l: \text{launch} \\ \text{field}}} = \underbrace{\begin{bmatrix} M_1 \\ M_2 \\ \vdots \\ M_N \end{bmatrix}}_{\substack{M: \text{mode} \\ \text{field}}} \quad (\text{Eq. 1-4})$$

where I represents the launch fields from input SMFs, N is the number of modes, M is an array of the mode fields guided by the FMF. A is a diagonal matrix representing coupler internal attenuation, which can be caused by splitters, waveguides or fibers inside the coupler. A different mode basis can be chosen to simplify the calculation of Γ . Γ is the mode conversion matrix, which is quantified with an overlap integral at the coupling plane, which locates at the entry facet of the FMF's core, as shown in Figure 1-7. The overlap integral is calculated as:

$$\gamma_{i,j} = \frac{\int E_{\text{launch},i}^* \cdot H_{\text{mode},j} dA}{\sqrt{\int E_{\text{launch},i}^* \cdot H_{\text{launch},i} dA} \sqrt{\int E_{\text{mode},j}^* \cdot H_{\text{mode},j} dA}} \quad (\text{Eq. 1-5})$$

where $E_{\text{launch},i}$ and $H_{\text{mode},j}$ are the transverse electric field of the i^{th} launch field at the coupling plane and the transverse magnetic field of the j^{th} fiber mode, respectively. A is the fiber cross-sectional area. The notation * indicates the complex conjugate.

The $N \times N$ transfer matrix of the whole coupler can be written as:

$$H = \Gamma \cdot A \quad (\text{Eq. 1-6})$$

1.3.2.1 Mode dependent loss

For the purpose to investigate the performance of different kinds of mode couplers, the coupler insertion loss (CIL) and mode dependent loss (MDL) are chosen and defined as:

$$CIL = \frac{\sum(\lambda_n^2)}{N} \quad (\text{Eq. 1-7})$$

$$MDL = \frac{\max(\lambda_n^2)}{\min(\lambda_n^2)} \quad (\text{Eq. 1-8})$$

where λ_n ($n=1$ to N) are singular values of the coupler transfer matrix H . Singular values can be calculated through employing singular value

decomposition (SVD) of an $m \times n$ real or complex matrix M , which can be described as:

$$M = U\Sigma V^* \quad (\text{Eq. 1-9})$$

where U is an $m \times m$ unitary matrix, V^* is an $n \times n$ unitary matrix and Σ is an $m \times n$ matrix with nonnegative real numbers on the diagonal. The diagonal elements of Σ are defined as the singular values of M . The difference between singular values by SVD and well-known eigenvalues by eigendecomposition (ED) can be summarized as:

1) SVD can be applied to any type of matrix, while ED is only defined for square matrices with $m = n$.

2) Singular values are always real, while eigenvalues can be real or complex.

3) The singular values of matrix M are the square roots of the eigenvalues of matrix MM^* .

MDL represents the maximum power difference for all the modes excited by the mode coupler and CIL shows the average insertion loss for all the ports.

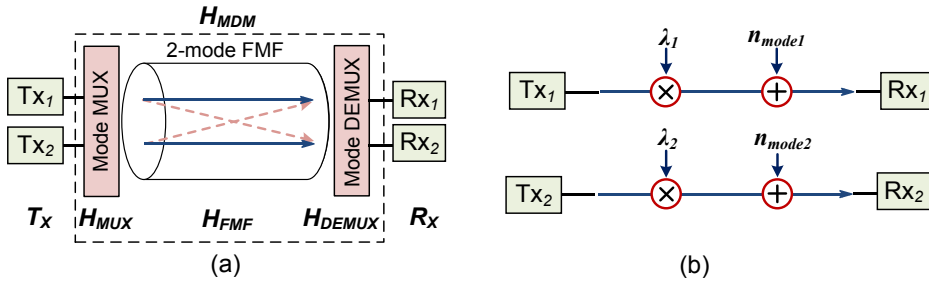


Figure 1-8 (a) Schematic diagram of an optical MDM MIMO system and (b) parallel and independent MDM channels after SVD.

In the following part, MDL will be discussed in different cases with examples. Figure 1-8 shows the schematic diagram of an optical 2×2 MDM system. Each part of the system can be described by a 2×2 matrix.

Case 1: Consider a case with unbalanced mode coupling happening in the mode MUX, for example: $H_{MUX} = \begin{bmatrix} 1 & 0 \\ 0.2 & 0.8 \end{bmatrix}$. For simplicity, mode coupling and loss in the FMF is neglected, therefore H_{FMF} can be regarded as an identity matrix. To achieve 0dB MDL, it can be calculated that a mode DEMUX with $H_{DEMUX} = \begin{bmatrix} 0.8 & 0 \\ -0.2 & 1 \end{bmatrix}$ is required, which gives $H_{MDM} = H_{MUX}H_{DEMUX} = \begin{bmatrix} 0.8 & 0 \\ 0 & 0.8 \end{bmatrix}$ with a CIL of 1.94dB. In order to achieve 0dB CIL in the meantime,

active component needs to be used to amplify one mode, which gives $H_{DEMUX} = \begin{bmatrix} 1 & 0 \\ -0.25 & 1.25 \end{bmatrix}$ with an element > 1 .

Case 2: Generally the same mode multiplexing components are employed at the MUX and DEMUX side, so accumulated MDL degradation can be observed. For example, $H_{MUX} = \begin{bmatrix} 1 & 0 \\ 0 & 0.7 \end{bmatrix}$ gives an MDL of 3.10dB and a CIL of 1.28dB. If no mode coupling occurs in the FMF and the same mode coupler is used as a DEMUX, it can be calculated that $H_{MDM} = H_{MUX}H_{DEMUX} = \begin{bmatrix} 1 & 0 \\ 0 & 0.49 \end{bmatrix}$, which gives 6.20dB MDL and 2.10dB CIL.

Case 3: Same situation as in case 2, except strong mode coupling within the FMF resulting in $H_{FMF} = \begin{bmatrix} \frac{\sqrt{2}}{2} & \frac{\sqrt{2}}{2} \\ -\frac{\sqrt{2}}{2} & \frac{\sqrt{2}}{2} \end{bmatrix}$. The MDL decreases to 4.43dB with

CIL=2.56dB. Mode coupling impact on MDM has been analyzed in [60]–[62]. With MDL, it has been verified strong mode coupling is beneficial to minimize the probability of system outage. It should be noticed that strong mode coupling can also be introduced in mode MUX/DEMUX as the spot-based mode coupler, which will be discussed later.

Case 4: Same situation as in case 2, except that mode switching occurs within the FMF with $H_{FMF} = \begin{bmatrix} 0 & 1 \\ 1 & 0 \end{bmatrix}$, which contributes to 0dB MDL with a slightly higher CIL of 3.1dB. This case shows it is possible to minimize the MDL by swapping the lossy modes with the modes having more powers.

Figure 1-8 (b) shows the parallel and independent 2×2 MDM channels after SVD, where channel gains λ_1 and λ_2 are the singular values of H_{MDM} and n_{mode1} and n_{mode2} are the noises of two channels [63]. If both channels are assumed with a similar noise level, the channel with a smaller channel gain will have lower signal-noise-ratio, which results in poorer performance. Therefore a larger MDL induces system capacity loss and increases system outage probability [9].

1.3.2.2 Scalability

MDM and WDM are two fundamentally different schemes [13]: wavelength crosstalk in WDM can be negligible while MDM exhibits severe linear crosstalk among parallel modes so that the definition of the scalability for MDM and WDM is slightly different.

For an existing SMF link, WDM has a full scalability to provide a variable number of wavelength channels through switching on or off some wavelengths

depending on the link capacity requirement. However, for MDM, the case is different. In order to achieve a reliable optical system, a robust MDM link needs to follow the rule shown below [9]:

$$N_{Tx} \leq N \leq N_{Rx} \quad (\text{Eq. 1-10})$$

where N_{Tx} , N and N_{Rx} are the count of transponders, spatial modes guided by the FMF and receivers. This means all the receivers have to be activated simultaneously to minimize the outage possibility. Therefore for real applications, mode channels will or have to be fully used to lower the per-bit delivery cost.

In this thesis, the scalability of a mode multiplexing solution shows the ability to offer an efficient mode multiplexing with low MDL and CIL to a larger number of parallel mode channels.

Hereafter, mode coupler solutions based on phase plate, spot launch and photonic lantern are under analysis based on the matrix representation.

1.3.2.3 Mode coupler solutions

1) Phase plate mode coupler

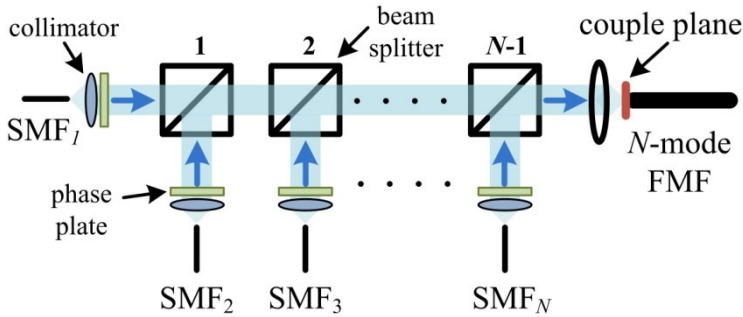


Figure 1-9 Phase plate mode coupler

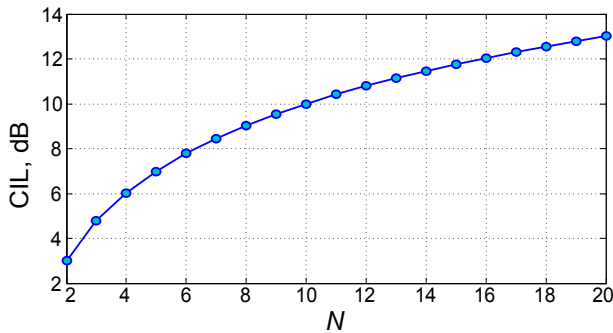


Figure 1-10 CIL for phase plate mode coupler versus the number of spatial modes N .

Figure 1-9 shows the schematic diagram of the phase plate mode coupler supporting N spatial modes, where to selectively launch or detect one specific spatial mode, a corresponding phase plate needs to be utilized. Assuming ideal phase plates selectively excitation of each LP mode with negligible crosstalk, Γ can be simplified to an $N \times N$ identity matrix. To balance the insertion losses for different ports since different launch fields go through different numbers of beam splitters, beam splitters with different splitting ratios are assumed to be used. In this case, diagonal elements of A , see (Eq. 1-4) can be expressed as:

$$\alpha_n = \frac{1}{N} \tag{Eq. 1-11}$$

Using (Eq. 1-7) and (Eq. 1-8), MDL is zero and CIL can be calculated as follows:

$$CIL = \frac{1}{N} \tag{Eq. 1-12}$$

CIL in dB for phase plate mode coupler versus the number of spatial mode channels is plotted in Figure 1-10. It should be noticed that ideal phase plates and beam splitters with the optimum splitting ratio are assumed for use, which is difficult to fabricate in practice. The detailed discussion about phase plate mode coupler is presented in Chapter 3.

2) Spot coupler

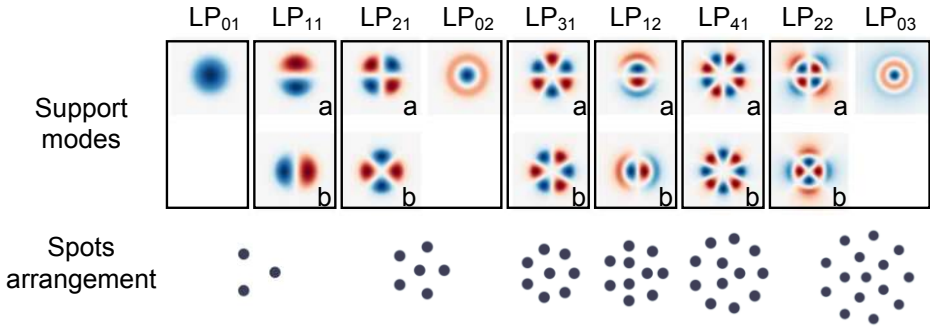


Figure 1-11 Spot arrangements for supporting different modes as a spot-based mode coupler. [57]

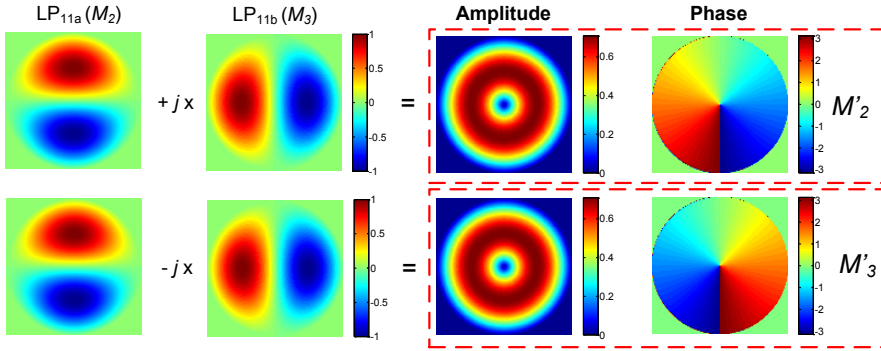


Figure 1-12 Using a helical mode basis for simplifying the calculation of Γ .

Figure 1-11 shows the spot arrangements in order to support different modes. The spot coupler starts with three spots, arranged in an equilateral triangle to support LP_{01} and LP_{11} modes. To scale up for more modes, the construction rules of the spots are: 1) adding one spot for each non-degenerate mode and two spots for each degenerate mode. 2) a new spot is added in the center as one circularly symmetric mode (LP_{0m}) is added. For example, to support LP_{21} modes, two spots need to be added and for LP_{02} mode, one spot is added in the center, which results in an arrangement with 6 spots (one spot in the center and five in an outer ring), as shown in Figure 1-11.

Without using lossy beam splitters, coupler internal attenuation can be neglected and A is rewritten as an identity matrix. In order to simplify the calculation of Γ , helical modes are used to replace the LP modes with azimuthal order $l \neq 0$ [57]. Helical mode is also known as orbital angular momentum (OAM) [64], [65]. As illustrated in Figure 1-12, the unitary transformation between the LP_{11} modes and the modes M'_2 and M'_3 can be described as:

$$\begin{bmatrix} M'_2 \\ M'_3 \end{bmatrix} = \begin{bmatrix} \frac{\sqrt{2}}{2} & j\frac{\sqrt{2}}{2} \\ \frac{\sqrt{2}}{2} & -j\frac{\sqrt{2}}{2} \end{bmatrix} \begin{bmatrix} M_2 \\ M_3 \end{bmatrix} \quad (\text{Eq. 1-13})$$

In this case, (Eq. 1-4) for a 3-spot coupler can be rewritten as:

$$\underbrace{\begin{bmatrix} \gamma_1 & \gamma_1 & \gamma_1 \\ \gamma_2 & \gamma_2 e^{\frac{j2\pi}{3}} & \gamma_2 e^{-\frac{j2\pi}{3}} \\ \gamma_2 & \gamma_2 e^{-\frac{j2\pi}{3}} & \gamma_2 e^{\frac{j2\pi}{3}} \end{bmatrix}}_{H: \text{transfer matrix}} \begin{bmatrix} I_1 \\ I_2 \\ I_3 \end{bmatrix} = \underbrace{\begin{bmatrix} M_1 \\ M'_2 \\ M'_3 \end{bmatrix}}_{\text{New mode basis}} = \underbrace{\begin{bmatrix} 1 & 0 & 0 \\ 0 & \frac{\sqrt{2}}{2} & j\frac{\sqrt{2}}{2} \\ 0 & \frac{\sqrt{2}}{2} & -j\frac{\sqrt{2}}{2} \end{bmatrix}}_{\text{Unitary transformation}} \begin{bmatrix} M_1 \\ M_2 \\ M_3 \end{bmatrix} \quad (\text{Eq. 1-14})$$

where γ_1 and γ_2 are the overlap integrals of one spot with LP_{01} mode and M'_2 or M'_3 , respectively. Therefore, to compute the CIL and MDL by using (Eq. 1-7) and (Eq. 1-8), only γ_1 and γ_2 need to be calculated instead of all 9 elements of H in (Eq. 1-14). The detailed discussion about spot coupler is presented in Chapter 5.

3) Photonic lantern

A photonic lantern based mode coupler adiabatically tapers down N SMFs, which are arranged according to the same structure as the spot coupler, into a few-mode front end, guiding N spatial modes. A can also be regarded as an $N \times N$ identity matrix with neglecting fiber or waveguide losses. (Eq. 1-4) is rewritten as:

$$\Gamma \begin{bmatrix} I_1 \\ I_2 \\ \vdots \\ I_N \end{bmatrix} = \Gamma \begin{bmatrix} M'_1 \\ M'_2 \\ \vdots \\ M'_N \end{bmatrix} = \begin{bmatrix} M_1 \\ M_2 \\ \vdots \\ M_N \end{bmatrix} \quad (\text{Eq. 1-15})$$

Few-mode front end modes
 M : mode field (FMF)

If the modes supported in the few-mode front end matches the guided modes by an FMF, Γ in (Eq. 1-15) becomes a unitary matrix. In this case, lossless mode conversion is realized. An example for a photonic lantern to support 4 LP modes is given in Figure 1-13. As shown in the upper figure of Figure 1-13, during tapering down 6 SMFs, modal propagation constants start to separate and 4 supermodes are generated at the front. It can be seen in the lower figure that as SMFs are tapered down in a small core separation, supermodes can evolve into the FMF modes, which gives negligible MDL and CIL.

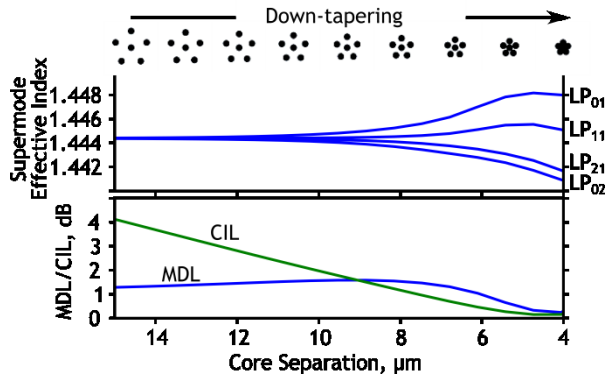


Figure 1-13 Photonic lantern for supporting 6 spatial modes. [55]

Fiber lanterns have been demonstrated for their excellent performance: low CIL and MDL [55], [66] with the advantage of direct-splicing with FMFs. Photonic lanterns can also be realized on a laser-inscribed 3D waveguide (3DW) device [67], which has more freedom in arranging waveguides spatially and advantages in integrating them with silica-based Planar Lightwave Circuits (PLCs). The discussion in detail about photonic lantern is presented in Chapter 6.

1.3.3 Digital signal processing

One important factor, which enables high capacity MDM systems to be realized in lab trials, is from the tremendous development in electronics and digital signal processing (DSP). For almost all demonstrations, optical coherent receivers and high-speed real-time oscilloscopes are utilized for detecting and sampling the received signals. Front-end impairments, chromatic dispersion (CD), timing offsets and carrier frequency offset (CFO) can be compensated by DSP [68], [69]. Carrier phase estimation (CPE) is implemented after the multiple-input and multiple-output (MIMO) equalizer in time or frequency domain. Figure 1-14 gives the DSP block for recovering 3 spatial modes after polarization division multiplexing (PDM) coherent receivers.

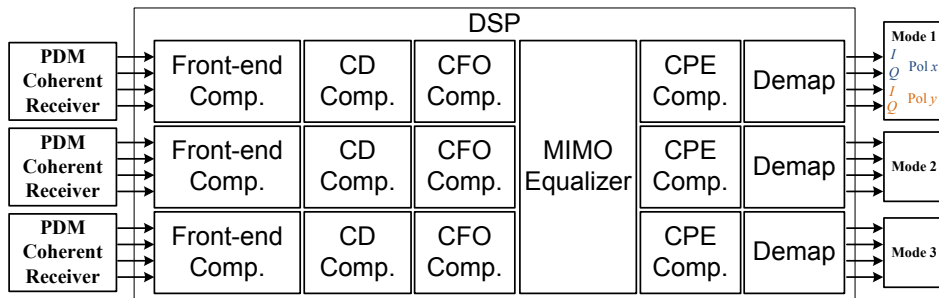


Figure 1-14 DSP block for recovering 3 spatial modes. [70]

Figure 1-15 shows a schematic diagram of a 2×2 MIMO equalizer. S_1 and S_2 represent two transmitted signals. It is assumed that mode coupling only occurs in mode MUX and DEMUX. Figure 1-15 (b) shows the separation of two modes in time domain due to the differential group delay (DGD). DGD is caused by the different propagation constants of different modes. As shown in Figure 1-15 (c), a 2×2 MIMO equalizer with a finite-impulse-response (FIR) butterfly filter structure can recover the mixed signals. In order to cover the time delay between two signals, the equalizer window needs to be wider than the DGD.

In early MDM demonstrations [20], [47], the time-domain data-aided (DA) Least-Mean-Square (LMS) algorithm is used for initializing the taps of the

MIMO equalizer. After convergence, decision-directed (DD) LMS or constant modulus algorithm (CMA) is employed. To recover optical PDM signals over N spatial modes, the MIMO equalizer requires a $2N \times 2N$ FIR filter. There is large computational complexity, as a large number of taps for each filter are required for compensating the accumulated DGDs. Recently, frequency domain equalizer (FDE) was applied in optical communication [71], [72]. Block-by-block processing and fast Fourier Transform (FFT) implementation result in tremendous reduction in computational complexity [63].

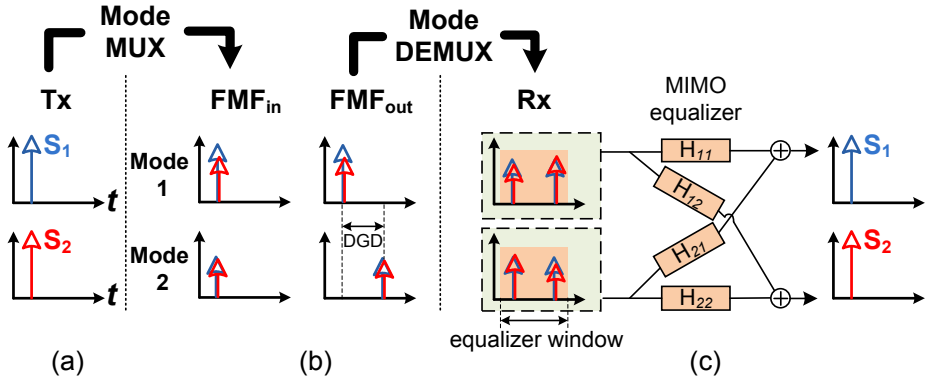


Figure 1-15 (a) Transmitted signals; (b) mode coupling induced by mode MUX with the DGD between two modes after FMF transmission and (c) MIMO equalizer with a wide equalizer window to handle DGD.

1.4 Preview of the Thesis

The thesis is structured as follows:

Chapter 2 discusses MMF's capacity enhancement by MGDM. First, the principles of MGDM and mode selective spatial filtering are introduced. Second, the transmission results with 3 parallel mode groups are presented. Then, integrated MGDM coupler solutions and optical MIMO demultiplexing for MMF links are discussed.

Chapter 3 investigates the principles and applications of selective mode excitation, where the use of binary phase plates is analyzed in both simulation and experimental measurements. A multi-mode phase mask is proposed, which enables to separate LP modes with a single phase mask. The design and analysis of a demonstrated mode crossbar switch for LP_{01} and LP_{11} modes based on a spatial light modulator follow afterwards.

Chapter 4 focuses on the photonic integrated solutions for mode coupling. This chapter introduces a push-pull scheme for LP_{11} mode excitation and its

extended solution for a 3-mode coupler, where silicon-on-insulator (SOI) based grating couplers are used as vertical emitters. The MDM transmission results over a 3-mode FMF and a 19-cell photonic bandgap fiber (PBGF) are both presented as utilizing the proposed SOI device as a mode MUX. An Indium Phosphide (InP)-based 45° vertical mirror is introduced as another compact vertical emitter solution. The measured results for the fabricated vertical mirrors are presented.

Chapter 5 introduces spot-based mode coupler solutions, which excite a linear combination of modes instead of pure fiber modes. Firstly, a prism-based 3-spot coupler is proposed and demonstrated with high capacity MDM transmission over a 120km FMF. Then, a 3DW based 3-spot coupler is experimentally verified with an all-FMF re-circulating loop. The last part of this chapter investigates multi-segment phase masks, which are more scalable to a larger number of modes, compared to the multi-mode phase mask, introduced in Chapter 3.

Chapter 6 discusses photonic lantern based mode couplers. Combined MDM and WDM transmission over an FMF distance of 900km and only MDM transmission over a record distance of 1500km are both demonstrated employing fiber lanterns as mode couplers.

Chapter 7 concludes the thesis, by summarizing the research results obtained in this PhD work and with an outlook on the future study topics in MDM networks.

The research work presented in Chapter 2 to 5 was done as part of the EU FP7 MODE-GAP project [12], which targets the 100 fold enhancement of the overall capacity of core networks and develops few-mode and photonic bandgap fibers, long-haul transmission and associated technologies. The work about fiber lanterns as presented in Chapter 6 was carried out during the internship in Bell Laboratories, Holmdel, New Jersey.

Chapter 2 Mode Group Control for Mode Group Division Multiplexing

This chapter is based on the publications [74]–[76] made during the Ph.D project. In this chapter, the enhancement of MMF’s capacity by mode group division multiplexing (MGDM) is described. 30Gb/s 3×3 MGDM transmission over a short-distance MMF is experimentally demonstrated with a proposed mode selective spatial filtering technique. Chapter 2.3 introduces a photonic integrated mode group multiplexing solution with optical multiple-input and multiple-output (MIMO) tracking.

2.1 Multi-mode Fiber

Compared to SMF, MMF has a larger fiber core, which provides higher alignment tolerance for fiber interconnections. Therefore, MMFs are popular in short-reach optical networks. Modal dispersion, caused by non-identical propagation constants of the different modes constrains the capacity of MMF links and results in a frequency-selective fading channel with transmission nulls at some frequencies.

2.1.1 Modal dispersion

The frequency response of an MMF is determined by modal dispersion, chromatic dispersion and excitation conditions [77]. Since the applications of MMF are mainly short reach links such as data center, in-building or access networks, the chromatic dispersion can be neglected compared to the modal dispersion. Figure 2-1 (a) and (b) shows the measured 2km SI-MMF’s impulse responses and frequency responses, respectively, under center and offset launch cases. A laser operating at 1550nm is modulated by an external modulator driven by a 100ps pulse. It can be seen that most of the power excited by center launch is dominant at fundamental mode (red curve), which provides a

frequency response with small fluctuation ($< 3\text{dB}$). With launch offset getting larger, more higher order modes are excited, which results in a frequency fading channel due to the interference among these modes.

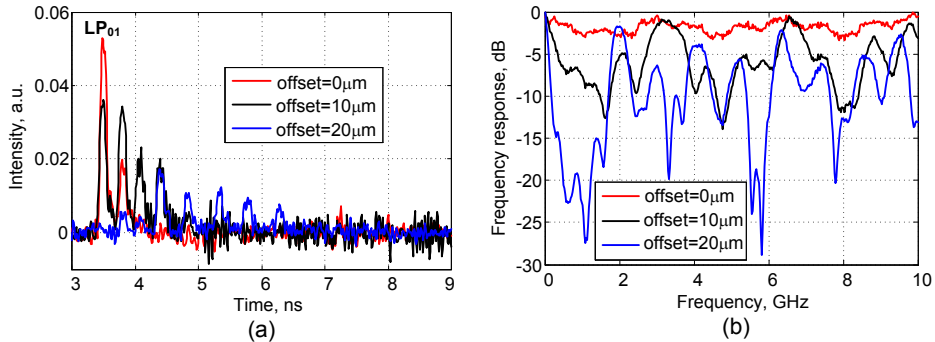


Figure 2-1 Measured 2km MMF's (a) impulse responses and (b) frequency responses with center/offset launch.

2.1.2 Proposed techniques

Driven by the ubiquitous video and cloud computing applications, the required capacity of optical communication networks has grown exponentially over the years. To enhance the link capacity to 10Gb/s and above with installed MMFs, several techniques have been proposed in order to overcome the modal dispersion:

1) Launch condition optimization: center/offset launch [77], [78], see Figure 2-2 (a), and mode or mode group selective launching [79]–[81]. An example for LP_{21} mode excitation is illustrated in Figure 2-2 (b).

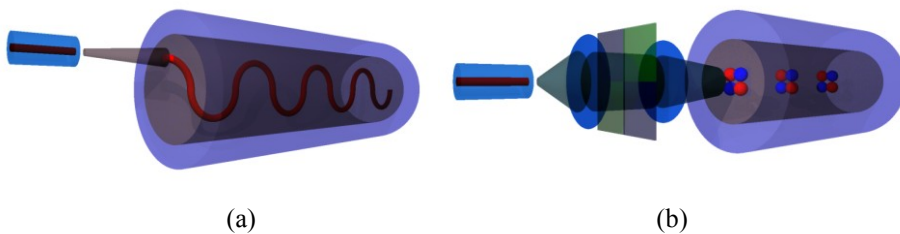


Figure 2-2 (a) Offset launch and (b) mode selective launch.

2) DSP based frequency fading cancellation: Adaptively modulated orthogonal frequency division multiplexing (OFDM) [82]–[84] and Zero-padded (ZP) OFDM [85]–[87].

Adaptively modulated OFDM, also called discrete multi-tone modulation (DMT), is able to enhance the capacity of MMF links with adaptive bit and

power loading algorithms. The algorithms measure the signal-to-noise-ratio (SNR) for a specified frequency range and use this information to adjust the bit allocation for each subcarrier [82]. This technique requires a feedback loop from the receiver for the transmitter to acquire channel state information.

ZP-OFDM inserts a sequence of zeroes as a guard in each OFDM frame to minimize the influence caused by frequency fading channel. It outperforms the widely-used cyclic-prefix (CP) OFDM but requires higher computation complexity caused by matrix operations [86].

3) Multiplexing in the spatial domain: mode group division multiplexing (MGDM) [38], [88].

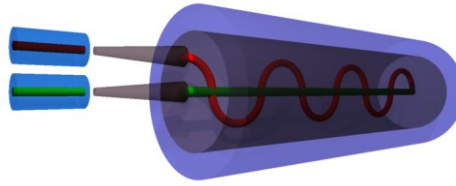


Figure 2-3 Schematic diagram of MGDM realized by center and offset launch.

2.2 Mode Group Division Multiplexing

With MGDM in a heavy-mode MMF, one can partition the whole set of guided modes in many subsets and launch each of them separately. Moreover, as a subset of modes exhibit less modal dispersion than the entire set of all modes do. Therefore, the bandwidth of a subset can be larger than that of the entire set [89], [90]. It should be noted that in this thesis, mode group refers to a set of modes, which are excited together under one launch condition. It is possible for some modes being excited by two different launch conditions. In this case, two mode groups will have an overlap of the modes, which can be seen as a crosstalk. In some literature, a mode group also represents a group of modes sharing a similar propagation constant.

2.2.1 Mode-selective spatial filtering

To separate mode groups in MGDM system, mode-selective spatial filtering (MSSF) was proposed in [91], [92], where a lens with a small numerical aperture (NA) was used to mitigate the crosstalk between the mode groups yielded with different radial offsets, as shown in Figure 2-4 (a). A microscope objective lens with $5\times$ magnification and $NA=0.1$ was utilized to measure the near field pattern (NFP) at the output facet of a 20m long $185/250\mu\text{m}$ graded-index (GI) MMF. Figure 2-4 (b) give the near field patterns with different radial

offset launchings, at a wavelength of 660nm. It can be seen that there is no spatial overlap between different mode groups therefore the crosstalk is negligible. Multi-segment photo detector (PD), proposed in [93], [94] is able to realize the detection of individual mode group.

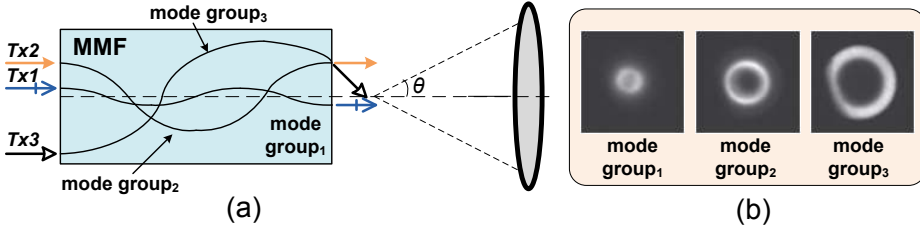


Figure 2-4 (a) The principle of MSSF through the use of a lens with small NA and (b) near field patterns for three mode groups with MSSF.

The main benefit of minimizing crosstalk through MSSF is to decrease the complexity of signal recovery, since the calculation for matrix inversion, especially in the case of high dimensions is complex and expensive. The rough number of computations for inversion of a $N \times N$ real matrix is N^3 . For a basic joint detection scheme with H , a high-speed transmission optical MGDM system would place a heavy burden on the computation power of the circuits. For a 3×3 MGDM system, shown in Figure 2-5, let the 3×1 vector $X(t)$ represent 3 electrical signals that modulate the power of the 3 optical light sources. In the MMF, 3 optical signals propagate through 3 different mode groups. At the receiving side, each spatially selective receiver detects a mixture of all mode groups. The 3×1 vector $Y(t)$ represents the 3 output electrical signals after photo-detection and can be written as:

$$Y(t) = HX(t) + n(t) \quad (\text{Eq. 2-1})$$

where $n(t)$ is a 3×1 additive noise vector. Entries c_{i1} , c_{i2} , c_{i3} of transfer matrix H , see Figure 2-8 (a), describe the signal transfer from transmitter x_1 , x_2 and x_3 to receiver y_i . Besides the diagonal items, all other items in H mean crosstalk. The crosstalk can be induced by imperfect selective launching, imperfect MSSF and the mode coupling in the MMF, especially when it is bent with a small radius. To recover the received signals, H can be estimated by sending some training symbols. Zero-Forcing (ZF) is applied to cancel out crosstalk and recover the signals in a joint detection by multiplying $Y(t)$ with the inverse transfer matrix H^{-1} .

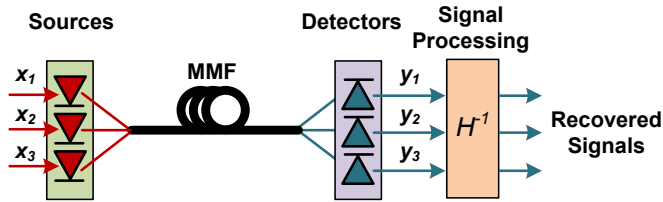


Figure 2-5 A 3×3 MGDM system.

In this study, optical fibers are used as MSSF elements for selectively detecting mode groups. Since an MMF guides a large number of modes, geometrical optics, also called ray optics, can be used to describe mode group propagation in terms of rays. It has been demonstrated that a PD with SMF pigtail can thus spatially detect mode groups with limited crosstalk [75]. The schematic diagram of realizing MSSF with SMFs is shown in Figure 2-6 (a), where three rays represent the three mode groups that were launched by three transmitters with different radial offsets. The angle which a ray makes with the fiber's axis is increasing when the ray approaches the axis. If at the output facet of the MMF, this angle is too large to fit within the NA of the fiber pigtail of a PD, this ray is not detected. Figure 2-7 gives the power distribution of mode groups after a 20m long 185/250 μ m GI-MMF launched by different radial offsets and detected by an SMF. It can be seen that the power distribution of mode groups in the fiber is fixed and main power of each mode groups is distributed at the radial position close to its launching offset.

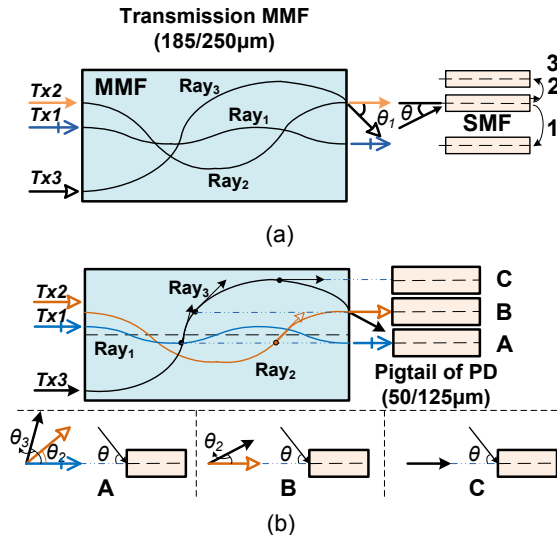


Figure 2-6 The realization of MSSF with fiber pigtail (a) SMF and (b) MMF.

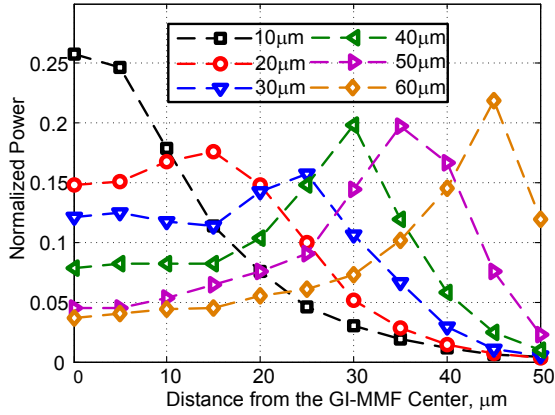


Figure 2-7 The power distribution of mode groups excited with different offsets along fiber radial axis.

A large coupling loss was observed because an SMF with limited mode field diameter is used to catch the light from one mode group. SMFs can only couple the power from a small spot of the mode group, which is distributed in 2D. The other proposed solution to realize MSSF with an optical fiber but with lower coupling loss is to use a PD with an MMF pigtail, whose core size is smaller than the transmission one, to limit the crosstalk of neighboring mode groups. For instance, in position A in Figure 2-6 (b), the angle of Ray₃ θ_3 , is larger than the NA of the detecting GI-MMF with a core/cladding 50/125 μm , so Ray₃ would be filtered out and the crosstalk only exists for two mode groups. In position B there is no power from Ray₁, so only Ray₂ and Ray₃ are detected. In position C only Ray₃ is detected with the same rule. So with the MSSF function see Figure 2-6 (b), H_{MSSF} can be expressed as Figure 2-8 (b) shows.

$$H = \begin{pmatrix} c_{11} & c_{12} & c_{13} \\ c_{21} & c_{22} & c_{23} \\ c_{31} & c_{32} & c_{33} \end{pmatrix} \quad H_{MSSF} = \begin{pmatrix} c_{11} & c_{12} & 0 \\ 0 & c_{22} & c_{23} \\ 0 & 0 & 1 \end{pmatrix}$$

(a)
(b)

Figure 2-8 Transfer matrix for a 3×3 MGDM system (a) without MSSF and (b) with MSSF.

2.2.2 Modal noise

Figure 2-9 gives the speckle patterns at the end of a 20m long 185/250 μm GI-MMF with center and 20 μm offset launch as a distributed feedback laser (DFB) is used. The speckle pattern is an intensity pattern produced by mutual

interference of the modes in the fiber when light source is with a narrow spectral width (a long coherence length) [95] such as vertical cavity surface-emitting laser (VCSEL) and DFB. Depending on the phase relations between the modes and mode coupling in the fiber, the speckle pattern can change randomly. Modal noise occurs as a receiver with a small detection area cannot detect all the modes which are carrying signals. In this case, the variation of the speckle pattern will cause a changing power in the receiver signal. Modal noise arises from interference effects between the modes instead of originating from external sources such as the typical noises in electronics.

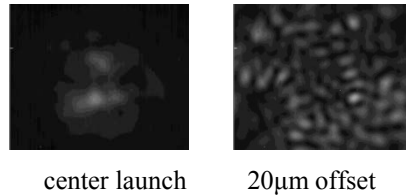


Figure 2-9 Speckle patterns at the MMF's end with center and offset launch.

A receiver with a smaller detection area, compared to the core size of a transmission MMF, is employed in MSSF, therefore modal noise has an effect to MSSF based receiver. In order to investigate the modal noise, the maximum power fluctuation for different radial offset launching over a time period of 20s was measured. The observed power fluctuation is within 0.2dB in the case the 185/250 μm GI-MMF is coupled with a 50/125 μm GI-MMF, which is smaller than the case when an SMF is used [75]. This can be explained by a larger number of modes are detected by the 50/125 μm MMF which averages out sharp interference variation. Therefore, increasing detection fiber's core size can minimize not only coupling loss but also modal noise.

2.2.3 MGDM transmission

The experimental setup of a 30Gbit/s 3×3 optical MGDM system employing two different kinds of detection fibers is shown in Figure 2-10 (a). A Mach-Zehnder modulator (MZM) is driven by a 10Gbit/s 2^7-1 random pattern to modulate the light of a 1550nm wavelength laser diode. The modulated light is amplified by the EDFA before it is split into three different arms. Three streams are decorrelated by the transmission through fibers with different length. These fibers are connected to a fiber concentrator, which is a linear array of single-mode waveguides with a spacing of two adjacent waveguides of 30 μm at the concentrated side [40]. Considering the large power loss of the large radial offset launching, the positions of selective launching are chosen as depicted in Figure 2-10 (b). A 20m long 185/250 μm GI-MMF is used as the MGDM

transmission medium. No strong mode mixing between mode groups was observed in the experiment due to the short length of the transmission fiber. The output light from the 185/250 μm GI-MMF is detected by an MSSF receiver. Either SMF or MMF is chosen for MSSF, as shown in Figure 2-10 (c) and (d), respectively.

1) For SMF-based MSSF, Figure 2-11 (a) shows bit error ratio (BER) curves versus different bit rates for the 3 mode groups. The performance of the subchannel which consists of a higher order mode group is better than that of the subchannel composed of a lower order one. The worst performance of subchannel y_1 compared to the other two subchannels can be explained because the interference from higher order mode groups into lower order ones is more serious than the reverse case; this is due to the MSSF function and the spatial power distribution of mode groups.

2) Utilizing a 50/125 μm GI-MMF to realize MSSF, the positions of selective detection are shown in Figure 2-10 (d). Figure 2-11 (b) gives the eye diagrams of received signals y_1 , y_2 and y_3 . It can be seen that the eye diagram of y_3 is clear and the crosstalk from the other mode groups can be neglected. This is due to the small power of the mode groups excited by x_1 and x_2 with small and medium offset at the position where y_3 is detected. The interference from the other mode groups to the detected y_1 and y_2 can be observed from eye diagrams. The estimated transfer matrix is determined by the received power obtained through training symbols in which transmitters send signals in turn. The rows in H_{MSSF} in Figure 2-11 (b) are normalized. It can be seen that the crosstalk, represented by the entries of H_{MSSF} which are encircled, only occurred at neighboring mode groups. In the process of the signal recovery, x_2 is recovered based on the 2×2 submatrix at the low right corner of H_{MSSF} through the ZF algorithm. The recovered eye diagram of x_2 is shown in Figure 2-11 (b). With the aid of the recovered x_2 , x_1 is recovered in the same way based on the 2×2 submatrix at the upper left corner of H_{MSSF} . The 3×3 transfer matrix is reduced into two 2×2 submatrices due to the limited mode group crosstalk. A matrix dimension reduction means less computation and less calculation error. Optimized joint detection which separates the transfer matrix into small submatrices through MSSF is also applicable to MGDM systems with higher dimensions, i.e., a larger number of mode group channels when radial offsets, detection positions and NA of the detection devices are carefully chosen.

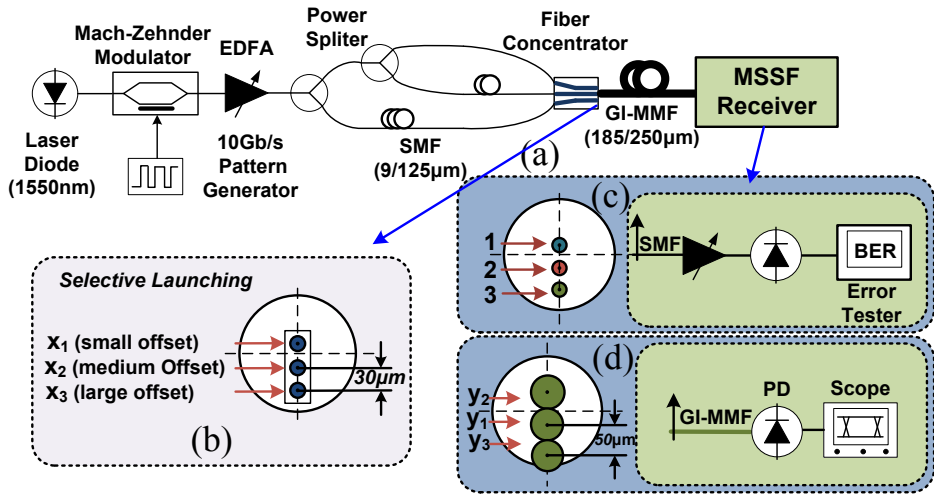


Figure 2-10 (a) Experimental setup of a 30Gbit/s 3 × 3 optical MGDM system with joint detection; (b) selective launching by fiber concentrator; and selective detection by (c) SMF and (d) MMF.

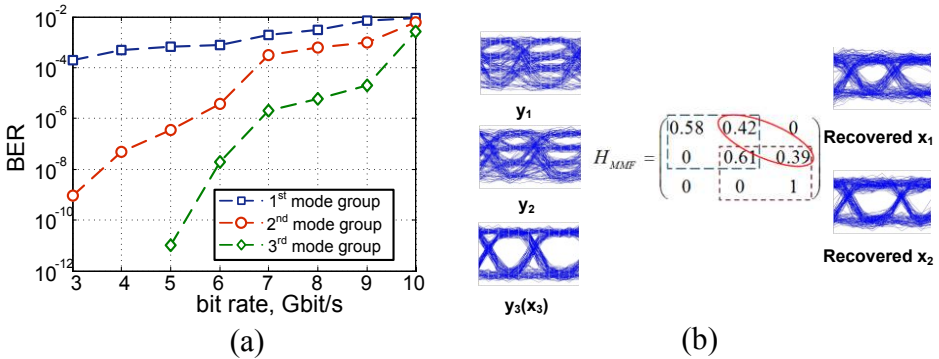


Figure 2-11 (a) BER versus different bit rates for the 3 mode groups with SMF detection and (b) estimated transfer matrix and eye diagrams for received signals y_1, y_2, y_3 and recovered x_1 and x_2 with MMF detection.

2.3 Optical MIMO Tracking

2.3.1 Integrated MGDM (de)multiplexer

The complexity and scalability of the mode group (de)multiplexer has a significant impact on the practicality of MGDM schemes. Up to now, fiber concentrators [74], [75] and multimode couplers [96] have been employed to

realize the (de)multiplexing function. A multimode coupler can only support a fairly limited number of mode group channels due to the control and calculation complexity in fusing more fibers. Also the support by a fiber concentrator is limited, as it is challenging to decrease the pitch between neighboring waveguides without inducing too much crosstalk.

A low-cost and scalable integrated mode group MUX/DEMUX design based on silicon-on-insulator (SOI) is proposed in [76]. Through arranging 2-dimensional (2D) vertical grating couplers along the axis of an MMF, center and offset launching can be realized, by which fundamental and higher order mode groups are excited, respectively. The high refractive index of SOI enables mode group excitation with a waveguide spacing less than $10\mu\text{m}$, which means more parallel channels could be excited in a $50\mu\text{m}$ MMF. The schematic diagram of the integrated mode group (de)multiplexing section is given in Figure 2-12 (a). Figure 2-12 (b) and (c) gives the Scanning Electron Microscope (SEM) images of a 1D grating coupler and three 2D vertical grating couplers with a radial distance of $5\mu\text{m}$ and sharing end reflectors to decrease the coupling loss.

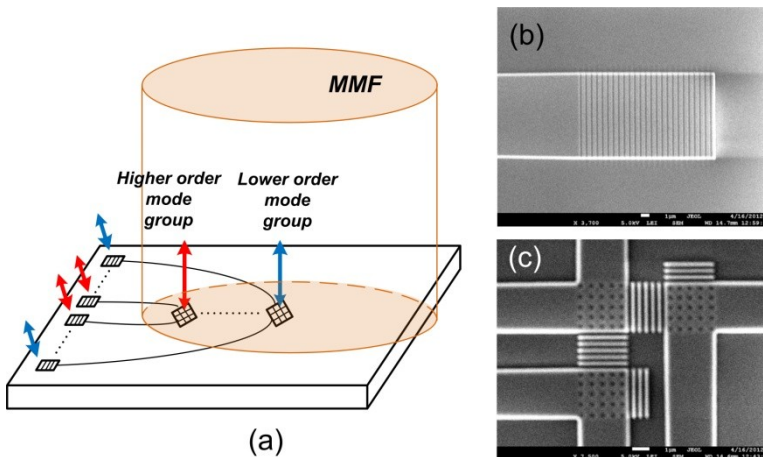


Figure 2-12 (a) The schematic diagram of the integrated mode group (de)multiplexing section; SEM images of (b) an 1D grating coupler and (c) three 2D vertical grating couplers.

2.3.2 Optical MIMO demultiplexing

Multiple-input and multiple-output (MIMO) demultiplexing is typically done by DSP in the electronic domain. However, for high bit rate optical transmission systems, DSP capacity for signal recovery may become insufficient when the number of modes or mode group numbers is going up.

Compared to DSP-based MIMO demultiplexing, optical MIMO demultiplexing [97], which includes an endless phase shifter (EPS) and tunable coupler (TC), shown in Figure 2-13 (a) and (b), is insensitive to the bit rate.

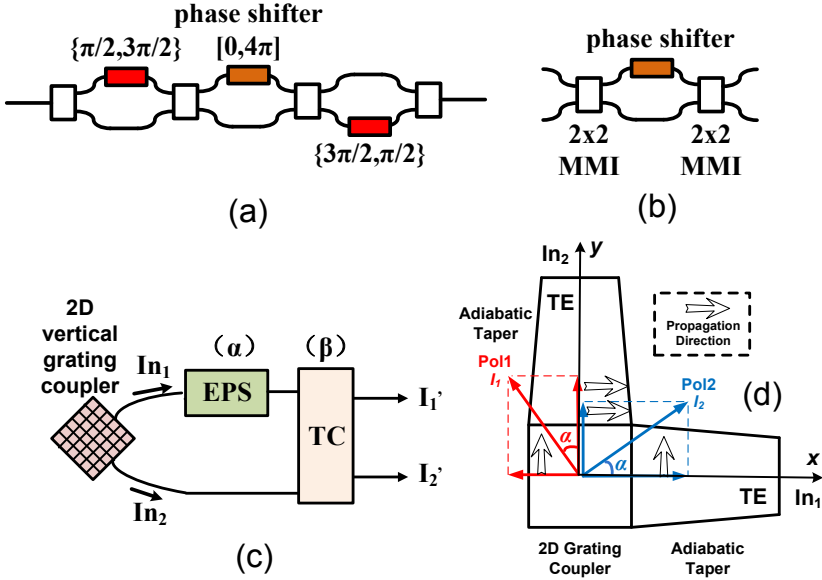


Figure 2-13 The structure of (a) EPS and (b) TC; (c) optical MIMO demultiplexing structure based on a 2D vertical grating coupler as a polarization splitter and mode-selective spatial filter and (d) dual-polarization detection by a 2D grating coupler.

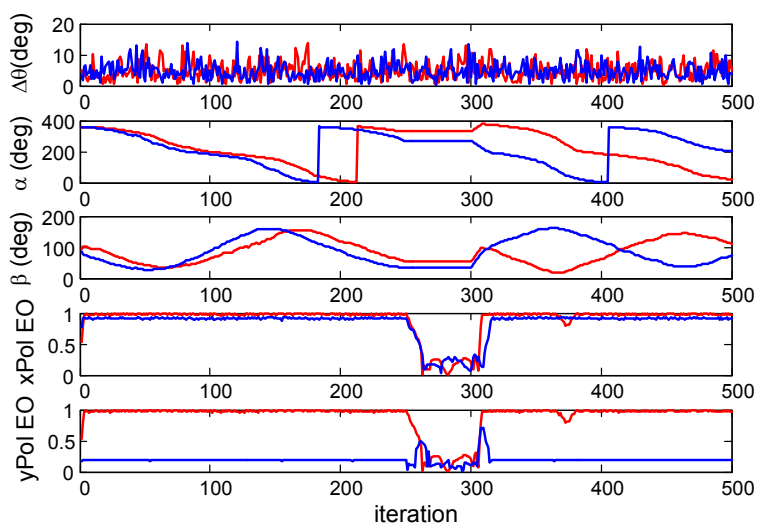
Figure 2-13 (c) shows the basic structure of the optical MIMO demultiplexing suitable for photonic integration. A vertical grating coupler accepts light in a cone perpendicular to the substrate, which is similar to the MSSF realization using the NA of an SMF. As shown in Figure 2-7, the peak power of a mode group occurs at a radial position close to its launching offset. Through positioning the vertical 2D grating couplers radially along the MMF’s output, the MSSF function could help each coupler detect the mode group of interest with a low mode group crosstalk. Therefore, to separate each mode group from the MGDM channel after MMF transmission, a 2D vertical grating coupler is proposed to use, which in the meantime plays a role as a polarization beam splitter. As shown in Figure 2-13 (d), a PDM optical signal, composed of two polarization tributaries I_1 and I_2 , illuminates a 2D grating coupler. After decomposing the state of polarization (SOP) into two orthogonal directions x and y , optical light oscillating perpendicular to the propagation direction can be horizontally coupled into an adiabatic taper, used for mode matching between the 2D grating coupler and an single-mode waveguide.

2.3.3 Simulation results

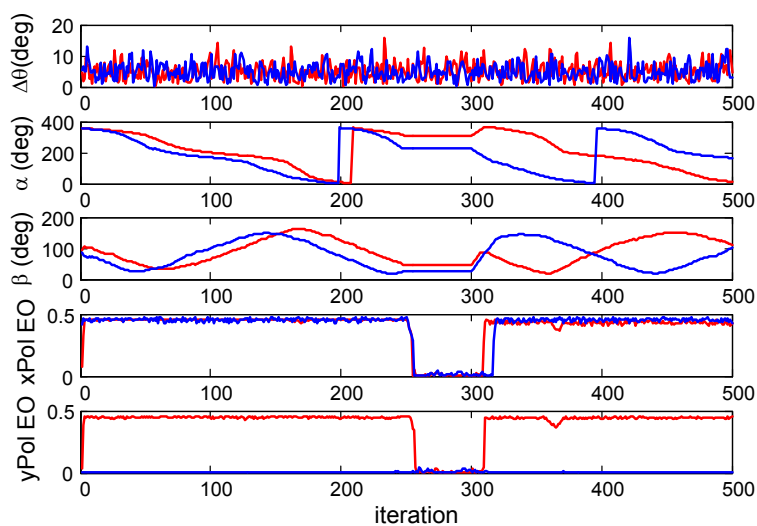
In the simulation, a pseudorandom sequence (PRBS) with a length of 2^9-1 is used to generate two quadratures of a QPSK signal through 12 bits delay with respect to each other. With 25 symbols shift of the QPSK signal, two PDM streams are created to compose a PDM-QPSK signal which is used to modulate one mode group. The signal carried by the other mode group is generated by a different PRBS with the same length. The mode group crosstalk is assumed to happen only between neighboring mode groups. To test the tracking ability of the optical MIMO demultiplexing, the SOPs of MGDM signals are rotated, which are realized by multiplying with several rotation matrices. In each iteration, the total rotation differential angle $\Delta\theta$ on the Poincare sphere is calculated. Before the DQPSK demodulation, the radio frequency (RF) signal power is measured.

Assuming in an ideal MSSF case, the mode group crosstalk can be neglected. In this case, the maximum $\Delta\theta$ is set at 15° . An EPC and a TC, as described in Figure 2-13 (c), are activated to track the changes of SOPs. The phase shifters in EPS and TC are adjusted 6 times in each iteration. Through comparing the recorded RF powers with increasing and decreasing the phase, a new phase is updated according to the case with minimum RF signal power. When the two polarizations of one mode group are kept orthogonal before entering the 2D vertical grating coupler, one polarization can be separated from one output port of the TC and the orthogonal polarization goes to the other output, see the red curves in Figure 2-14 (a). Figure 2-14 (a) shows the tracking process with the phase information of the EPS and TC (α and β) and the eye openings (EOs) of one quadrature of two polarizations which are separated from two outputs of the TC. During the simulation, the RF signal power from upper output of the TC is recorded.

The PDM signals carried by different mode groups will endure variable deterioration in polarization orthogonality [98]. The blue curves in Figure 2-14 (a) give the simulation results when the polarization orthogonality deteriorates with 15° . It can be seen that one polarization, regarded as xPol, still can be nicely tracked with good EO, but the other cannot be separated through the other output port of the TC. However, if the tracking structure is duplicated, both polarizations can be tracked simultaneously. Starting from iteration 250, the tracking stops for 60 iterations, and it can be seen that the eye closes during this period and is back to be open very fast when the tracking is turned on.



(a)



(b)

Figure 2-14 The tracking process of optical MIMO demultiplexing for PDM-DQPSK MGDM signals (a) without and (b) with the mode group crosstalk from a neighboring mode group.

Figure 2-14 (b) shows the simulation results for a case in which there is -10dB MG crosstalk from a neighboring mode group. The red and blue curves represent the cases in which polarization orthogonality of the mode group of interest is being kept constant or not, as the simulations show in Figure 2-14 (a).

Considering the short reach application of the MGDM, the polarization-dependent loss is neglected in the simulations. It can be seen the optical MIMO demultiplexing is still working with high mode group crosstalk which basically could be reduced through the MSSF [75]. The tracking process takes more time to go back to a good EO in the case where mode group crosstalk is present.

2.4 Summary

This chapter presented MMF related research work carried out in the early Ph.D stage. Transmission of three parallel mode group channels over a 20m long GI-MMF with a total capacity of 30Gb/s was demonstrated in the chapter. Limited by the pitch of the fiber concentrator, the MMF with a large core diameter of 185 μm was chosen to use. MSSF realized by the small NA of optical fibers was proposed to separate different mode groups. For these measurements, mode group detection was realized individually through moving the position of the detecting fiber, which was mounted on a translation stage. To simultaneously detect all mode groups for practical applications, fiber bundle which has been widely used as MCF coupler [99] can be employed. However, it is challenging to achieve a small core pitch in order to minimize the core-to-core crosstalk. Most reported MCFs have a core pitch larger than 35 μm [32], [100]–[102], which means a limited number of mode groups can be excited or detected in a standard MMF 50 μm or 62.5 μm cross-section without using imaging optics. The proposed integrated mode group coupler solution with 2D grating couplers can support more mode groups. However, large coupling loss can still be expected due to the field mismatch between the fiber modes guided by the MMF and a single grating coupler.

The research presented in this chapter focuses on the solutions to enhance the capacity of MMF but little attention has been paid to the system's reliability [9], [13]. Offset launch for mode group excitation yields a group of modes which will create different mode group distributions at the detection side due to the constructive and destructive interference between the modes. Fiber bending or imperfect splicing influences the amplitude and phase of the modes, which results in a changing mode group distribution. Due to the small detection area, some mode groups may not be detected properly and system outage will occur in this case. Selective mode excitation which has been employed to selectively yield and detect one mode or degenerate modes over MMFs [33], [103], [104] can lower this outage possibility since most power can be kept by the original mode. Selective mode excitation will be discussed in next chapter.

Chapter 3 Selective Mode Excitation

In this chapter, selective mode excitation is researched to excite pure fiber modes. Chapter 3.3 presents a single multi-mode phase mask to separate different LP modes as a compact solution for mode demultiplexing. Chapter 3.4 demonstrates a mode crossbar switch in the first time for LP₀₁ and LP₁₁ modes employing an spatial light modulator as a switch controller.

3.1 Selective Mode Excitation

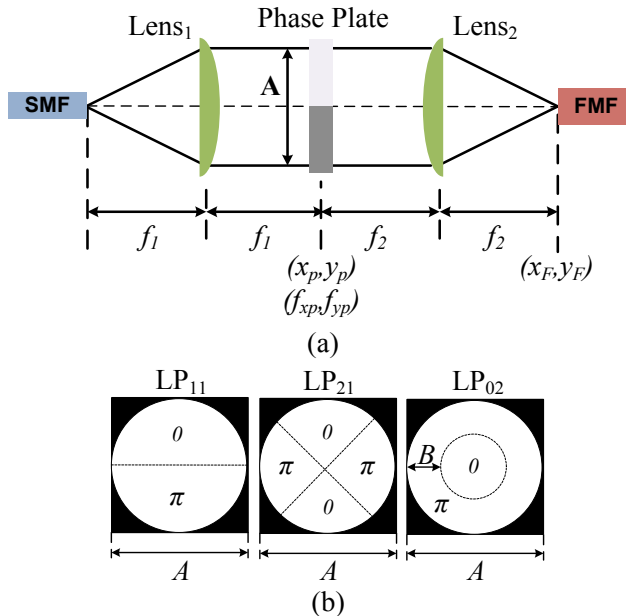


Figure 3-1 (a). Mode excitation scheme using phase plate; (b) phase plates for LP₁₁, LP₂₁ and LP₀₂ mode excitation.

To selectively excite a single LP mode only, the optical launch field should have the same field distribution and the state of polarization (SOP) as the mode of interest, which can be realized through spatially tailoring the collimated SMF's output. Binary phase plates [20], [23], [47], [105], and spatial light modulators (SLM) [58], [106], [107] have been demonstrated for selectively exciting modes. SLMs are usually based on polarization-sensitive liquid crystals. To support polarization multiplexed light, extra polarization separation and conversion setups are required. Phase plates can be made of glass which are able to support both polarization states.

A $4f$ setup is usually applied for free space selective mode excitation, as shown in Figure 3-1(a), where a phase plate is located in the Fourier plane. Output optical beam from the SMF gets collimated by the 1st lens with a beam width of A , written as $I_p(x,y)$. If the transmittance of the phase plate is written as $t_p(x,y)$, the field at the back focal point of the lens₂ is the Fourier transform of the product of $t_p(x,y)$ and $I_p(x,y)$:

$$\begin{aligned} U_F(x_F, y_F) &= U_F(f_{xp}, f_{yp}) \Big|_{f_{xp}=\frac{x_F}{\lambda f_2}, f_{yp}=\frac{y_F}{\lambda f_2}} \\ &= \iint_{-\infty}^{+\infty} I_p(x_p, y_p) t_p(x_p, y_p) e^{-j2\pi(x_p f_{xp} + y_p f_{yp})} dx_p dy_p \quad (\text{Eq. 3-1}) \end{aligned}$$

where f_{xp} and f_{yp} are spatial frequency coordinates in the phase plate plane, regarded as the Fourier plane. x_p, y_p and x_F, y_F are spatial coordinates of the phase plate and FMF input plane, respectively. This Fourier transform process does the phase modulation to intensity modulation conversion. The coordinates of the samples of x_p can be described as: $[-A/2:\Delta x_p:A/2-\Delta x_p]$, ranging from $-A/2$ to $A/2-\Delta x_p$ in steps of Δx_p . Due to the relation between the spatial and frequency domains in Fourier Transform, f_{xp} can be described as: $[-1/2\Delta x_p:1/A:1/2\Delta x_p-1/A]$. There is a relation: $x_F=f_{xp}\lambda f_2, y_F=f_{yp}\lambda f_2$, so that x_F can be described as: $\lambda f_2 [-1/2\Delta x_p:1/A:1/2\Delta x_p-1/A]$. λ and f_2 are the wavelength of the light and the focal length of the lens₂, respectively. Figure 3-1 (b) shows the phase plate designs for mode LP₁₁, LP₂₁ and LP₀₂. B is the width of outer ring with a π phase shift and $B=A/4$.

Figure 3-2 gives the theoretical mode profiles (left to right: LP_{11a}, LP_{21a} and LP₀₂) in a 6-mode fiber. For the circularly asymmetric modes such as LP₁₁, there exist two degenerated modes called as LP_{11a} and LP_{11b}. There is an assumption that the SOP is matched. With a 90° rotation of the phase plate, LP_{11b} can be obtained respectively. For LP₂₁ mode, to generate degenerated LP_{21a} and LP_{21b} modes, the phase plate needs to be rotated with 45°. According to (Eq. 3-1 and coordinates relations shown above, Figure 3-2 shows the simulated launch fields at FMF plane modulated by phase plates, see Figure 3-1 (b), with Gaussian-distributed LP₀₁ mode as the input beam. Variables:

$\lambda=1550\text{nm}$, $f_1=18\text{mm}$, $f_2=23\text{mm}$ and an SMF with a core of $9\mu\text{m}$ and an NA of 0.11 are used for simulating the phase-plate launch fields. Figure 3-3 gives the vertical cross-section of the theoretical mode profiles of a 6-mode SI-FMF with a core diameter of $24.7\mu\text{m}$ in blue curves and the phase plate launch fields in red curves. It can be seen that binary phase plate is able to create a similar optical field at the focal point to match the corresponding fiber mode.

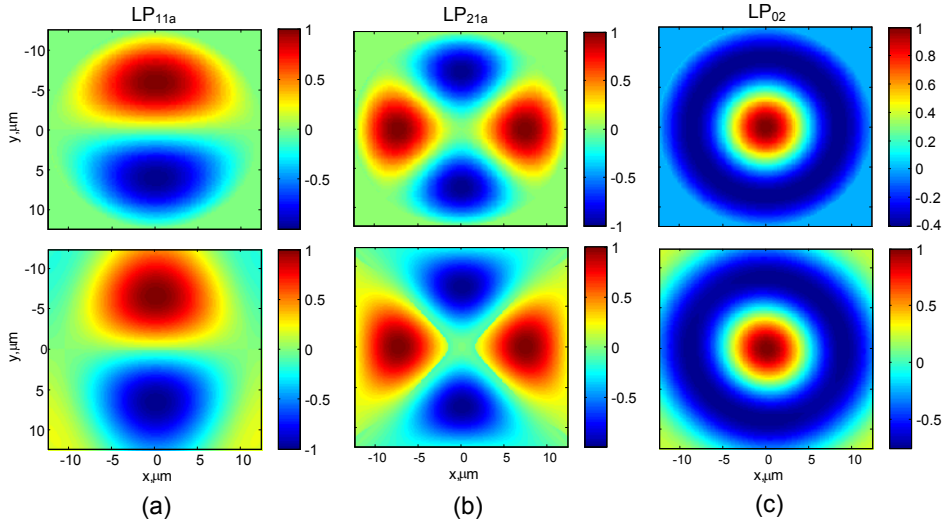


Figure 3-2 Theoretical mode profile (upper) and phase plate launch field (lower) for (a) LP_{11} , (b) LP_{21} and (c) LP_{02} mode.

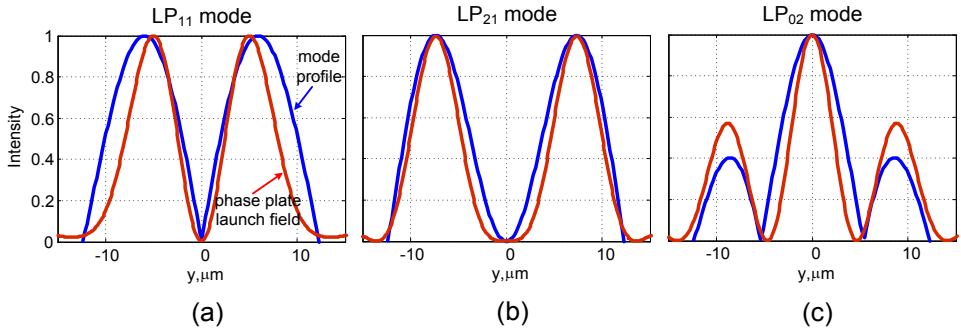


Figure 3-3 Vertical cross-section of the theoretical mode profile (blue curve) and phase plate launch field (red curve) for (a) LP_{11} , (b) LP_{21} and (c) LP_{02} mode.

3.2 Mode Detection

When the setup shown in Figure 3-1 (a) is used in reverse, each LP mode can selectively be detected. Figure 3-4 (a) and (b) give the simulated fields projected on the input facet of the SMF for each LP mode without and with 45 and 90° rotation in the LP_{11a} and LP_{21a} receivers, respectively. LP₀₁ and LP₀₂, due to the circularly symmetric distribution, are insensitive to the mode rotation. But for LP₁₁ and LP₂₁ modes, coupling losses can be expected with mode rotations for a short and straightly-placed FMF [108].

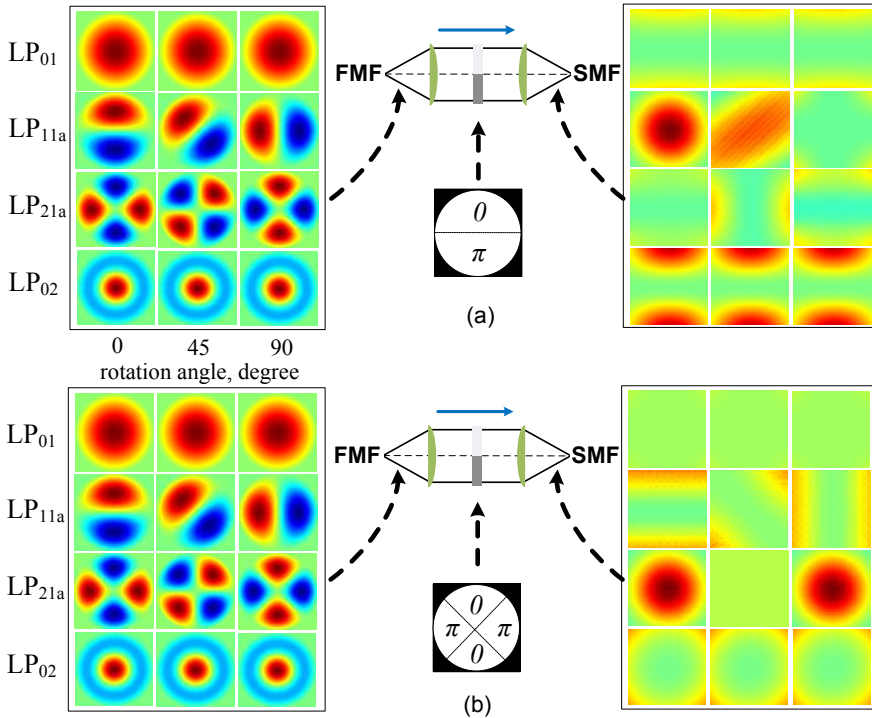


Figure 3-4 The simulated fields projected on the SMF for 4 LP modes with mode rotation (a) in the LP_{11a} receiver and (b) in the LP_{21a} receiver.

Figure 3-5 shows the normalized coupled powers of both degenerate modes as a function of the mode rotations in the corresponding LP_{11a} and LP_{21a} mode receivers. The simulated crosstalk from other modes is smaller than -20dB for all rotation angles, which verifies the mode selectivity of phase plate mode coupler. As the transmission FMF becomes longer, more mode coupling happens due to fiber bends or some structural defects, especially for the degenerate LP modes such as LP_{11a}, LP_{11b} and LP_{21a}, LP_{21b}. Therefore, a

combination of the degenerate modes: $LP_{1ma} + j LP_{1mb}$, which gives a ring-shaped mode distribution is used to evaluate the influence of mode rotations to phase-plate mode DEMUX. It can be observed in Figure 3-5 that constant powers can be detected with all rotation angles, which means that a phase plate mode coupler is a robust solution to not only detect but also separate different LP modes. The assumption for using the mode combination is reasonable, since a circular FMF behaves as a mode scrambler for the degenerate modes. It should be noted that it is challenging to further separate degenerate modes for circular core fibers such as LP_{11a} and LP_{11b} , which need to be recovered by an MIMO equalizer in digital domain.

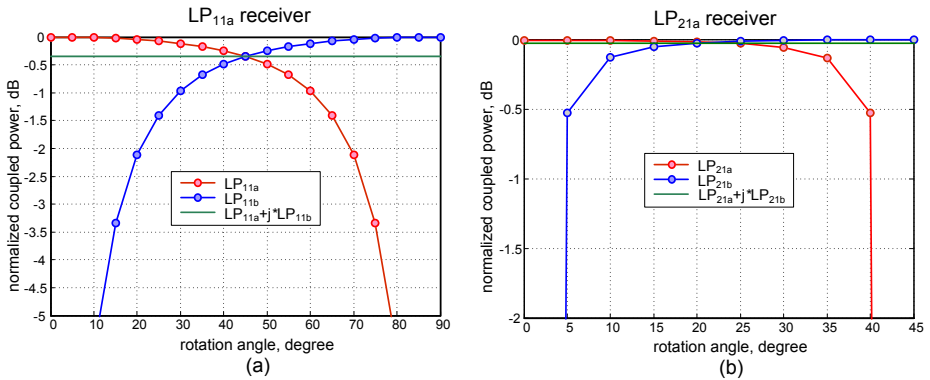


Figure 3-5 Normalized coupled power in dB for the degenerate modes in (a) LP_{11a} and (b) LP_{21a} mode receiver.

3.3 Multi-mode Phase Mask

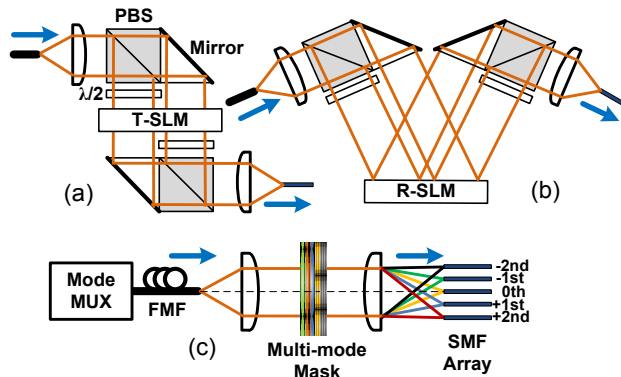


Figure 3-6 PDM setup for a (a) transmissive and (b) reflective SLM; (c) a single multi-mode phase mask for separating all modes.

This section is based on the publication [51] made during this Ph.D project. A multi-mode phase mask (MMPM) is proposed as a flexible mode division demultiplexing solution, which is able to demultiplex all mode channels simultaneously with one multi-level phase plate, which can be fabricated as diffractive optical elements (DOEs) [109], [110]. An MMPM is able to image different LP modes to different receiving ports. A programmable phase-only SLM is chosen to realize this spatial separation and track mode rotations for different modes. The SLM is composed of a 2D liquid crystal array, where each pixel can change its phase shift individually with different applied voltage. Since general liquid crystals can only modulate phase effectively for one polarization, the setup for a transmissive and reflective SLM to support PDM optical signal is illustrated in Figure 3-6 (a) and (b), respectively.

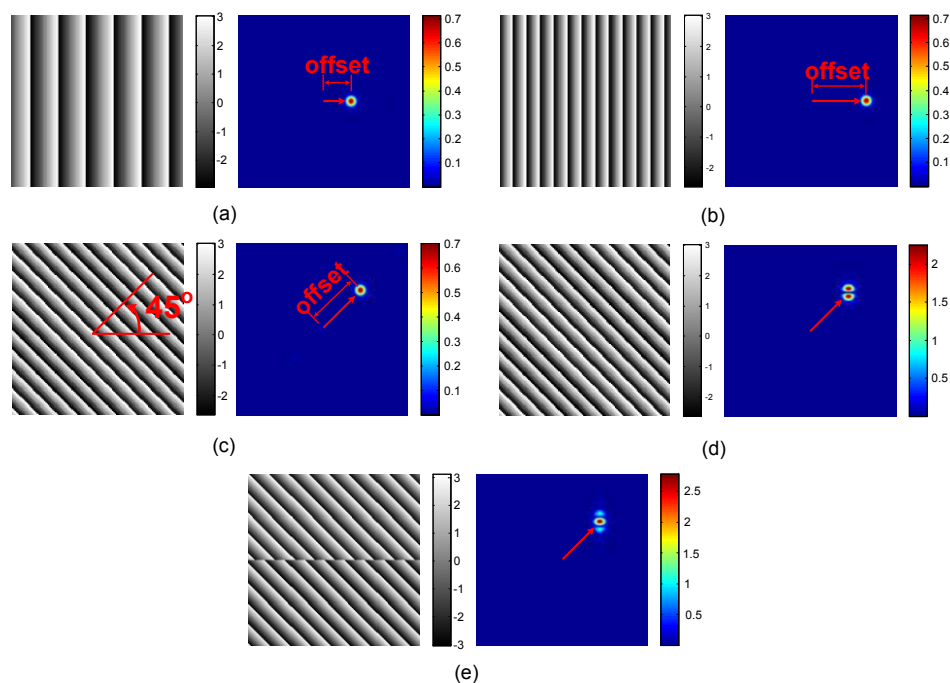


Figure 3-7 Blazed grating steers the beam in (a) a small offset, (b) a big offset and (c) 2D. Steering LP_{11} mode with (d) only a blazed grating and (e) a mode-related mask.

Figure 3-6 (c) shows the basic setup for demultiplexing all modes with the proposed MMPM. Since the SLM is programmable, this mode demultiplexing solution has a large range of applications. Examples of the blazed gratings are shown in Figure 3-7 with the blazed gratings (left) and the corresponding simulated diffracted beams (right). As shown in Figure 3-7 (a) and (b), the

density of the grating determines the offset of a diffracted beam. Figure 3-7 (b) shows the possibility to steer a beam in 2D with tilting the grating.

The MMPM can be created by superimposing all mode-related masks together. Each mode-related mask is the summation of a binary phase mask and a blazed grating which determines the routing port of the mode of interest at the SMF array's input. The example of the LP_{11} mode-related mask is given in Figure 3-7 (e). It can be seen in Figure 3-8 that every mode only passing through one related binary mask would generate a Gaussian-like spot in the center, marked by a red circle, which can be coupled into an SMF in the detection side. For other modes, the overlap integral between the complex diffracted profile and the fundamental mode of the SMF is close to zero which gives low mode crosstalk.

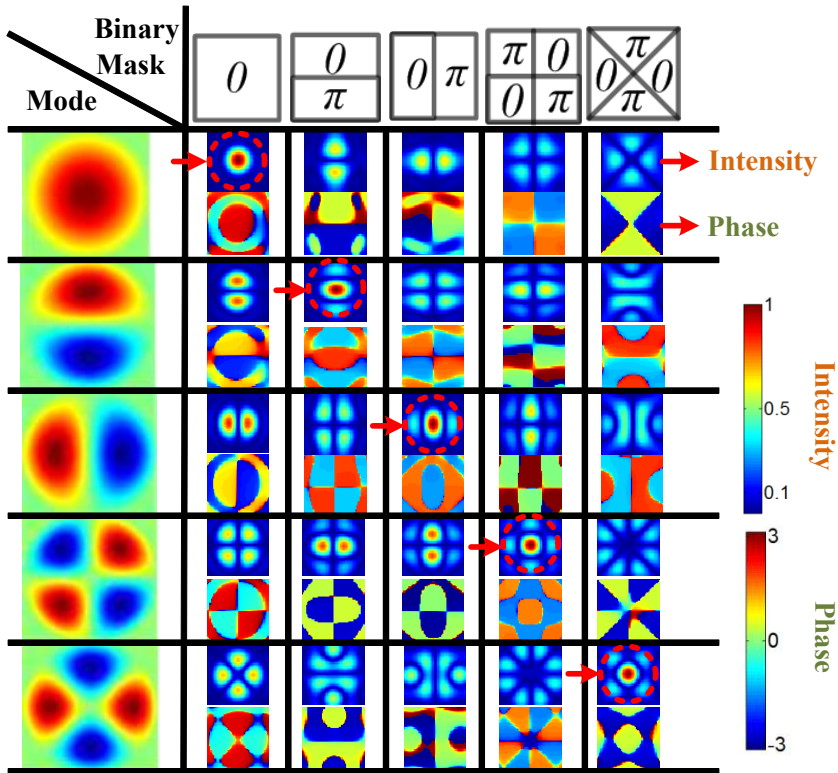


Figure 3-8 Converted mode profiles when different modes go through different binary phase plates. (upper: intensity; lower: phase, in rad)

Figure 3-9 (a) shows the mode-related phase masks and the summarized MMPM where different blazed gratings are used for each mode. Figure 3-9 (b) gives the far fields at the plane of a SMF array as LP_{01} , LP_{11a} , LP_{11b} , LP_{21a} and

LP_{21b} pass through the MMPM, respectively. The periods of blazed gratings are precisely calculated to couple different modes into different array's ports with a spacing of d . Figure 3-9 (c) and (d) show a case with mode dependent rotations where LP_{11} modes rotate 22° and LP_{21} modes rotate 12° . With the corresponding rotation of the mode-related phase mask, these mode rotations can be compensated and each mode is routed to the desired port.

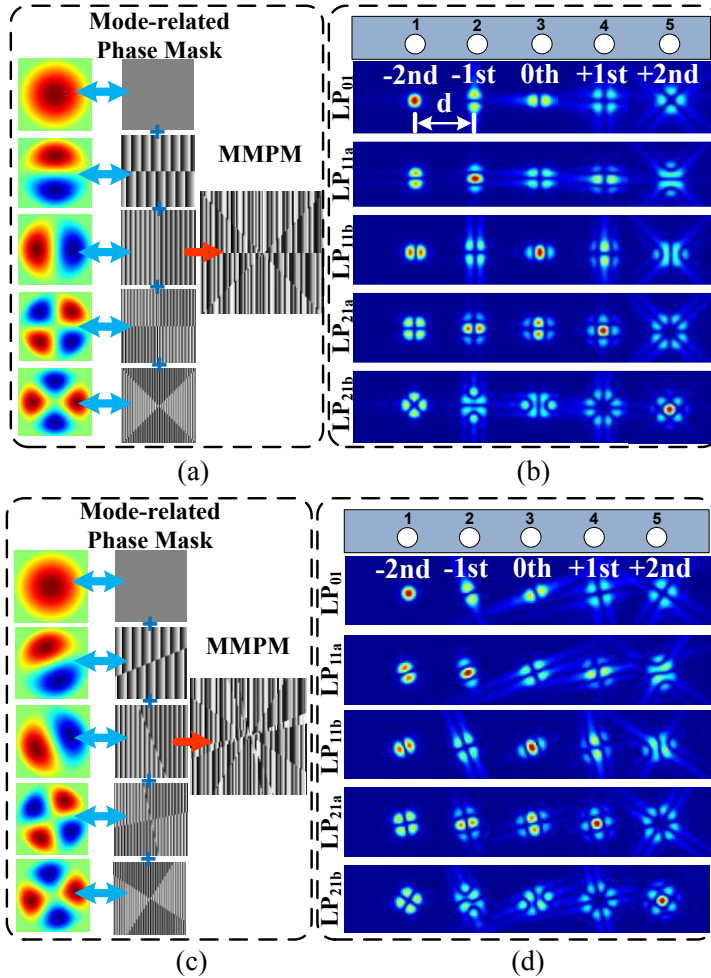


Figure 3-9 (a) Mode-related phase masks and the summarized MMPM; (b) simulated far fields as different modes pass through the MMPM (top to down: LP_{01} , LP_{11a} , LP_{11b} , LP_{21a} and LP_{21b}); (c) and (d) mode-related phase masks rotate with corresponding angles to compensate for mode-dependent rotations.

To investigate the performance of the MMPM for demultiplexing N spatial modes, an $N \times N$ transfer matrix M is used. N is also the number of SMF array's ports. The matrix entries $m_{i,j}$ of M are calculated through the overlap integral between the SMF's fundamental mode and the far field of the j -th mode which is diffracted by the multi-mode mask to the i -th array's port, as shown in Figure 3-9 (b) and (d). λ_n ($n=1$ to N) are singular values of M . The definition of the MDL is given in (Eq. 1-7). For an MDM system with 3 and 5 spatial modes, the MDL of this demultiplexer is 1.06dB and 1.87dB, respectively. When each mode-related phase mask uses different blazed gratings, different modes are routed to different ports, as shown in Figure 3-6 (c). In this case, the demultiplexer will achieve a maximum loss, which is $[10 \cdot \log_{10}(N) + \text{CIL}]$ (dB). The coupler insertion loss, defined in Eq. 1-8, is caused by the binary phase plates which are a phase-only approximation for each mode. The CIL for demultiplexing 3 and 5 modes is calculated as 0.66dB and 1.29dB, respectively. The CIL could be greatly reduced if an optimized mask for each mode is designed through simulated annealing algorithms [103].

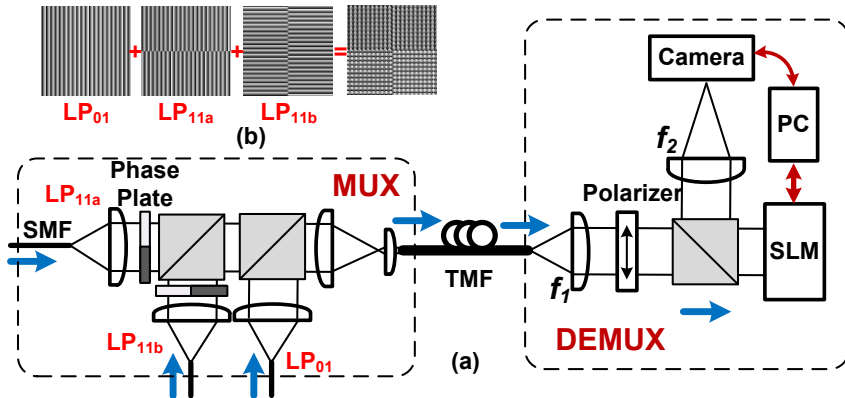


Figure 3-10 (a) Experimental setup for demultiplexing 3 spatial modes with one MMPM; (b) mode-related masks for LP₀₁, LP_{11a} and LP_{11b} modes and the superimposed MMPM.

Figure 3-10 (a) shows the experimental setup for demultiplexing one polarization of 3 spatial modes: LP₀₁, LP_{11a} and LP_{11b} modes with one MMPM. This setup can also support PDM as the setup proposed in Figure 3-6 (a) and (b) is applied. The mode MUX setup uses binary phase plates for LP₁₁ mode excitation and beam splitters to combine 3 beams. With this mode MUX, >25dB high mode extinction ratio between LP₀₁ and LP₁₁ modes are measured, as demonstrated by [47]. A 10-km SI-FMF with a core size of 19.4 μ m which guides LP₀₁, LP_{11a} and LP_{11b} modes is used as the test fiber. In the mode DEMUX, two lenses with $f_1=15$ mm and $f_2=150$ mm are deployed. Figure 3-10 (b)

gives the mode-related masks for 3 spatial modes and the superimposed MMPM which is realized by a reflective SLM with a resolution of 1920×1080 . To avoid the crosstalk from undiffracted light at the centre due to SLM's imperfections, same blazed grating is used for all mode-related masks but with different rotations (LP_{01} : 0° , LP_{11a} : 90° and LP_{11b} : 180°) to diffract different modes to different directions but with a same offset D . The simulated and experimental results for the diffracted far fields without and with the use of the MMPM are given for all 3 spatial modes in Figure 3-11, respectively. A camera is used to capture these far fields at the SMF array's plane. It can be seen that if SMFs are placed at the appropriate positions (e.g. using a 2D SMF array), each mode can be spatially separated and detected with low crosstalk from the other modes. The positions of mode detection are pointed with red arrows in Figure 3-11.

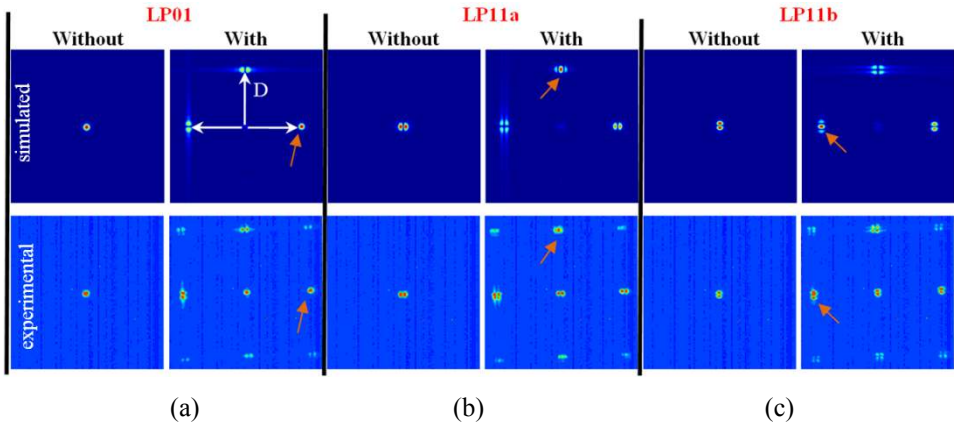


Figure 3-11 Simulated (upper) and experimental (lower) results for the diffracted far fields without and with employing the MMPM shown in Figure 3-10 (a) for (a) LP_{01} , (b) LP_{11a} and (c) LP_{11b} mode respectively.

3.4 Mode Crossbar Switch

This section is based on the publication [111] made during this Ph.D project. A mode crossbar switch scheme between LP_{01} and LP_{11} mode is realized for the first time, which utilizes the orthogonality of modes and spatially tailors two mode profiles at the same time. The aim of this research is to investigate the possibility for building a reconfigurable optical add/drop multiplexer (ROADM) which enables the operation at a mode layer.

The mode switch is directly realized in the optical domain therefore signal format transparency is preserved and devices for costly optical-electronic-

optical (OEO) conversions can be saved. A binary phase plate [47] is used in the mode MUX for LP_{11} mode excitation. An SLM acts as a crossbar switch controller. The mode crosstalk from LP_{11} to LP_{01} mode is measured at the LP_{01} mode drop port over C-band. The results show that low mode crosstalk ratio can be achieved when cross-bar switch is applied in an MDM transmission link.

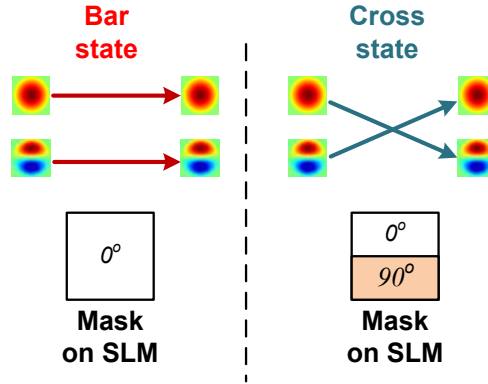


Figure 3-12 Masks for realizing bar and cross switch for LP_{01} and LP_{11} modes.

The SMF crossbar switch which can map the input ports to the output ports with or without interchange, corresponding to the states of cross or bar is demonstrated in [112]. For the mode crossbar switch, the interchange happens between different modes. The basic principle of a mode crossbar switch between the LP_{01} and LP_{11} mode is to convert the bipolar field distribution of the LP_{11} mode into unipolar and do the reverse conversion for the LP_{01} mode. This can be done for two modes simultaneously through phase modulation in spatial domain. The pattern to create the 0 and π phase shift (see Figure 3-12, which is the same pattern on the phase plate in the MUX) is emulated on an SLM in the cross state to spatially change the phase of two modes from an FMF, which are collimated by a lens and illuminate the SLM, as shown in Figure 3-13 (b). The spatially phase-tuned optical field is focused by a second lens and the far field pattern at the focal point which approximately matches the desired mode is coupled into an FMF. The SLM gives the flexibility to rotate the pattern to match the LP_{11} mode profile and eliminates the rotation angle θ to a minimum.

Figure 3-13 shows the setup of the MDM link with a mode crossbar switch and LP_{01} mode drop unit, where lenses with a focal length of 3mm are utilized. The light from a tunable laser is passed into a 50:50 power splitter to feed power into two inputs of the MUX. All lenses inside the setup have a focal length of 15mm. The MUX and the crossbar switch are linked with a 10m FMF. A reflective SLM with 1920×1080 resolution is used to carry out the mode switch. Due to the polarization sensitivity of the SLM, a linear polarizer is put

in front of the beam splitter to increase the modulation efficiency. A camera is used to capture the LP_{11} mode pattern to gain the knowledge of mode rotation. When the SLM is off, the LP_{01} and LP_{11} mode from the input FMF inside the crossbar switch generate corresponding modes in the output FMF. Figure 3-14 (a) gives the mode profiles for the LP_{01} and LP_{11} mode over a 10km FMF in the bar switch state. When the 0 and π phase shift pattern is projected by the SLM, the cross switch (LP_{01} to LP_{11} and LP_{11} to LP_{01}) is realized, see Figure 3-14 (b). At LP_{01} mode drop port, a reference output power is measured by a power meter when only LP_{01} mode in bar state and LP_{11} mode in cross state is excited in the MUX. Then the output power from the other mode is measured and the LP_{11} to LP_{01} mode crosstalk ratio can be determined with respect to the reference output power, as shown in Figure 3-13 (c). Mode crosstalk is measured in the case that the output power from the 10km FMF keeps the same as LP_{01} and LP_{11} mode is excited in the MUX individually. These measurements are repeated at 6 wavelengths over C-band. Due to the wavelength-dependence of modal characteristics, the LP_{11} mode will rotate slightly at different wavelengths, which influences the performance, especially in cross state. In the experiment, the SLM is optimized at 1537.40nm with the minimum θ , where the mode crosstalk ratios for both bar state and cross state are better than -10dB, see Figure 3-15. Around 3dB extra loss is observed for the cross state case.

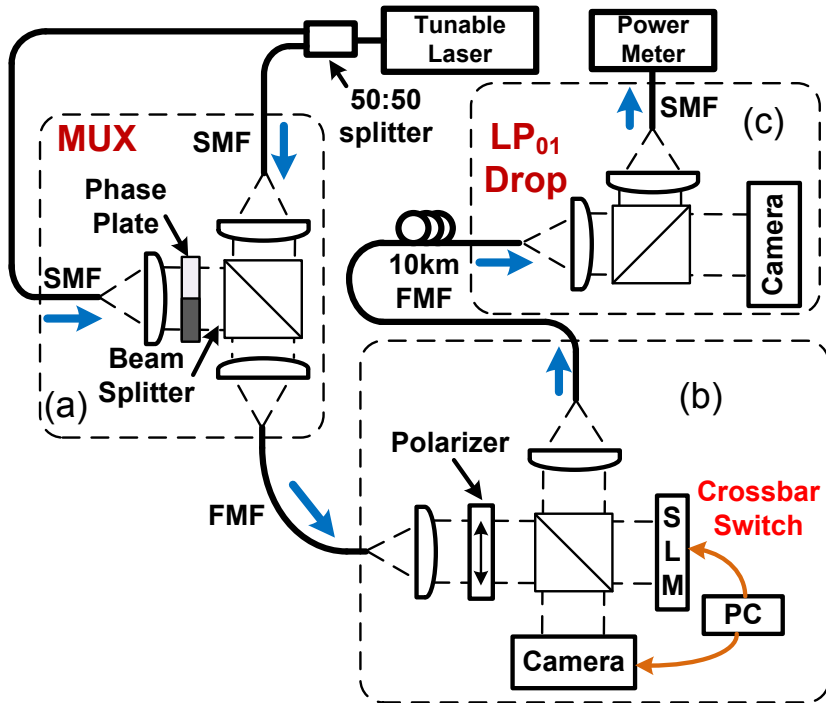


Figure 3-13 MDM link with a mode crossbar switch and LP_{01} mode drop: (a) MUX, (b) mode crossbar switch and (c) LP_{01} mode drop unit .

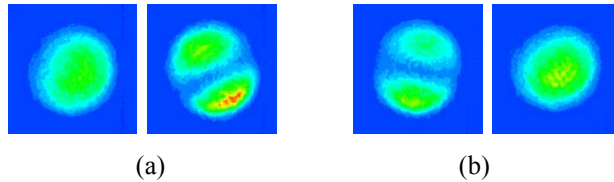


Figure 3-14 The field profiles of the LP_{01} and LP_{11} mode at LP_{01} mode drop unit: (a) bar state and (b) cross state realized by an SLM.

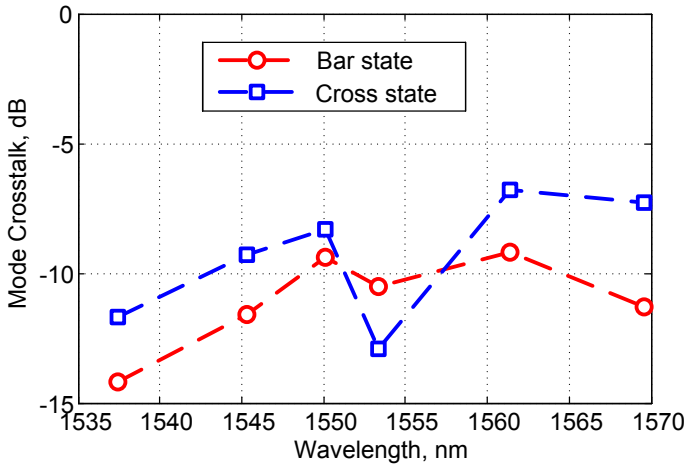


Figure 3-15 Measured mode crosstalk in dB at LP₀₁ drop port in both bar state and cross state versus different wavelengths

3.5 Summary

This chapter verified that binary phase plates are able to create optical fields, which can match fiber spatial modes. Therefore mode (de)multiplexing with high mode extinction ratio can be realized by the phase plated based mode coupler. In order to combine the spatially-tailored optical fields for excitation of different spatial mode, passive beam splitters are utilized in phase-plate mode couplers [47], which give the whole component in a large footprint. A compact mode DEMUX based on one multi-mode phase mask (MMPM) is proposed and demonstrated to separate different spatial modes. However, its scalability to a larger number of modes is still limited due to the diffraction losses from the superimposition of blazed gratings. Chapter 5 will describe another mode DEMUX based on a multi-segment phase plate with much lower insertion loss.

A mode crossbar switch is demonstrated in this Chapter for the first time. Using the SLM as a mode switch controller, the achieved mode crosstalk level is from -7dB to -15dB over a 35nm wavelength range. This crosstalk level exceeds the proposed -25dB threshold above which MIMO equalization needs to be applied to recover the signals [113], [114]. Otherwise, mode coupling will be induced by fiber non-circularity, material impurity and imperfect fiber splice [115] even though high mode extinction ratio can be achieved at mode MUX/DEMUX through selective mode excitation. Therefore, as pointed out in the introduction, wavelength crosstalk in WDM can be negligible while MDM exhibits severe linear crosstalk among parallel modes, which makes it

challenging and less interesting to add/drop a subset of modes at a network node.

In chapter 5, scalable spot-based mode couplers are researched which excite a linear combination of modes instead of pure fiber modes. Design complexity and insertion loss can both be dramatically minimized compared to the mode multiplexing solutions relying on selective mode excitation.

Chapter 4 Photonic Integrated Mode Coupler

This chapter focuses on the photonic integrated solutions for mode multiplexing, based on the publications [49], [50], [59] made during this Ph.D project. This chapter describes a Silicon-on-Insulator (SOI) based mode (de)multiplexer, employing grating couplers as vertical emitters to realize 2-dimensional top coupling. It is for the first time that MDM and WDM transmission over FMF is demonstrated with a photonic integrated mode multiplexer. A 45° vertical mirror based on Indium-phosphide (InP) platform is also investigated.

4.1 Silicon-on-Insulator Mode Coupler

To support high capacity MDM transmission, more optical components, such as lasers, modulators and photo-detectors, need to be employed in order to support multiple modes. In this case, photonic integration is advantageous as it enables more compact MDM transceivers at a lower cost. For the purposes of MDM, the mode multiplexing functionality needs to be integrated into a photonic integrated circuit. This integration avoids the inherent issues of bulky free-space optics and allows many optical components to be combined in a small area. Vertical coupling to MCFs based on a planar arrangement of grating couplers was demonstrated in [116]. An integrated mode coupler for a ring-core MMF using a circular coupler was introduced in [117]. In [97], the all-optical MIMO demultiplexing proposed in [118] was experimentally demonstrated. Compared to the previous works, the integrated mode couplers based on Silicon-on-Insulator (SOI) technology¹ described in this Chapter are suitable for typical solid-core FMFs guiding LP₀₁ and LP₁₁ modes. Moreover, the mode coupler can

¹ In the framework of ePIXfab set-up by CEA/LETI .

² With the help from Pinxiang Duan in the TU/e cleanroom.

selectively excite each mode with a high extinction ratio, thus it is able to decrease the complexity of the DSP at the receiver, especially for the case with large DGD [58].

In this section, mode selective excitation schemes: push-push for LP_{01} mode and push-pull for LP_{11} mode are analyzed. Mode coupling efficiency (CE) based on the proposed schemes is simulated and discussed. By implementing push-pull and center launch configurations to excite LP_{11} and LP_{01} mode, respectively, a photonic integrated mode coupler [49], [59] is experimentally demonstrated with three spatial modes in two polarizations encoded with 128-Gb/s 16QAM at four wavelengths for a total of 3.072Tb/s transmission over 30km of few-mode fiber.

4.1.1 Push-pull and push-push scheme

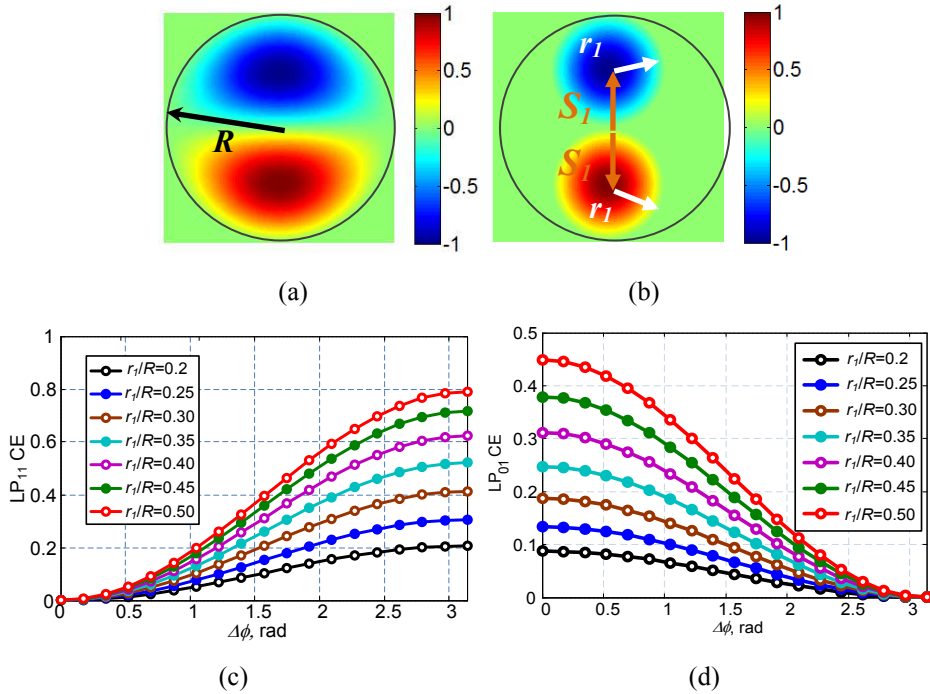


Figure 4-1 (a) LP_{11a} mode field; (b) a pair of spots with a phase difference of π ; (c) LP_{11} mode CE with the push-pull scheme at optimum spot offset versus spot radius r_1/R and $\Delta\phi$ and (d) CE for LP_{01} mode with a pair of spots as $s_1/R = 0.65$ versus r_1/R and $\Delta\phi$.

To selectively launch one specific mode with high CE and low crosstalk to the other modes, a field as similar as possible to that of the desired mode needs to be generated. Both the amplitude and phase of the generated field determine

the CE. The LP_{01} mode field is unipolar, and the LP_{11} mode has a bipolar field distribution, as shown in Figure 4-1 (a). The LP_{11a} and LP_{11b} mode fields are orthogonal, and rotated $\pi/2$ with respect to each other in the FMF's core cross-section area. In [49], a push-pull scheme was proposed to excite the LP_{11} modes where two Gaussian-like spots are used with a phase difference $\Delta\varphi$ of π , see Figure 4-1 (b). The CE can be quantified with an overlap integral:

$$CE = \frac{|\int E_{mode}^* \cdot E_{Launch} dA|^2}{\int |E_{mode}|^2 dA \cdot \int |E_{Launch}|^2 dA} \quad (\text{Eq. 4-1})$$

where E_{Launch} and E_{mode} are the electric fields of the mode coupler's launch field and fiber mode, respectively. A is the fiber cross-sectional area. The notation * indicates the complex conjugate. Figure 4-1 (c) gives the simulated LP_{11} mode CE at optimum offset $S_l/R=0.5$ versus the spot radius r_l/R and $\Delta\varphi$. It can be seen around 80% CE (<1dB loss) can be achieved by the push-pull scheme with optimum variables. When a pair of spots are in-phase, as in a push-push case, the flat phase-front of the LP_{01} mode can be matched, which results in a high CE of the LP_{01} mode [50]. Figure 4-1 (d) shows the simulated CE for LP_{01} as $S_l/R=0.65$ versus r_l/R and $\Delta\varphi$. As $\Delta\varphi = 0$, the CE for LP_{01} reaches the maximum. Therefore, depending on $\Delta\varphi$, a pair of spots can be used to selectively launch LP_{01} and LP_{11} mode.

To support the 3 spatial modes (the LP_{01} and two LP_{11} modes) simultaneously, the push-pull scheme was extended to a 5-spot design [49]. As shown in Figure 4-2 (a), a single spot with a radius of r_2 is placed in the center for LP_{01} excitation or detection. The LP_{01} mode CE versus r_2/R is shown in Figure 4-2 (b). 4 spots with the same radius of r_l are arranged in a ring with an offset of S_l . Two pairs of opposite spots driven with phase difference $\Delta\varphi = \pi$ are used for launching the two degenerate LP_{11} modes, respectively. To provide the space for the center spot, S_l is enlarged. Figure 4-2 (c) shows the simulated LP_{11} mode CE of a pair of spots with $S_l/R=0.65$ versus r_l/R and $\Delta\varphi$. Due to the fact that the launching fields and fiber modes are orthogonal, high mode extinction ratio can be achieved. With $r_l/R=0.29$, $r_2/R=0.36$ and $S_l/R=0.65$, negligible mode dependent loss can be achieved with CE around 29% (an optimum CIL of 5.3dB) for both modes.

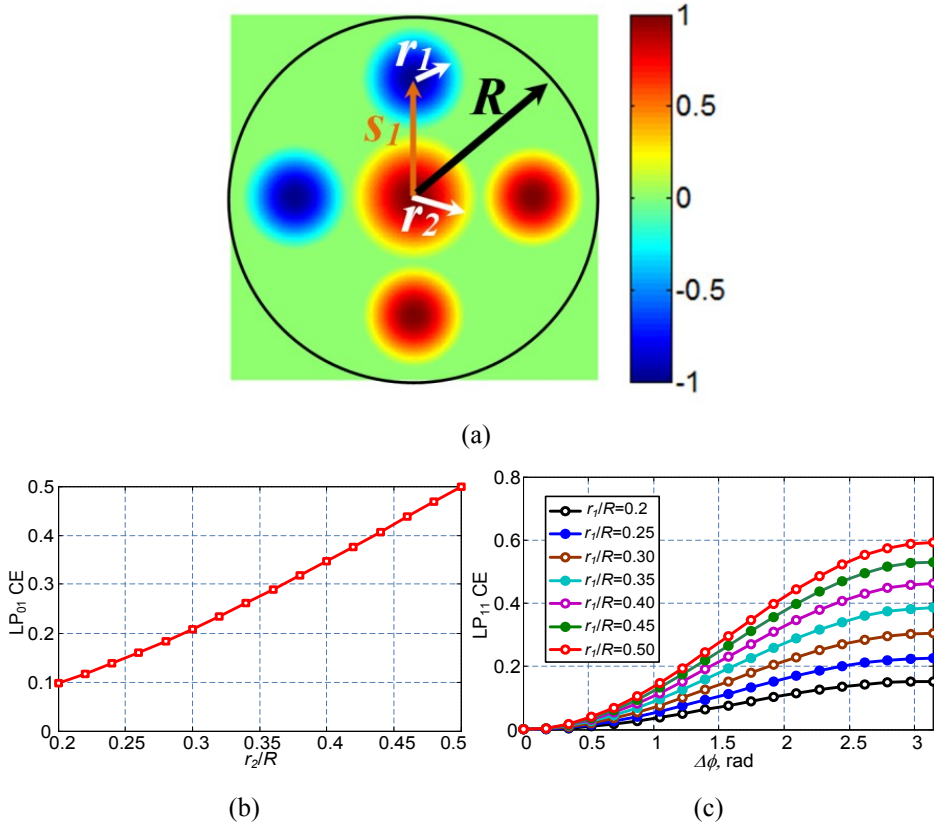


Figure 4-2 (a) The arrangement of 5 spots for LP_{01} and LP_{11} modes excitation with high mode extinction ratio; CE for (b) LP_{01} mode with the center spot versus r_2/R and (c) LP_{11} mode with a pair of spots as $s_1/R=0.65$ versus r_1/R and $\Delta\phi$.

4.1.2 Vertical coupler

Edge coupling with a spot-size convertor or lensed fiber, and top coupling with a grating coupler are the two dominant approaches for the coupling between SOI-based photonic integrated circuits and optical fibers. However, it is challenging for the facet coupling to stack multiple waveguide layers together with a small spacing to realize 2D coupling for SDM, especially for coupling into an FMF, where 2D patterns need to be positioned with micron accuracy. Top coupling provides more freedom for the 2D arrangement of vertical emitters. For the purpose of MDM, small grating couplers based on SOI are designed for coupling into FMFs without the use of imaging optics.

For adequate coupling of the multiple modes and their polarization varieties from the SOI chip into an FMF, vertical out-of-plane coupling is required. A chirped grating coupler with period $\Lambda = \lambda/n_{eff}$, where n_{eff} is the average effective index of the waveguide in the grating region can diffract the light vertically. However, the coupling efficiency into the fiber is low due to the large Bragg back-reflection. With the introduction of a linear chirp in the grating, a destructive interference between the diffracted fields by the front and rear surfaces of each rectangular slot can reduce the back reflection [119]. Two 2D vertical grating couplers with 5 periods varying from 640nm to 520nm (grating chirp parameter: $\Delta = 30\text{nm}$) and 6 periods varying from 640nm to 515nm ($\Delta = 25\text{nm}$) are designed. To improve the coupling efficiency, three rectangular shaped slabs ($0.15 \times 3.48\mu\text{m}$) with a spacing of 220nm are used as an end reflector at the back end of the grating couplers for both designs.

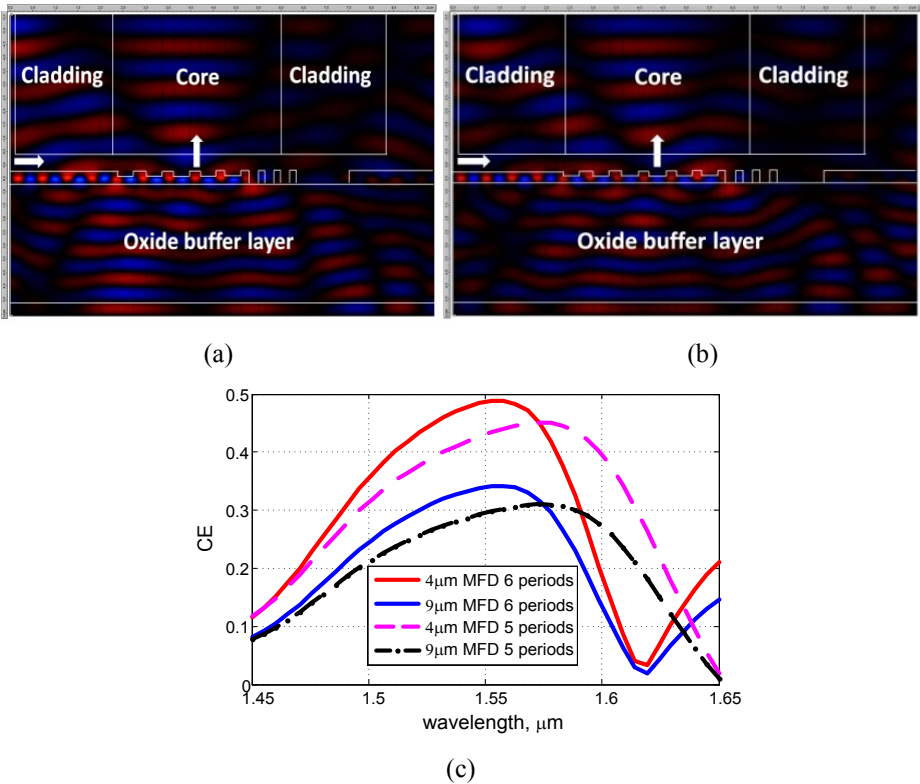
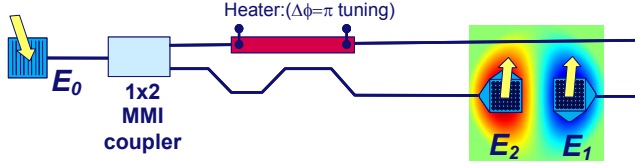


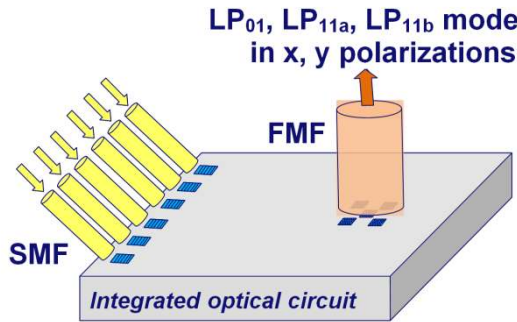
Figure 4-3 Diffracted fields from the designed small grating coupler with (a) 5 and (b) 6 periods; (c) simulated CEs versus wavelength for two designs.

Figure 4-3 (a) and (b) show the simulated field diffracted by the 5 and 6 periods chirped grating couplers, respectively. Figure 4-3 (c) shows the

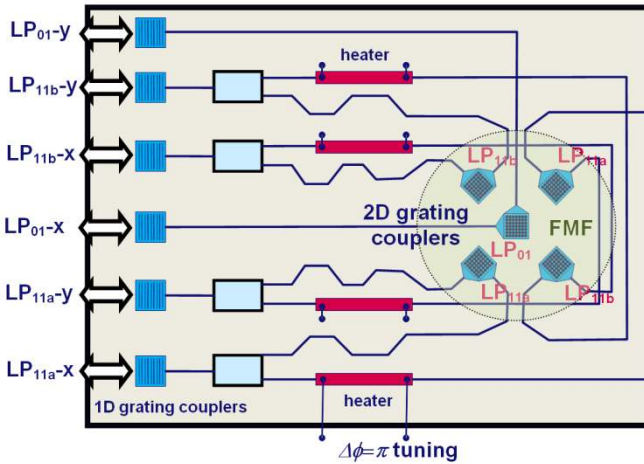
simulated CEs of the designed grating couplers with a Gaussian-distributed mode with a Mode Field Diameter (MFD) of $4\mu\text{m}$ or $9\mu\text{m}$ through the overlap integral between the radiation profile and the mode.



(a)



(b)



(c)

Figure 4-4 (a) Push-pull scheme realized by a pair of grating couplers for LP_{11} mode excitation; (b) circuit schematics and (c) input and output ports for multiplexing LP_{01} and LP_{11} modes

4.1.3 Circuit design

The push-pull scheme [49] was proposed to excite the LP_{11} modes, creating two Gaussian-like spots with a phase difference $\Delta\phi$ of π , since the LP_{11} mode has such a bipolar field distribution. As shown in Figure 4-4 (a), to create such a bipolar field for LP_{11} mode coupling, two 2D grating couplers are driven in a push-pull configuration with opposite phase. To further illustrate this concept, a full 6-channel integrated mode coupler is sketched in Figure 4-4 (b), where the center 2D grating coupler is for launching or detecting the LP_{01} mode. The mode coupler connects 6 individual SMFs through one-dimensional grating couplers to the five 2D grating couplers for FMF coupling, as shown in Figure 4-4 (c). The five small 2D vertical grating couplers, as shown in Figure 4-4 (c), excite 6 mode channels: the x- and y-polarization of the LP_{01} and of the degenerate LP_{11} modes (LP_{11a} and LP_{11b}).

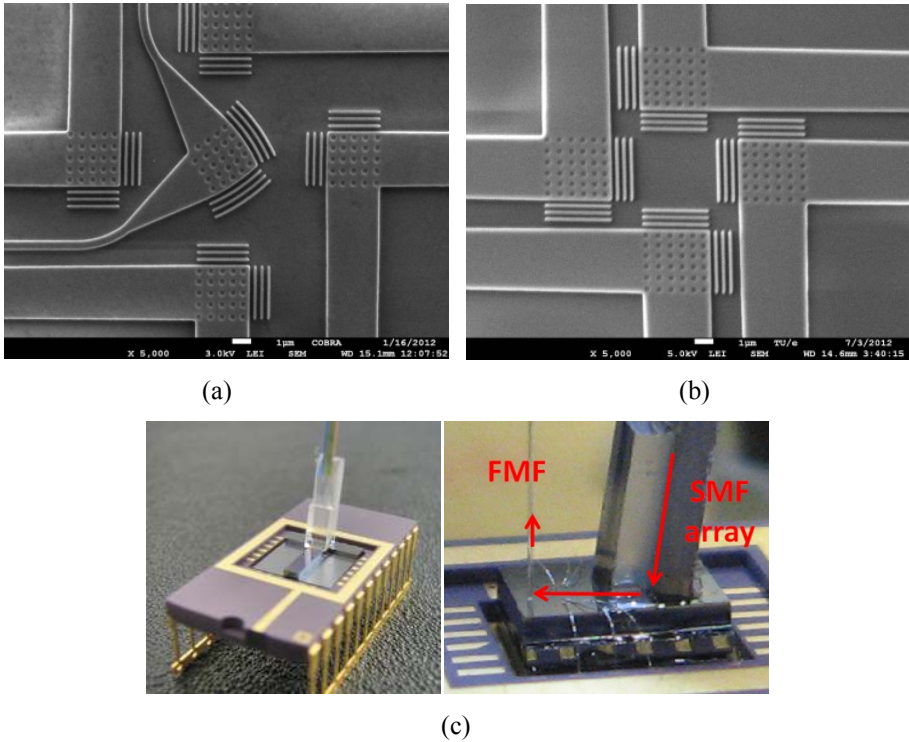


Figure 4-5 SEM pictures of the FMF coupling area with (a) five [49] and (b) four [50] vertical grating couplers; (c) pictures of the packaged integrated mode coupler.

SEM² pictures of the FMF coupling area with five [49] and four [50] vertical grating couplers are shown in Figure 4-5. An integrated mode coupler has been packaged with an SMF array for 6 SMF ports and wire-bonded to an electronic circuit, see Figure 4-5 (c)³.

4.1.4 Thermo-optic phase tuning

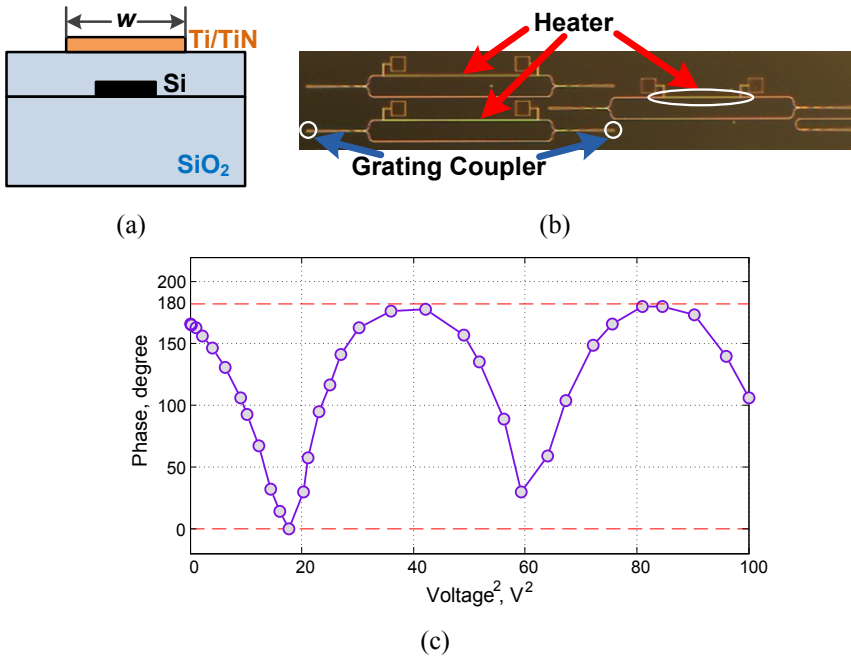


Figure 4-6 (a) Layer stack with a 2D heater; (b) Mach-Zehnder interferometer with a heater on one arm for characterizing thermo-optic phase tuners; (c) Thermo-optic phase tuning results versus applied voltage.

The layer stack of the SOI device consists of a 220nm thick silicon waveguide layer, buried in an isolation layer with a thickness of 600nm, as shown in Figure 4-6 (a), which is a compromise between optical losses induced by the Ti/TiN heater layer and thermal tuning efficiency. The thickness of the Ti/TiN layer is 110nm. The thermo-optic tuning effect is tested through measuring the output power when applying power to the heater which is above one arm of the MZI. The standard 1D grating couplers are utilized for optical coupling in and out. The resistance of a heater can be expressed as: $R = \rho L / Wt$, where ρ is the

² With the help from Pinxiang Duan in the TU/e cleanroom.

³ Device packaging was carried out by Dr. Brad Snyder in Tyndall national institute, Cork, Ireland.

resistivity, and L , W and t are the length, width and thickness of the heater, respectively. Mach-Zehnder interferometer with a heater with $W = 5\mu\text{m}$ and $L = 450\mu\text{m}$ on one arm is used for characterizing the thermo-optic phase tuners, as shown in Figure 4-6 (b). Figure 4-6 (c) shows the thermo-optic phase tuning results for the heater. 70nm shallow etching is used for the grating couplers.

4.1.5 Circuit characterization

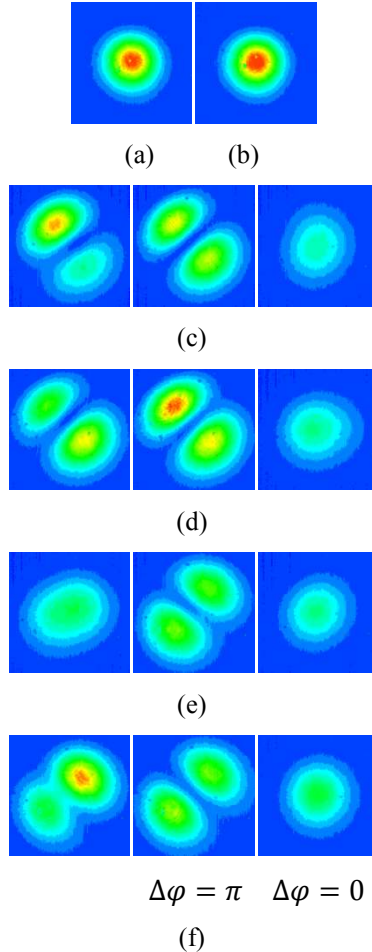


Figure 4-7 (a) LP_{01x} , (b) LP_{01y} , (c) to (f) push-pull launching cases by adding optical power into 4 LP_{11} mode input ports individually (left to right: without phase tuning, π and 0 phase difference).

A 3-meter long SI-FMF with a core size of $19.4\mu\text{m}$ is used to test the fabricated mode MUX. Figure 4-7 (a) to (f) show the launched mode profiles when adding optical power into each SMF input port individually. It shows that the grating coupler pair can selectively launch LP_{01} or LP_{11} modes with different phase differences through the heater tuning. Figure 4-8 (a) shows the insertion losses versus wavelength for all 6 channels when the chip is used as a mode MUX. 20dB insertion loss for the LP_{01} mode is achieved. The insertion loss for a SMF-to-SMF loop involving two 1D grating couplers is plotted as a blue curve in Figure 4-8 (a). The coupling loss from an SMF to an on-chip wavelength via a 1D grating coupler is around 4dB. Besides on-chip losses, extra loss comes from the grating coupler design with few periods (only 5 periods in our case) of the small vertical grating coupler. This lowers the light diffraction efficiency of the grating and thus induces a quite high loss. Due to the limited space, the large spacing between 2 grating couplers, see Figure 4-6 (a), causes more loss for LP_{11} mode excitation than the LP_{01} mode excited by the center grating coupler, as analyzed in Chapter 4.1.1. This loss issue can be nicely solved with the use of larger grating couplers and imaging optics, which collimate beams into the FMF.

To characterize the chip as a mode DEMUX, a bulky phase plate based mode-multiplexing setup is used [47]. 30dB total link loss for LP_{01} mode is achieved (from the input of the phase plate based MUX to the integrated DEMUX's output), as shown in Figure 4-8 (b). Besides the 8.2dB loss from the MUX [47] and the loss from the SOP mismatch between the center 2D grating coupler and the input LP_{01} mode, the loss of the chip is around 20dB, which is the same as a mode MUX. Moreover, it has been demonstrated that a pair of grating couplers can also selectively detect LP_{01} and LP_{11} modes with a mode extinction ratio of more than 20dB as low mode coupling happens in the FMF. With strong mode coupling, heaters are not necessarily needed in demultiplexing, but in that case, MIMO compensation is inevitable for data recovery.

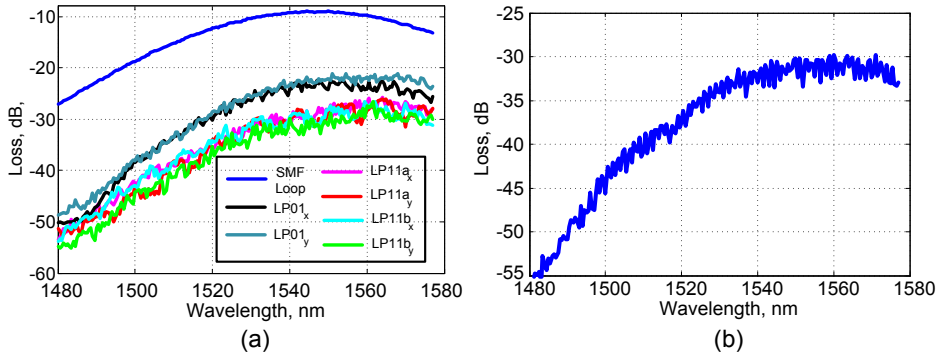


Figure 4-8 (a) Insertion losses for LP₀₁ and LP₁₁ modes versus wavelength when the chip is used as a mode MUX; (b) Total loss for detecting LP₀₁ mode with the center 2D grating coupler.

The length difference between the two waveguide arms after the splitter to feed light to a pair of 2D grating couplers in diagonal positions should be small enough to prevent Mach-Zehnder Interferometer spectral filtering effects and thus provide a sufficiently wide spectral operation range. E.g., for a free spectral range (FSR) $\gg 10\text{nm}$ (1.33THz) at $\lambda=1.5\mu\text{m}$, with an effective waveguide refractive index $N_{\text{eff}}=3.5$, a length difference $\Delta L < 64\mu\text{m}$ needs to be satisfied.

4.1.6 High-order mode excitation

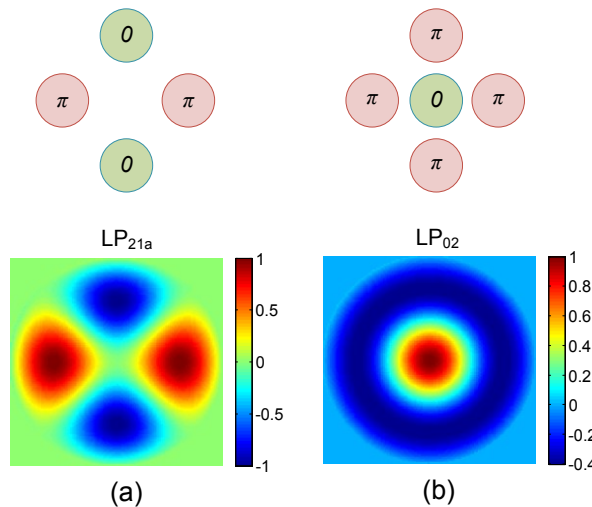


Figure 4-9 Using 5-spot arrangement to excite (a) LP_{21a} and (b) LP₀₂ mode.

The proposed structure with five 2D grating couplers can support other high-order modes, e.g., one of two degenerate LP_{21} modes and LP_{02} mode with high spatial overlapping efficiency [47]. As 4 outer grating couplers satisfy the π phase difference, the output field profiles can nicely overlap with the profile of the LP_{21a} mode, see Figure 4-9 (a). To generate the LP_{02} mode, shown in Figure 4-9 (b), the outer grating couplers need to deliver the same phase, but with π phase difference with the center one. Limited by the number of grating couplers, it is challenging to excite the LP_{21a} and LP_{21b} modes simultaneously.

4.1.7 3-mode FMF

Figure 4-10 shows the experimental setup for MDM combined with WDM transmission utilizing the integrated mode coupler as a mode MUX⁴. The -3dB wavelength bandwidth of the integrated mode coupler is larger than 40nm, which can cover the entire C-band [49]. To verify the broad bandwidth performance of the integrated mode coupler, four external-cavity lasers (ECLs), operating at 192THz to 195THz with a 1THz frequency spacing (about 8nm) are passively combined and modulated by a $LiNbO_3$ IQ-Modulator driven by two digital-to-analog convertors (DACs) operating at 32Gbaud. The DACs drive the IQ-modulator with QPSK or 16QAM symbols. Unlike the standard way of emulating PDM through a polarization beam combiner (PBC) with a delay line, the signal is directly split via 6 different delay lines to cancel correlation into six tributaries, which are amplified and fed into the six input ports of the integrated mode coupler, where the 2D grating coupler has the ability to combine orthogonal polarizations as the PBC. In order to maximize the fiber-to-chip efficiency, an inline polarization controller (PC) is used to tune the SOP of the optical signal entering the 1D grating coupler. The delays with respect to the $LP_{11a/y}$ port for decorrelating the tributaries are denoted in Figure 4-10.

⁴ The measurements were carried out with the helps from Vincent Sleiffer, Dr. Yongmin Jung and Dr. Maxim Kuschnerov in Coriant GmbH, Munich, Germany.

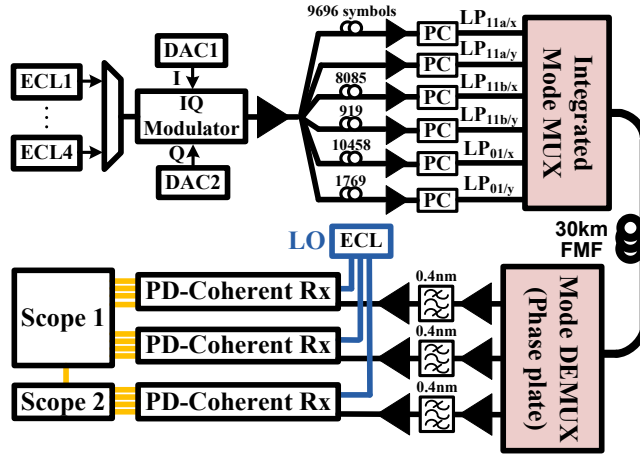
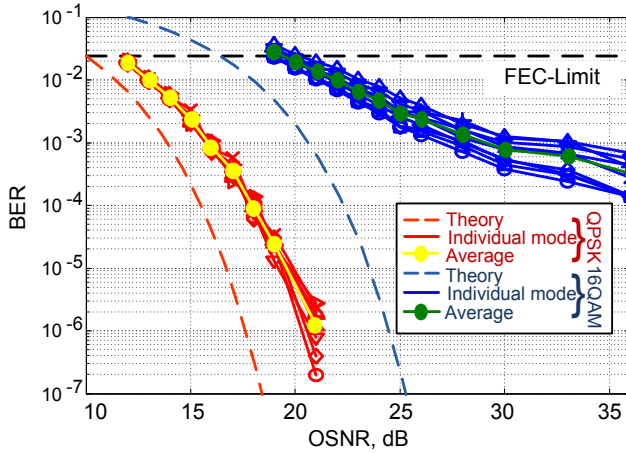


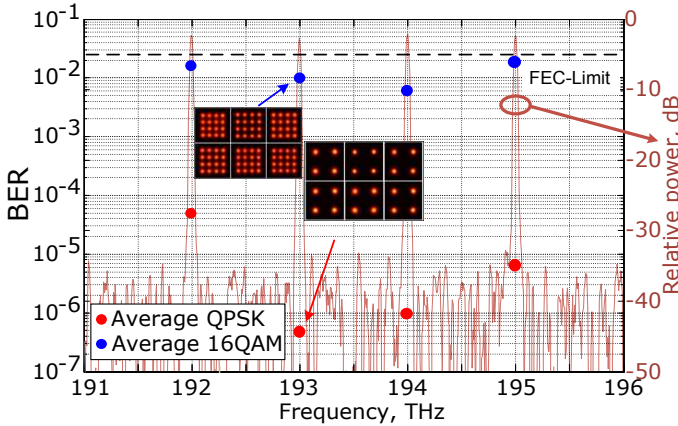
Figure 4-10 Experimental setup for MDM and WDM transmission.

A 10m SI-FMF with a core diameter of $19.4\mu\text{m}$ is coupled to the output of the integrated mode MUX and then spliced with a 30km low DGD GI-FMF (DGD = 0.06ps/m , dispersion = $20\text{ps/nm}\cdot\text{km}$, LP_{01} and LP_{11} attenuation = 0.191dB/km and 0.198dB/km , respectively) with a core diameter of $11\mu\text{m}$. Negligible splice losses between two FMFs with different core sizes is observed. After a phase plate based mode DEMUX, the signals at the measured wavelength are selected by three 0.4nm optical tunable filters and sent into three PDM coherent receivers. A tunable ECL is also tuned to the measured wavelength and used as local oscillator (LO). The 12 electrical signals are captured by two time-synchronized digital real-time oscilloscopes sampling at 40GS/s and 50GS/s . The captured data are processed offline with 6×6 MIMO based DSP to recover all the signals. After resampling and removing receiver imperfections, CD compensation is performed and the start of the frame is determined by a correlation technique[120]. Subsequently a 6×6 DA time-domain equalizer is used to determine the channel impulse response employing 401 T/2 spaced taps, using 100,000 symbols for convergence and leaving 500,000 symbols (2 million bits per spatial and polarization mode) for bit-error counting. A 20% forward error correction (FEC)-overhead is assumed which gives an FEC-limit at a BER of 2.4×10^{-2} . Figure 4-11 (a) shows the back-to-back (through 10m of SI- FMF) BER for all 6 mode-channels and the average BER versus the optical signal noise ratio (OSNR) with QPSK and 16QAM modulation formats, where red and blue solid lines represent the 6 individual mode-channels. Figure 4-11 (b) shows the frequency spectrum and BERs for the transmission with 4 WDM channels. The recovered 16QAM and QPSK constellations for all mode-channels at 193THz are also given in Figure

4-11 (b). The insertion loss of the integrated mode coupler is around 20dB and 25dB for coupling to LP_{01} and LP_{11} modes respectively. After transmission over 30km FMF and passing through the mode DEMUX, the received powers approach the noise limits of the optical amplifiers, which results in average BERs for 128-Gb/s 16QAM transmission being close to the FEC-limit due to the high OSNR requirement [20].



(a)



(b)

Figure 4-11 (a) BER versus OSNR after back-to-back transmission and (b) frequency spectrum and BER (red and blue dots) for 4 WDM channels after 30km FMF transmission.

4.1.8 PBGF

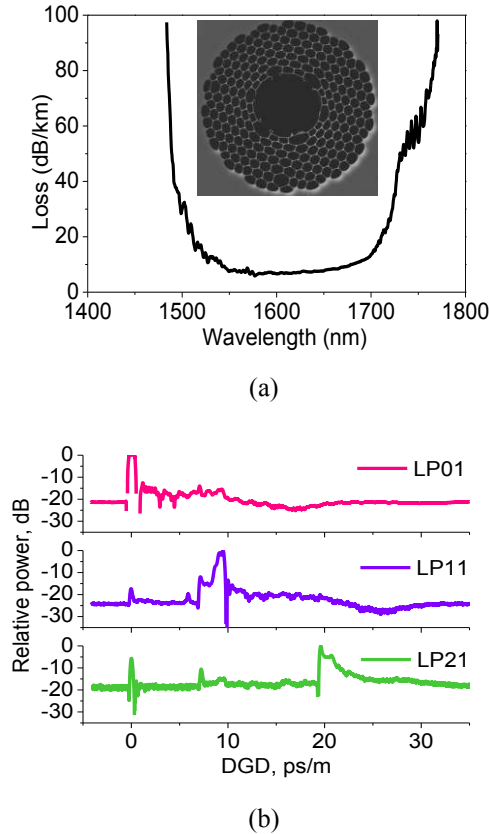


Figure 4-12 (a) Transmission loss spectrum and SEM picture of the 19c HC-PBGF and (b) time-of-flight measurement for pure LP₀₁, LP₁₁ and LP₂₁ mode.

Hollow-core photonic bandgap fiber (HC-PBGF) is proposed as a transmission medium with lower nonlinearity compared to solid core fibers so that it has the advantage to significantly relax the capacity limitation resulting from fiber nonlinearities [121], [122] and potentially lower loss in 2000nm. HC-PBGF guides the light in the central air core, which is surrounded with a regular lattice of air holes to generate a photonic bandgap. The dominant loss in the HC-PBGF comes from surface scattering [121], induced by the overlap of the fiber modes with the air-glass interface. A 19-cell thin-core-surround HC-PBGF design is able to decrease significantly the surface scattering. Figure 4-12 (a) shows the transmission loss spectrum and SEM picture of the fiber, manufactured by Optoelectronics Research Centre at University of Southampton. It has a -3dB bandwidth larger than 120nm with a minimum loss of 5.86dB/km. Figure 4-12

(b) shows the results of a time-of-flight measurement [122] for pure LP_{01} , LP_{11} and LP_{21} modes⁵. The DGD between LP_{01} and LP_{11} modes is around 9ps/m, which is larger than the typical DGD in solid core fiber FMF (i.e. 0.04ps/m for a 3-mode fiber) and results in 1.7ns modal delay after 193m transmission.

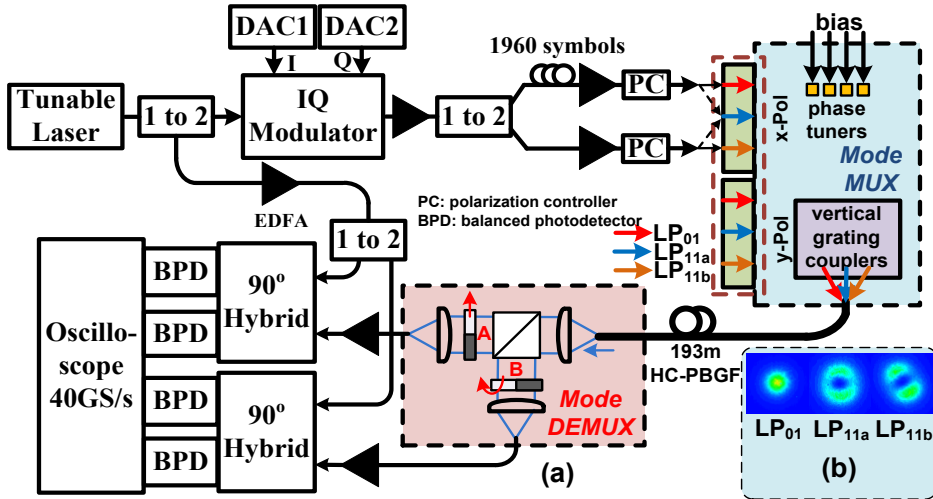


Figure 4-13 (a) Transmission setup, and (b) mode profiles for LP_{01} , LP_{11a} and LP_{11b} modes.

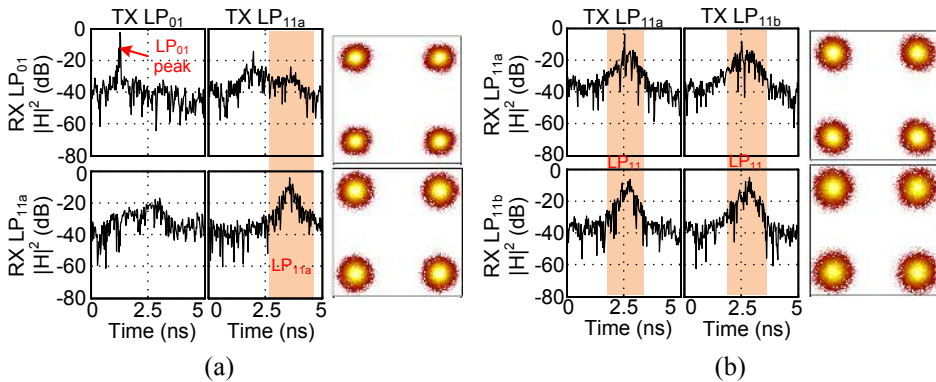


Figure 4-14 Equalizer taps (left) and constellations (right) after transmission for (a) LP_{01} and LP_{11} modes, and (b) LP_{11a} and LP_{11b} .

⁵ The results in Figure 4-12 are provided by Dr. Yongmin Jung, Optoelectronics Research Centre (ORC), University of Southampton, UK.

To characterize the performance of the SOI mode coupler for HC-PBGF transmission, a transmission link ($2 \times 20\text{Gbps}$ QPSK⁶) supporting two modes is established as shown in Figure 4-13. At the mode DEMUX side, binary phase plates are employed for separating two different modes for analysis. Depending on the transmitted modes, the phase plate at port A is inserted or taken away to select the LP_{01} or $LP_{11a/b}$ mode and the one at port B is rotated by 90° where appropriate to select the corresponding LP_{11} mode, see the DEMUX block in Figure 4-13 (a). Figure 4-13 (b) shows the mode profiles for the 3 spatial modes. The equalizer taps after convergence and constellations for the transmission of LP_{01} and LP_{11} , and degenerate LP_{11} modes (LP_{11a} and LP_{11b}) are given in Figure 4-14 (a) and (b), respectively. Robust transmission can be seen for both cases from the QPSK constellations. A sharp peak for LP_{01} mode and a wide plateau for LP_{11a} mode can be observed in Figure 4-14 (a) with a separation in time scale due to the existence of DGD. For two LP_{11} modes transmission, the DGD of the degenerate LP_{11} modes is negligible, as shown in Figure 4-14 (b). The wide plateau of the equalizer taps for LP_{11} modes may come from a large distributed mode coupling between the LP_{11} modes [123], which can also be observed in Figure 4-14 (b).

4.2 InP-based 45° Vertical Mirror

This section extends the mode coupler solutions with high mode extinction ratio as presented in [49], [50] for supporting four LP modes: LP_{01} , LP_{11} , LP_{21} and LP_{02} . In the view of spatial modes, there are in total 6 modes which each can have 2 polarization states. It translates into 12 MDM channels.

⁶ The measurements were carried out in TU/e with the helps from Roy van Uden in DSP and Dr. Chigo Okonkwo in coherent transmitters and receivers.

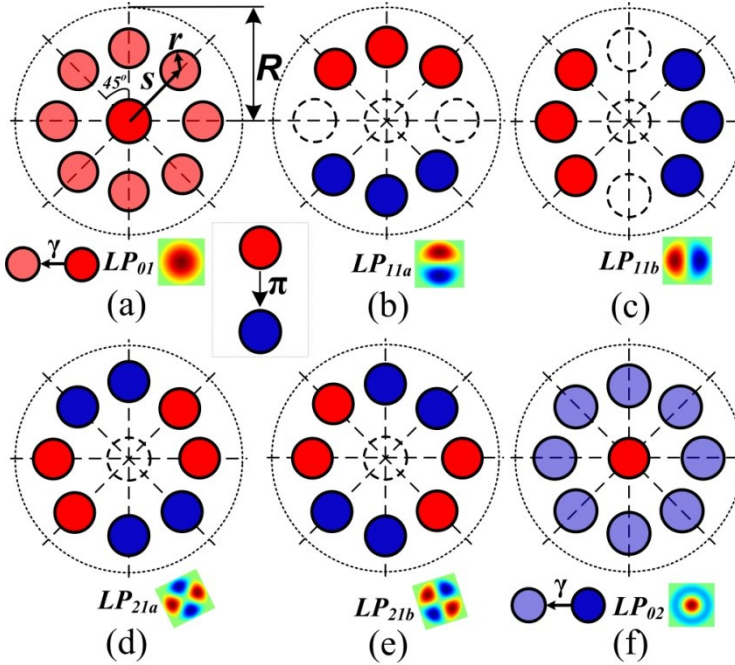


Figure 4-15 The arrangement of spots for exciting different spatial modes with high mode extinction ratio.

Figure 4-15 (a)-(f) illustrate the arrangement of 9 spots for exciting each spatial mode. R is the radius of the FMF. All spots have a radius of r and 8 spots are uniformly distributed along a circle with a radius of S . The push-pull scheme proposed in [49] is utilized to launch LP_{11} (see Figure 4-15 (b) and (c)) and LP_{21} modes (see Figure 4-15 (d) and (e)). Unlike the 6-spot arrangement used by a spot coupler [57], by using more spots, a high mode extinction ratio is achieved at the same time with excellent mode coupling efficiency. Due to the circular symmetry of LP_{01} and LP_{02} modes, large mode coupling might happen with improper launching conditions. Through properly positioning the spots and allocating different powers to the center spot and the outer 8 spots, see Figure 4-15 (a) and (f), the mode profiles of LP_{01} and LP_{02} can be nicely matched, which gives high coupling efficiency and low mode crosstalk. In LP_{01} launch condition, the simulated coupling efficiency (CE) for LP_{01} and LP_{02} mode can be seen in Figure 4-16 (a) and (b), respectively with $\alpha = 0.28$. α and β are defined as:

$$\alpha = r/R \quad (\text{Eq. 4-2})$$

$$\beta = S/R \quad (\text{Eq. 4-3})$$

Each spot arranged in the outer ring has an intensity, which is γ ($\gamma < 1$) times the intensity of the center one. The CE is calculated by using (Eq. 4-1). It can be seen in Figure 4-16 (a), as $\beta = 0.6$ and γ is around 0.4, larger than 60% LP_{01} mode CE is achieved and meanwhile the crosstalk in LP_{02} is negligible. The same case can be seen in LP_{02} launch condition as shown in Figure 4-16 (b). Figure 4-16 (c) and (d) show the CE for LP_{11a} and LP_{21a} modes with corresponding launch conditions, where all the spots have the same power level. It can be seen that at $\beta = 0.6$ and $\alpha = 0.28$, 6 spatial modes can be selectively excited with around 60% efficiency, which means less than 2.3dB coupling loss and better than -40dB mode crosstalk to the others modes due to the mode orthogonality.

For simultaneously exciting all modes, optical splitters, phase shifters and combiners are needed to feed each spot with the combined optical signals where each one has the proper power and phase, as illustrated in Figure 4-15. To guarantee the high mode extinction ratio, optical fibers or waveguides which deliver the light to the spots cannot couple with each other. Low crosstalk even at small gaps can be achieved for optical waveguides with high core-cladding index contrast. Moreover, premium optical splitter/combiner and phase tuner structures have been demonstrated in InP-based photonic integrated circuits [124].

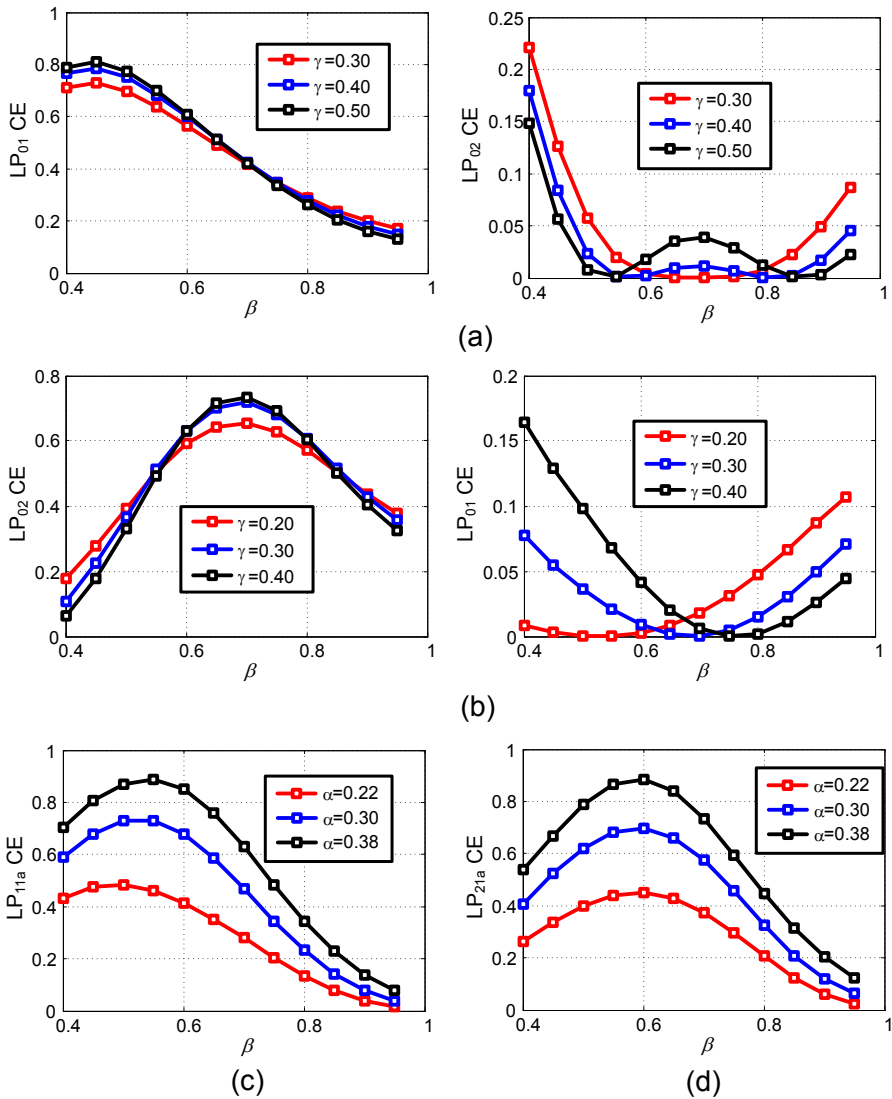


Figure 4-16 Coupling efficiency (CE) for different LP modes.

To implement the layout shown in Figure 4-17 (a) into an InP-based photonic integrated device, a 45° vertical mirror is proposed for realizing the top coupling. Figure 4-17 (a) shows the schematic of the total internal reflection, (TIR) of the 45° mirror which happens at the slanted boundary of the InP and air [125]. To reduce the loss from Fresnel diffraction at the top, anti-reflection (AR) coating can be applied. The mirror etching process is done through a Focused Ion Beam

(FIB) technique⁷. Different currents are used for the first raw etching step with a round scan to speed up the whole process and the second fine etching with a line scan for smoothing the mirror's surface. The depth of etch is set to $6\mu\text{m}$ and total time for the FIB etching is around 20 minutes. SEM images of the fabricated 45° vertical mirrors can be seen in Figure 4-17 (b).

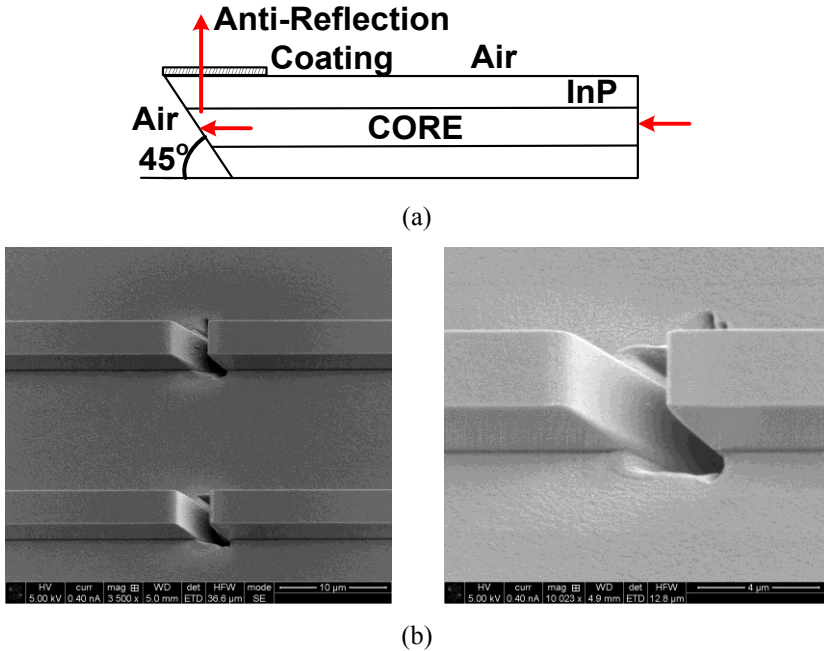
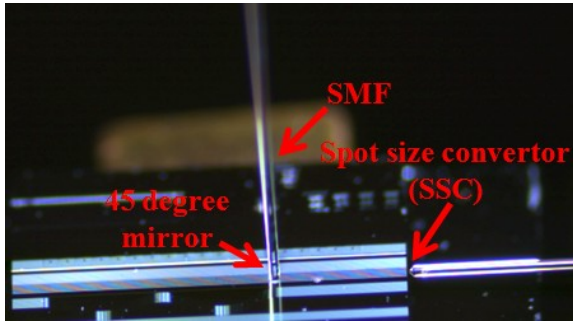


Figure 4-17 (a) Schematic of the TIR of the 45° mirror in an InP waveguide and (b) SEM images of fabricated 45° mirrors.

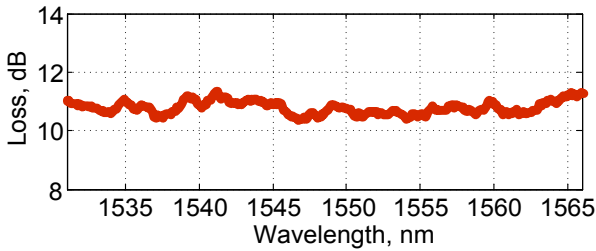
A waveguide structure with a width of $4\mu\text{m}$ as introduced in [126] is utilized for etching the 45° mirror. Figure 4-18 (a) gives the picture of the test setup where an SMF is placed vertically to catch the light from the mirror. The fiber-to-fiber insertion loss is around 11dB, see Figure 4-18 (b), which includes 1.5dB coupling loss from the Spot Size Converter (SCC) and 0.5dB waveguide loss. Therefore, the coupling loss from the vertical mirror to an SMF is less than 9dB, where 1.5dB (30%) loss is coming from the Fresnel reflection since no AR coating is utilized for the top boundary between the InP waveguide and air. It can be seen in Figure 4-18 (b), without the bandwidth limitation from a periodic structure as in the SOI grating coupler [49], the 45° mirror has a large -3dB

⁷ With the helps from Dr. Beatriz Barcones Campo and Barry Smalbrugge in the TU/e cleanroom.

wavelength bandwidth. The power variation in the mirror coupling test is less than 0.5dB when changing the SOP. Therefore the vertical mirror is able to support orthogonal polarizations for PDM. With an optimized design of the waveguide's layer stack and the usage of the AR coating, low-loss 45° vertical mirror based mode coupler can be achieved for implementing the spots' arrangement shown in Figure 4-15.



(a)



(b)

Figure 4-18 (a) Test setup for the vertical mirror top coupling and (b) SMF-to-SMF coupling loss with the vertical mirror versus the wavelength.

4.3 Summary

In this chapter, photonic integrated mode couplers were explored. It is for the first time that 3 spatial modes (LP_{01} and $LP_{11a/b}$ modes) MDM and WDM combined transmission over 30km FMF was demonstrated with a total capacity of 3.072Tb/s employing an SOI mode coupler. The 2D grating couplers based on SOI platform and FIB etched 45° vertical mirror based on InP platform were both investigated for the interface between a photonic integrated device and FMF, where 2D top coupling is required.

Selective mode excitation was realized on the SOI mode coupler with a structure of five 2D vertical grating couplers through push-pull scheme and center launch for LP_{11} and LP_{01} mode excitation, respectively. Vertical emitters for 2D top coupling can also be arranged in a more scalable structure as spot-base couplers [118], [127]. In this case, fewer vertical emitters need to be used.

In order to make the photonic integrated mode coupler as a practical mode multiplexing solution, coupling loss from the chip-to-FMF interface needs to be further minimized below 2dB. In this case, considering its advantages such as mass production and dense components integration, an integrated mode coupler is able to compete with other low-loss mode coupler solutions, such as the spot coupler and photonic lantern, which will be discussed in detail in Chapter 5 and 6, respectively.

Chapter 5 Spot-based Mode Coupler

This chapter introduces spot-based mode couplers, which are based on the publications [53], [56], [54] carried out during Ph.D project. Spot-based mode couplers are advantageous to achieve lower MDL and CIL, compared to the ones using selective mode excitation. Chapter 5.1 describes a prism-based 3-spot coupler solution, with which high capacity MDM transmission over a 120km FMF link is demonstrated. Chapter 5.2 demonstrates a 3D Waveguide (3DW) based 3-spot coupler, which is verified as a mode DEMUX in an all-FMF recirculating loop based MDM link. Chapter 5.3 investigates multi-segment phase masks, which are scalable and have a lower insertion loss than the multi-mode phase mask (MMPM) introduced in Chapter 2.

5.1 Prism-based Spot Coupler

5.1.1 3-spot mode coupler

This section is based on the publications [53], [128]. As a scalable mode (de)multiplexing solution, a spot-based mode coupler was proposed in [57]. Considering the fact that mode coupling is inevitable during propagation over the fiber and can be easily induced by bends, twists and structural defects randomly occurring along the fiber, spot-based mode couplers are practical for real applications.

A 3-spot coupler can realize mode (de)multiplexing for three spatial modes: LP_{01} , LP_{11a} and LP_{11b} . Figure 5-1 (a) shows the arrangement of the three Gaussian-like spots, where R is the radius of the FMF core which guides three spatial modes. Variables r and s are spot radius and offset respectively. To investigate the performance of the mode coupler, (Eq. 1-7), (Eq. 1-8) and (Eq. 1-14) are used for MDL and CIL calculations. Numerical simulation results in order to access the attainable CIL and MDL with spot size and offset scanning are shown in Figure 5-4 (b). As $r \approx 0.5R$ and $s \approx 0.5R$, $MDL = 0.6dB$ and $CIL = 2.1dB$ can be achieved for an SI-FMF with $R = 19.5\mu m$ and a

normalized frequency of $V = 3.83$. Three optical spots as analyzed need to be arranged as closely as possible in order to achieve the optimum coupling performance. The spot arrangements for more modes are illustrated in Chapter 1, see Figure 1-11.

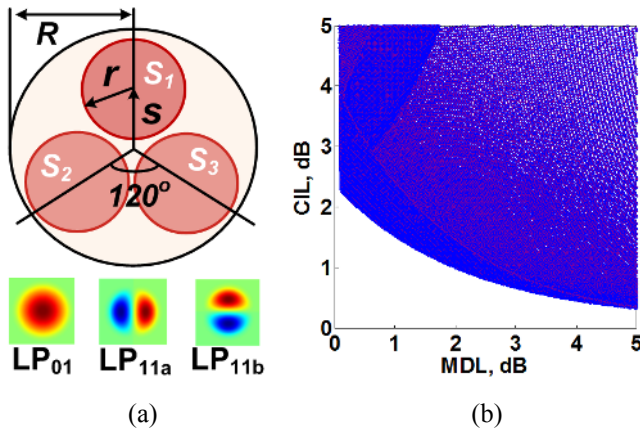


Figure 5-1 (a) 3-spot arrangement; (b) region of attainable CIL and MDL with spot size and offset scanning.

5.1.2 Coupler design

A number of promising MDM transmission systems based on spot-based mode couplers have been demonstrated recently, where free space [52], [53], [56], [129], [130] and photonic lantern [16], [55], [66] based solutions were employed. Free-space solutions using mirrors with sharp edges [52] or a 3-surface prism with small bevels [53] share the same purpose, namely to arrange three closely spaced beams in an equilateral triangular shape. Compared to the solution using separate mirrors, as shown in Figure 5-2, the single prism solution uses fewer optical components and high-precision manipulators.

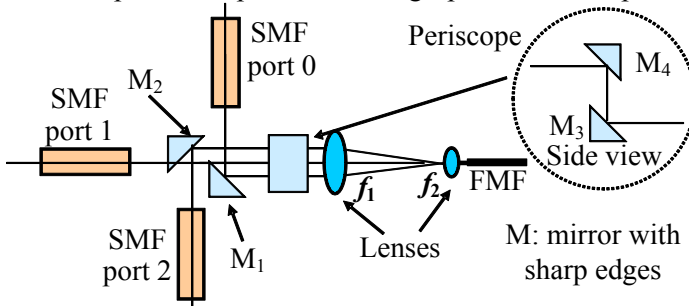


Figure 5-2 3-spot mode coupler using mirrors with sharp edges [52].

The schematic diagrams of the 3-surface prism based spot coupler are shown in Figure 5-3. As shown in Figure 5-3 (a), two vertical surfaces of the prism are perpendicular with each other and the top surface is 45° with respect to the vertical. In order to ensure the optimal injection with optical beams along the optical axis, a telecentric lenses setup composed of two lenses with focal length of f_1 and f_2 are utilized to image the three spots into the FMF, as shown in Figure 5-3 (d). P_1 represents the plane where the beams are combined by the prism. Optical beam offset and tilt can be checked in P_2 . P_3 is the plane of FMF input facet. Figure 5-3 (e) shows the captured FMF output fields launched by the individual spot. A ray tracing model of the 3-spot coupler with telecentric lenses is established in ZEMAX. The Gaussian beam waist D in P_1 is assumed to be $600\mu\text{m}$. Two commercial lenses with focal length of $f_1 = 200\text{mm}$ and $f_2 = 2.75\text{mm}$ are used for the ray tracing simulation. With varying F , which is the offset of the beam (see Figure 5-3 (c)), the normalized field intensity distribution of the corresponding optical beam in P_2 is shown in Figure 5-4. It can be seen that when $F=300\mu\text{m}$, the radius and offset of the beams, illuminating the FMF, are close to the optimum values for a SI-FMF with a core diameter of $19.4\mu\text{m}$ as analyzed. In this thesis, the Gaussian beam radius is defined as the radial value where the field intensity drops to $1/e^2$ of the maximum. Due to the demagnification, the spot offset F gives trivial influence to the performance of the coupler. As shown in Figure 5-4, a spot with $100\mu\text{m}$ offset in P_1 (i.e. $F = 200\mu\text{m}$ or $F = 400\mu\text{m}$) only induces a small offset in P_3 . The telescopic setup adjusts the 3 optical beams propagating along the optical axis and minimizes the influence from beam tilt. Figure 5-5 gives the normalized field intensity distribution of the three combined Gaussian beams ($F=300\mu\text{m}$ and $D=600\mu\text{m}$) in P_1 , P_2 and P_3 , respectively, as one beam is tilted with 0.01rad . The spot shift (indicated by a red arrow) caused by the beam tilt can be clearly observed in Figure 5-5 (b), which provides the instruction about how to adjust the angle of the input port through a tilt stage. The positions of the 3 spots at FMF input facet after the telescopic setup is shown in Figure 5-5 (c), where 3 spots are nicely positioned in an equilateral triangular structure. This demonstrates that the 3-spot coupler is insensitive to a small beam tilt. Note that, for simplification, the divergence of the Gaussian beams is not considered in ZEMAX simulations.

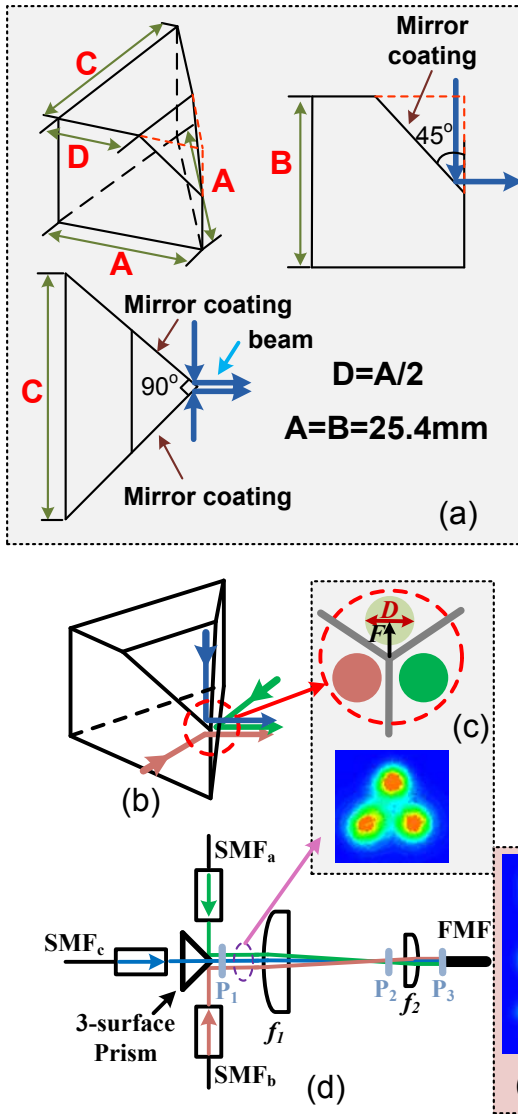


Figure 5-3 (a) Drawing of the customized prism; (b) the 3-surface prism for combining 3 optical beams; (c) image of the 3 combined optical beams; (d) the setup of the 3-surface prism based 3-spot mode coupler and telecentric lens system and (e) FMM output fields launched by different spots.

The bevels of the prism influence the attainable spacing between the spots, see Figure 5-3 (c). For the manufactured prisms⁸, the width of bevels is controlled to less than $10\mu\text{m}$, which is much smaller than the diameter of the collimated Gaussian beams ($600\mu\text{m}$). The tested CILs of the 3-spot mode coupler as a mode MUX and DEMUX is 3.9dB and 2.8dB, respectively for an SI-FMF with a core diameter of $19.4\mu\text{m}$. For a GI-FMF with a core diameter of $11\mu\text{m}$, which is used as the transmission fiber in this section, the CIL is 3.7dB and 3.5dB for mode MUX and DEMUX, respectively. The difference in CIL between MUX and DEMUX may mainly come from the different divergence of different FMF modes.

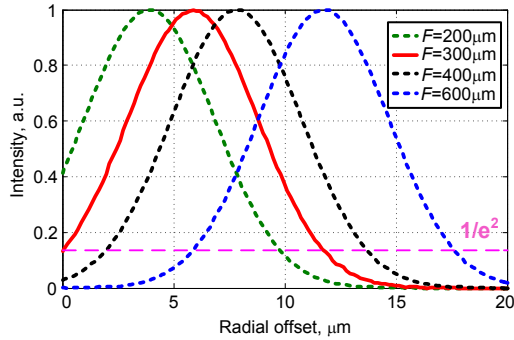


Figure 5-4 Normalized field intensity distribution of the modified beam in plane P_3 with the variation of F in plane P_1 (for $D=600\mu\text{m}$).

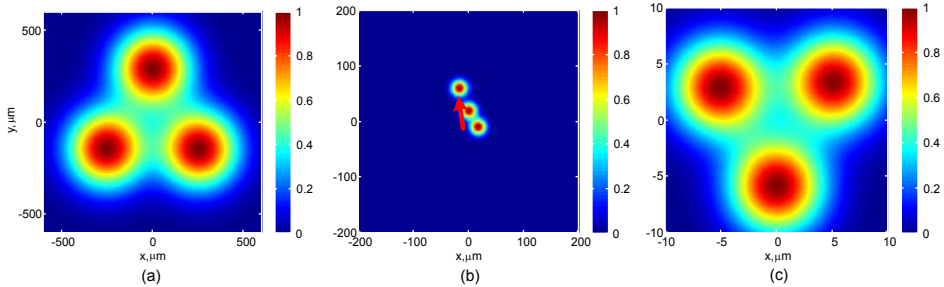


Figure 5-5 (a)-(c) Normalized field intensity distribution of three combined optical beams in P_1 , P_2 and P_3 , respectively.

⁸ The designed 3-surface prisms were fabricated by Wuhan Union Optic, China.

5.1.3 Transmission measurements

The experimental setup⁹ for MDM/WDM transmission with prism-based 3-spot mode couplers is shown in Figure 5-6. Eight ECLs, operating at 193.7THz to 193.7THz with a 100-GHz frequency spacing are passively combined and modulated by a LiNbO₃ IQ-Modulator driven by two DACs operating at 32Gbaud. The DACs are driving the IQ-modulator either with QPSK, 8QAM, 16QAM symbols or with pre-generated 32QAM FEC-encoded symbols. PDM is emulated by a stage with 700 symbols delay between two arms, which are multiplexed by a PBC. The signal is then split into three tributaries, which are amplified and fed into the input ports of the 3-spot coupler as a mode MUX. As indicated in Figure 5-6, with respect to the third tributary, first and second tributaries are delayed with 4414 and 2826 symbols, respectively.

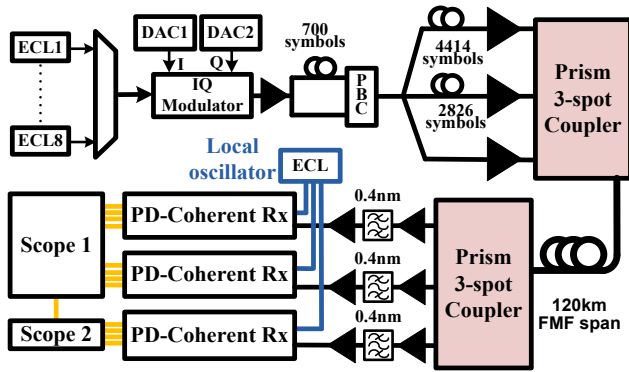


Figure 5-6 Experimental setup for MDM/WDM transmission with free-space prism 3-spot couplers.

Table 5-1 The DGD-compensated FMM span (@ 1550nm) (*MPI: multipath interference [123])

	Spool 1	Spool 2	Spool 3	Spool 4
Length, km	30	30	30	30
MPI*, dB	-26	-26	-25	-26
DGD, ps/m	0.039	-0.044	0.053	-0.047
Disp. LP ₀₁ , ps/(nm·km)	19.9	19.8	19.8	19.8
Disp. LP ₁₁ , ps/(nm·km)	20.1	20	20	20

⁹ The measurements were carried out with the helps from Vincent Sleiffer and Dr. Maxim Kuschnerov in Coriant GmbH, Munich, Germany.

A 120km DGD-compensated FMF span [131] composed of four spools is used as a transmission fiber link, see Table 5-1, calculated to have a compensated modal DGD less than 1 symbol duration. After the mode DEMUX, the signals are sent into three PDM coherent receivers. The output of an ECL is divided into three, used as LOs. The 12 electrical signals are captured by two time-synchronized digital real-time oscilloscopes sampling at 40GS/s and 50GS/s. The captured data is off-line processed with 6×6 MIMO DSP[132] to recover all the signals. After resampling and receiver skew compensation, CD is compensated and the start of the frame is determined by a correlation technique[120]. Subsequently a 6×6 DA time-domain equalizer is used to determine the channel impulse response employing 401 T/2 spaced taps, using 100,000 symbols for convergence and leaving 500,000 (2 million bits per spatial and polarization mode) for bit-error counting. Three time-different shots are taken and averaged per measurement point. Figure 5-7 shows the impulse responses of the FMFs with different lengths, where 1.875ns DGD of a 30km FMF spool can be observed in the black graph. The power of LP_{01} and LP_{11} modes are represented by the two peaks. Only one peak is observed after 120km FMF, see red curve in Figure 5-7, which means the DGD of the composite FMF span is accurately compensated as expected from the accumulation of DGDs of the separate spools.

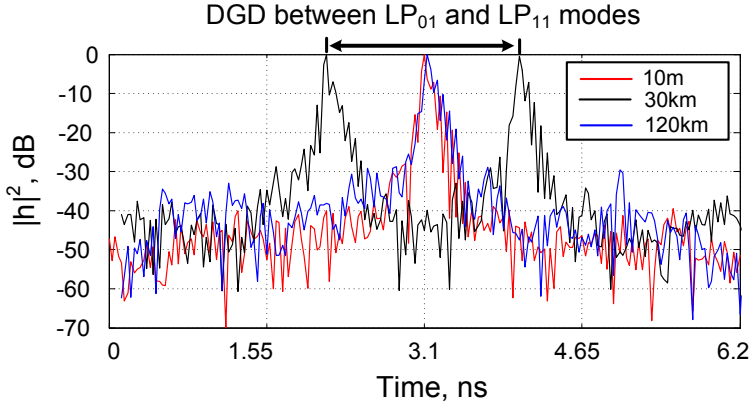


Figure 5-7 Impulse responses of the FMF with a length of 10m (as back-to-back), 30km and 120km, respectively.

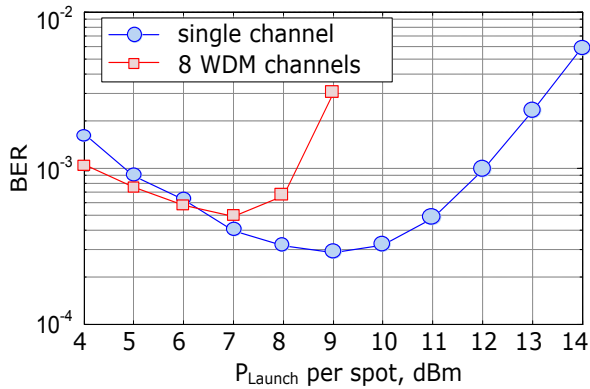
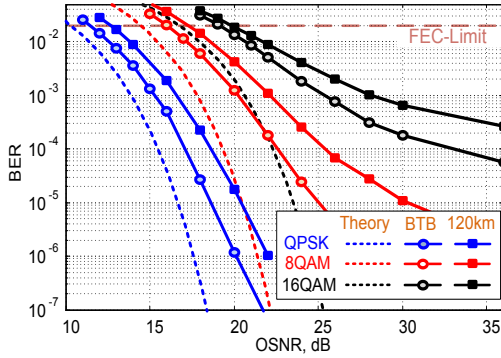


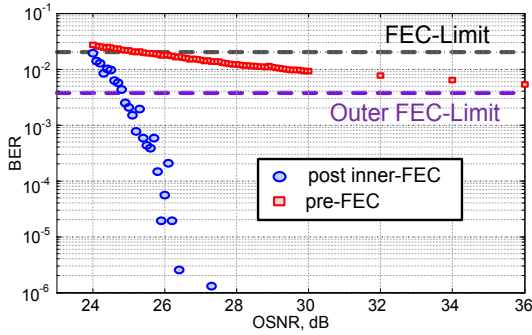
Figure 5-8 BER performance of single channel and 8 WDM channels for 120km FMF transmission versus launch power per spot (16QAM modulation formats).

Figure 5-8 shows the average BER performance versus the launch power per spot, transmitting 16QAM modulation, in order to determine the optimal launch power per spot. Nonlinear effects start to be observed when the launch power exceeds 9dBm and 7dBm for a single channel and 8 WDM channels, respectively. Note that the launch power is defined as the measured optical power at the FMF input facet per spot. Figure 5-9 (a) gives the average BER versus OSNR after 120km transmission at the optimum launch power for different modulation formats. Noise that is generated by a JDSU MAP broadband source is optically loaded at the transmitter side. Less than 2dB transmission penalty (at BER of 2×10^{-2}) can be observed after 120km transmission. With the implementation of the outer hard decision and inner soft decision turbo product code with a total overhead of 21%¹⁰, the pre-FEC BER threshold is 2×10^{-2} [133]. Figure 5-9 (b) gives the BER performance for single channel transmission versus OSNR with 32QAM modulation format. At an OSNR of 25dB/0.1nm, a pre-FEC BER of 2×10^{-2} is obtained. From there on the post inner-FEC BER is below the outer-FEC limit, which is 3.8×10^{-3} . Figure 5-9 (c) gives the frequency spectrum and BER performance for 8 WDM channels transmission with recovered 32QAM constellations for 6 mode channels. As can be observed all signals were performing below the FEC-limit and most shots were error-free after inner FEC and the others gave post inner-FEC BERs well below the outer FEC-limit, which would have resulted in error-free transmission. Around 2dB MDL was calculated through SVD of the converged taps.

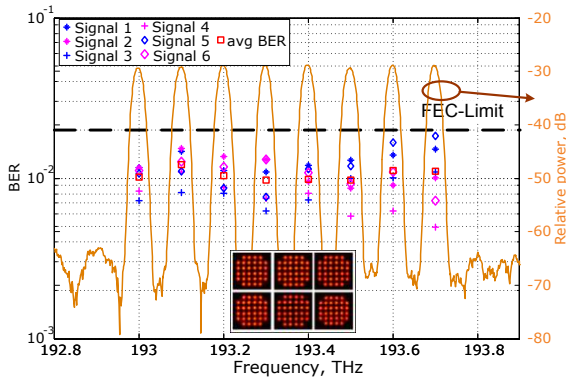
¹⁰ The FEC was implemented by Paolo Leoni, Universität der Bundeswehr München, Germany.



(a)



(b)



(c)

Figure 5-9 BER performance for 120km FMF transmission versus (a) OSNR for QPSK, 8QAM and 16QAM modulation formats, (b) OSNR for 32QAM and (c) frequency spectrum and BER for 8 WDM channels after transmission with recovered 32QAM constellations.

5.2 3D waveguide (3DW) Spot Coupler

5.2.1 3DW device

This section is based on the publication [56] made during the Ph.D project. The 3DW fabrication is based on the use of femto-second laser pulses, which are focused inside a fused silica substrate, as depicted in Figure 5-10 [134], [135]. Both the core and the cladding of the waveguides are made out of pure fused silica. This provides a solution to modify the refraction index of a glass locally and generates waveguides in 3D. Figure 5-11 (a) shows the schematic of the 3DW 3-spot coupler¹¹. 3 single-mode optical waveguides are located in one facet with a spacing of $250\mu\text{m}$, which can be packaged with an SMF array. These waveguides run to the other end without crossing, where they are arranged in an equilateral triangle distribution. The 3DW waveguides typically have an index difference between the core and the surrounding of 6×10^{-3} to 6.5×10^{-3} . The NA is approximately 0.10 to 0.13 [134]. Figure 5-11 (b) gives the image of 3-spot end which is scanned by an SMF when all three waveguides are illuminated. The waveguides have a spacing around $16\mu\text{m}$, which results in weak coupling between all the waveguides. It can be seen from Figure 5-11 (c), around 3dB SMF to SMF insertion loss is uniform for each waveguide and within a large wavelength range (C+L band). The measured waveguide crosstalk is less than -11dB.

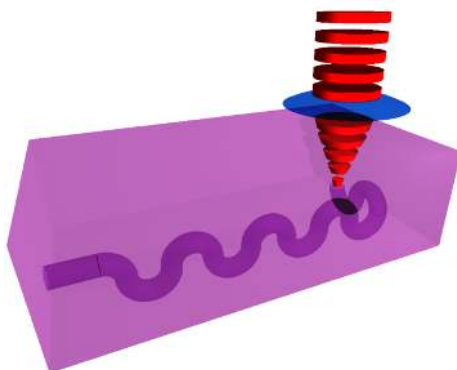


Figure 5-10 A waveguide is inscribed in 3D inside a glass substrate by a femto-second laser.

¹¹ The designed 3DW 3-spot coupler was fabricated by Translume, USA, with the helps from Dr. Philippe Bado and Dr. Ali Said.

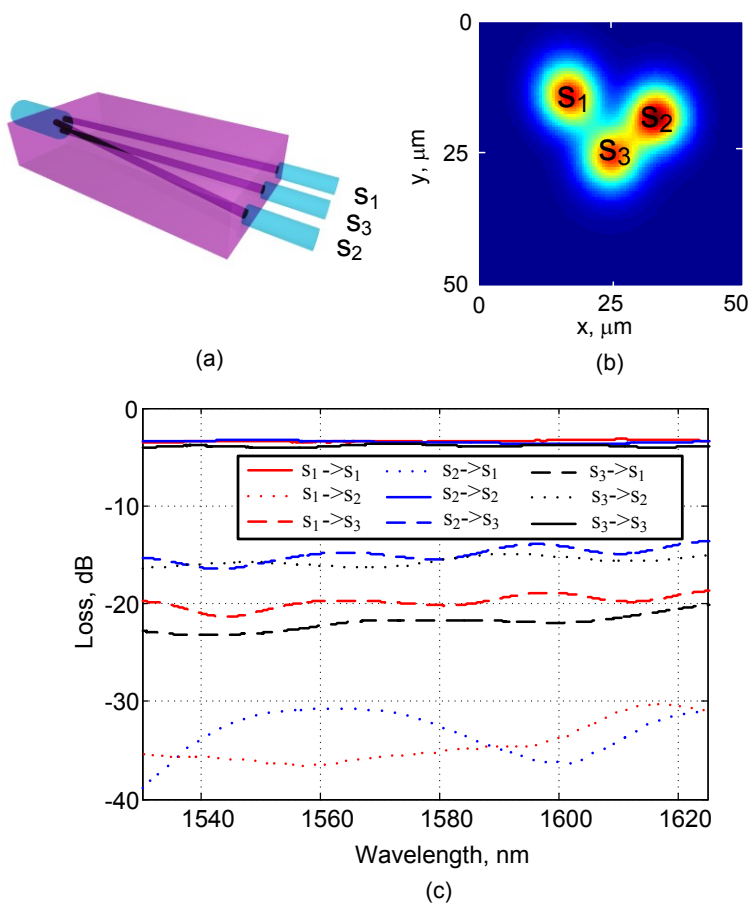


Figure 5-11 (a) Schematics of 3DW 3-spot coupler; (b) image of field distribution at FMF front-end scanned by an SMF; (c) measured insertion losses and coupling between three weakly coupled waveguides.

5.2.2 Transmission measurements

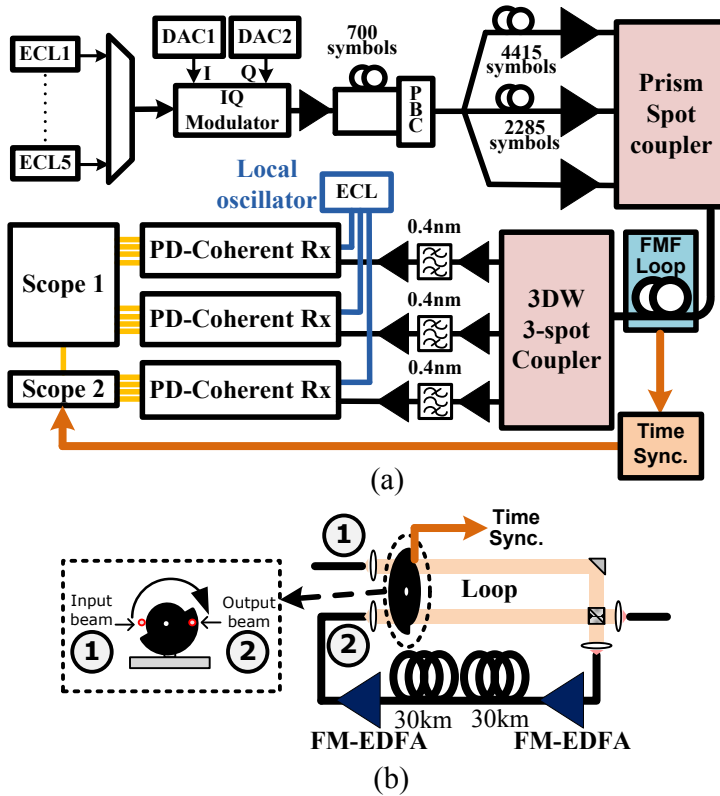


Figure 5-12 (a) Experimental setup containing an all-FMF re-circulating loop [24] and (b) chopper used as switching mechanism for the re-circulating loop.

Figure 5-12 (a) shows the experimental setup, containing a prism-based 3-spot coupler, an all-FMF re-circulating loop¹² and a 3DW 3-spot coupler as mode DEMUX. At the transmitter side five lasers running at 193.0, 193.1, 193.4 (channel under test (CUT)), 193.8 and 193.9 THz were passively combined using a polarization-maintaining coupler, and subsequently modulated using an IQ-modulator, driven by two DACs running at a 32 GBaud symbol rate that address the in-phase and quadrature port of the IQ-modulator. The electrical driving signal was formed by combining three PRBSs of length 2^{15} which were shifted by 8191 and 16383 symbols with respect to each other before combining them and mapping them onto 8QAM symbols.

¹² The all-FMF re-circulating loop was built by Vincent Sleiffer and Dr. Yongmin Jung. The measurements were carried out in Coriant GmbH, Munich, Germany.

After modulation, PDM was emulated by splitting the signal into two equally powered tributaries, delaying one by 700 symbols for de-correlation, and combining them again using a PBC. The 192-Gb/s DP-8QAM signal subsequently is split into three signals which are delayed by 2285 and 4415 symbols with respect to the original signal again for emulation of three different signals, and fed to the prism-based mode coupler, which launches the signals into a 3-mode FMF pigtail.

The FMF pigtail was connected to a free-space -3dB coupler. The input signal was coupled into the loop containing two few-mode EDFAs [22], and 60 km of FMF with the parameters listed in Table 5-2. The 60km FMF span has a DGD between the LP_{01} and LP_{11} modes of around 9 symbols. At the input and output of the loop a few-mode EDFA was placed to compensate for the span and coupling loss of the 3dB coupler.

A chopper was used inside the free-space -3dB coupler which provides the same functionality as an acousto-optic modulator (AOM) widely used in single-mode re-circulating loops, although careful control of timing is required, see Figure 5-12 (b). The free-space optics is tuned such that the output of the loop is blocked when the input is open, and vice versa. The chopper provides a signal which was used to control the timing to trigger the scopes at the receiver side after determining the loop time.

Table 5-2 60km FMF span (@ 1550nm)

	Spool 1	Spool 2
Length [km]	30	30
MPI [dB]	-26	-25
DGD [ps/m]	-0.044	0.053
Disp. LP_{01} [ps/(nm·km)]	19.8	19.8
Disp. LP_{11} [ps/(nm·km)]	20	20

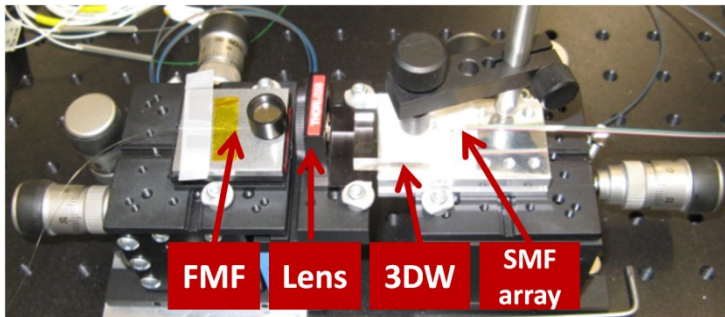


Figure 5-13 3DW-based 3-spot coupler with imaging optics.

At the output of the re-circulating loop, the 3DW device (with a dimension of $25.4\text{mm} \times 25.4\text{mm} \times 6.35\text{mm}$) was used to spatially demultiplex the three

signals. Figure 5-13 gives the picture of the 3DW device test setup. The 3DW device is packaged with an SMF array¹³. Imaging optics with a magnification of 2.44 is used to match the beam size between the 3DW device and the FMF. The 193.4THz CUT was filtered out using 0.4nm tunable filters and afterwards fed to three coherent receivers connected to two digital sampling scopes: an 8 port 40-Gsamples/s scope (20GHz electrical bandwidth) and a 4 port 50-Gsamples/s scope (16GHz electrical bandwidth). Both digital sampling scopes were carefully synchronized beforehand to assure all signals are received time-aligned. Afterwards, offline 6×6 MIMO-DSP was employed to reconstruct the sent signals.

Figure 5-14 (a) shows the back-to-back performance of the 192-Gb/s dual-polarization-8QAM signal over a short FMF with mode MUX and DEMUX. The performance shows a ~ 1.5 dB implementation penalty with respect to theory at the FEC-limit. Figure 5-14 (b) shows the optimization of the tap number after 2, 5 and 8 loops. Figure 5-15 (a) shows the transmission distance versus BER. After 480km an average BER over all modes of $\sim 1.3 \times 10^{-2}$ is reached. After 540km this BER increased to 3×10^{-2} , which is above the assumed FEC-limit at 2.4×10^{-2} . The constellations are indicating the recovered signals after 480km transmission. The DGD between the LP_{01} and LP_{11} mode in the 60km span is not fully compensated, which results in a DGD of 9 symbols and another peak appears after each loop. As observed in Figure 5-15 (b), from the impulse responses after 120, 300 and 480km transmission, the number of peaks grows in each loop as well as the number of taps needed to compensate this. For 480km the optimum number of taps is ~ 321 , see Figure 5-14 (b)

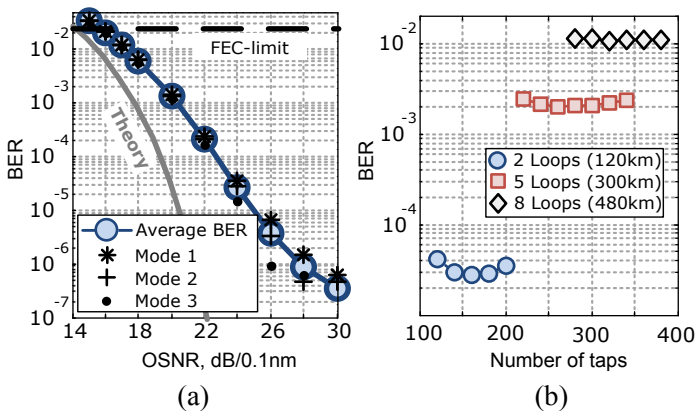
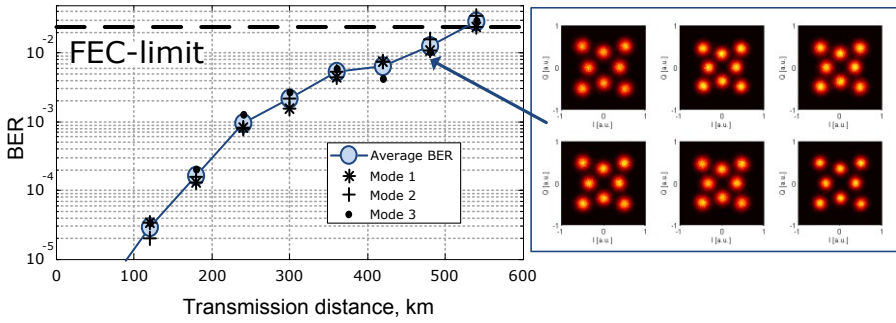
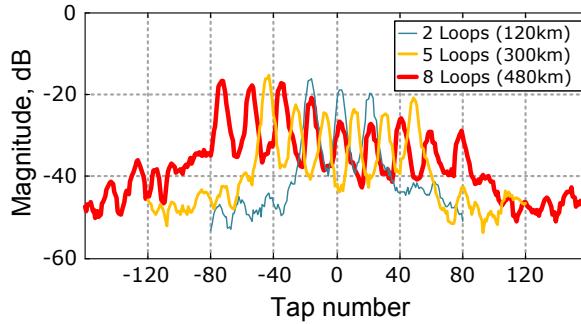


Figure 5-14 (a) Back-to-back curve, (b) Tap sweep for 120, 300 and 480 km,

¹³ Device packaging was carried out in Tyndall national institute, Cork, Ireland with the helps from Dr. Brad Snyder and Dr. Nicola Pavarelli.



(a)



(b)

Figure 5-15 (a) Transmission distance sweep; (d) impulse responses after 120, 300 and 480 km.

5.3 Multi-segment Phase Mask

This section is based on the publication [54] carried out during the Ph.D project. In this section, a single phase plate, called a multi-segment phase mask (MSPM) is introduced and demonstrated in both simulation and experimental tests. The proposed MSPM can be regarded as an optical beam splitter which is able to split optical power spatially and owns the advantages as good uniformity and applicability for arbitrary fibers. With a proper design of the MSPM, this scheme is able to demultiplex all mode channels simultaneously as the MMPM [51] introduced in Chapter 3.3 but with much less CIL. Without the need to use mode-related masks, utilized by the MMPM, the MSPM is less sensitive to the mode coupling which can be expected within long reach FMF transmission.

5.3.1 MSPM functions

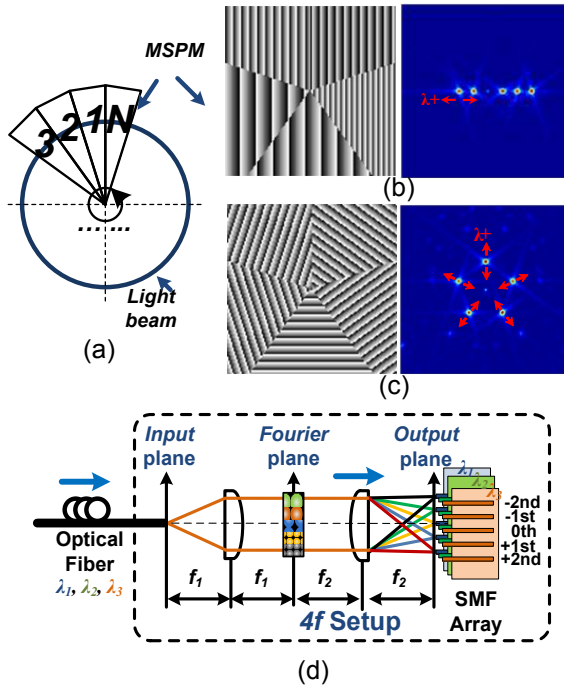


Figure 5-16 (a) Schematic of MSPM with N sliced sub-masks; (b) and (c) MSPM and the diffracted optical beams in the output plane (which is also the input plane of the SMF array) for 1D, and 2D SMF array application, respectively; (d) the 4f setup used for optical Fourier transform with multiple wavelengths;

Figure 5-16 (a) depicts an MSPM with N sliced sub-masks. The function of sub-masks is to split optical power and realize wavelength diffraction, as shown in Figure 5-16 (b) and (c). Each wedge-shaped sub-mask, which is patterned with diffraction grating, covers an area with a same size in order to equally split the power of the incoming optical beam. The 4f lens-based setup, as shown in Figure 5-16 (d) is utilized to realize an optical Fourier transform, where the MSPM is placed in the Fourier plane. To diffract the optical beam into the inputs of an SMF array, different diffraction gratings are patterned on different sub-masks. Figure 5-16 (b) shows the simulation results of splitting the Gaussian-like optical beam in a single wavelength into 5 tributaries. Depending on the design of the MSPM, a 1D or 2D SMF array can be chosen to receive the split beams. In a WDM system, an MSPM is able to split the power and separate the wavelengths simultaneously. For the MSPM shown in Figure 5-16 (b), all diffracted beams would be arranged in one line where red arrows

represent the movement path of the diffracted beam with the wavelength shift. It can be seen that limited by the space, the possibility of beam overlap is much higher in the 1D SMF array case than in the 2D SMF array case. Therefore, the usage of an MSPM for a 2D SMF array is able to provide a larger range of working wavelengths, as depicted in Figure 5-16 (d).

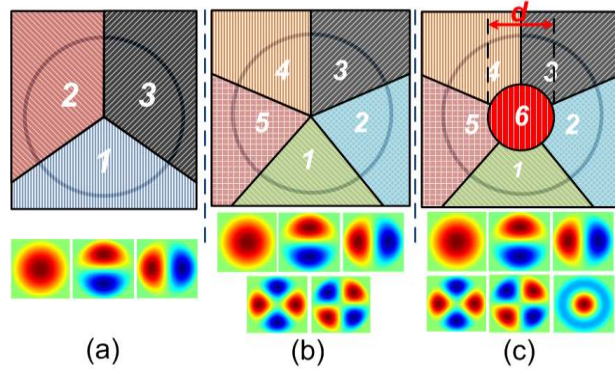


Figure 5-17 The sub-mask arrangement of the MSPM for demultiplexing different modes: (a) LP_{01} and $LP_{11a/b}$; (b) LP_{01} , $LP_{11a/b}$ and $LP_{21a/b}$; (c) LP_{01} , $LP_{11a/b}$, $LP_{21a/b}$ and LP_{02} .

In the application for mode demultiplexing, sub-masks of the MSPM can be regarded as an alternative implementation of a spot-based DEMUX, which is not designed for detecting one specific mode but for receiving the modes in a linear combination. In this study, MDM transmission with a single wavelength is investigated using the setup depicted in Figure 5-16 (d). The FMF is placed in the input plane of the 4f setup and the SMF array is located in the output plane to receive the separate power from all the modes. The design of the sub-masks needs to match the symmetry of the modes supported by the FMF. As shown in Figure 5-17 (a), initially the MSPM is divided into 3 parts to support LP_{01} and two degenerate LP_{11} modes. The sub-mask arrangements of the MSPM for demultiplexing more modes are shown in Figure 5-17 (b) and (c). The basic rule is adding one sub-mask for each non-degenerate mode (e.g. LP_{01} or LP_{02}) and two sub-masks for each degenerate mode, as the LP_{11} mode, which has two spatial modes: LP_{11a} and LP_{11b} . When a mode with a higher radial number is added, as LP_{02} , one sub-mask needs to be added at the center as shown in Figure 5-17 (c). The pattern of each sub-mask is not mode-dependent but determines the position of the diffracted light where the power is coupled into the SMF.

5.3.2 Simulations

The 4f Fourier optics model, developed in Chapter 2 is used to simulate the

MSPM-based mode DEMUX. To investigate the performance of the MSPM for demultiplexing N spatial modes, CIL and MDL are calculated using (Eq. 1-7) and (Eq. 1-8).

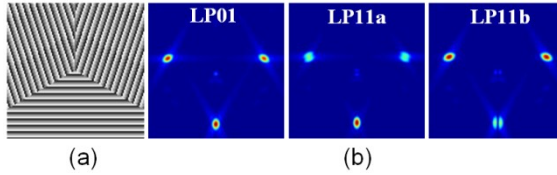


Figure 5-18 (a) MSPM for demultiplexing 3 spatial modes and (b) intensity profiles of the diffracted beams in the SMF array input plane.

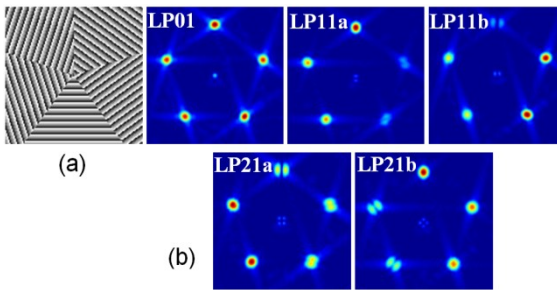


Figure 5-19 MSPM for demultiplexing 5 spatial modes.

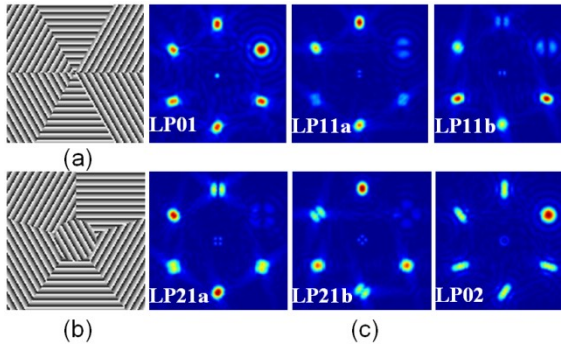


Figure 5-20 MSPM with (a) 6 sliced and (b) 5 sliced and one centred round sub-masks for demultiplexing 6 spatial modes.

Figure 5-18 (a) shows the MSPM for demultiplexing the 3 spatial modes (LP_{01} and $LP_{11a/b}$) and Figure 5-18 (b) gives the intensity profiles of the diffracted beams in the SMF array input plane. A 2D SMF array with a triangle arrangement is assumed to receive the 3 diffracted light beams. The calculated CIL and MDL is 0.9dB and 3.0dB, respectively. In the simulations, blazed gratings are utilized for sub-masks. Figure 5-19 (a) and (b) show the MSPM and

the intensity profiles of the diffracted beams for demultiplexing 5 spatial modes (LP_{01} , $LP_{11a/b}$ and $LP_{21a/b}$). The calculated CIL and MDL is 1.1dB and 5.9dB, respectively. Figure 5-20 (b) and (c) give the results for demultiplexing 6 spatial modes (LP_{01} , $LP_{11a/b}$, $LP_{21a/b}$ and LP_{02}). When a LP_{02} mode (with a higher radial number) is added, an additional round sub-mask needs to be located in the centre of the MSPM, see the 6th sub-mask in Figure 5-17 (c) and Figure 5-20 (b). The diameter of the centered round sub-mask affects the performance of the mode demultiplexer (DEMUX). Figure 5-21 shows the simulation results of the CIL and MDL versus the normalized diameter (d/D), where D is the diameter of the light beam. With the optimum $d = 0.3D$, the calculated CIL and MDL is 0.5dB and 6.9dB, respectively. Without the center sub-mask, for instance, for an MSPM with 6 sliced sub-masks, as shown in Figure 5-20 (a), the coupling efficiency for LP_{02} mode is very low which results in an MDL larger than 40dB.

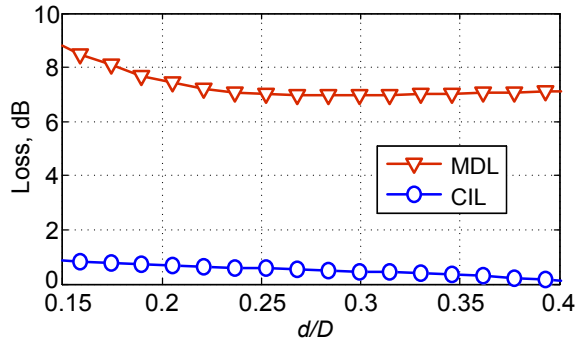


Figure 5-21 Simulated CIL and MDL versus the normalized diameter of the centered sub-mask for the 6-sliced MSPM.

5.3.3 Experimental results

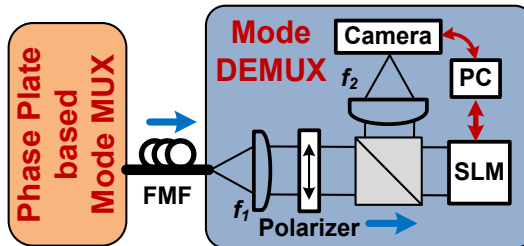


Figure 5-22 Experimental setup with the MSPM-based mode DEMUX.

Figure 5-22 shows the experimental setup for testing the MSPM-based mode DEMUX. The mode MUX is phase-plate based, which is able to provide high mode extinction ratio between different modes. A 10-km SI-FMF, which guides

the LP_{01} and $LP_{11a/b}$ modes is used as a transmission fiber. The core diameter of the FMF is $19.4\mu\text{m}$. In the MSPM-based DEMUX, two lenses with $f_1 = 15\text{mm}$ and $f_2 = 100\text{mm}$ are used to collimate the output beam from the FMF and focuses it into a camera operating at 1550nm respectively. A reflective SLM with a resolution of 1920×1080 pixels is utilized to emulate the proposed MSPM. Figure 5-23 (a) to (c) give the intensity of optical fields in the focal plane of the 2nd lens diffracted by the MSPM as shown in Figure 5-18 (a), Figure 5-19 (a) and Figure 5-20 (b) when LP_{01} mode is selectively excited in the FMF. Limited by the resolution of the camera, sharp diffracted patterns for the other modes are hard to capture. As the camera is replaced by a 2D SMF array to detect all diffracted light beams, signals over modes can be captured. Since the MSPM-based DEMUX is not designed to separate each mode but to receive the modes in a linear combination, all the mixed signals need to be recovered through MIMO based DSP in the receiver side.

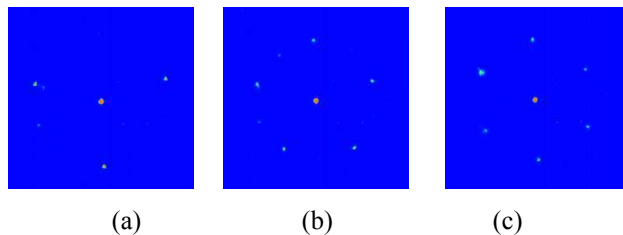


Figure 5-23 The intensity of the diffracted optical fields in the output plane of the DEMUX captured by a camera as LP_{01} mode is excited.

5.4 Summary

In this chapter, spot-based mode couplers, which excite a linear combination of modes instead of pure fiber modes were analyzed. Two 3-spot couplers realized by free space optics and laser-inscribed 3DW were demonstrated with transmission experiments.

1) The free space prism-based 3-spot coupler is able to achieve 3dB CIL and 2dB MDL. 7.68Tb/s transmission of combined MDM and WDM (8 wavelength channels) with 320Gb/s dual-polarization-32QAM over a 120km DGD-compensated FMF was demonstrated by employing the proposed prism-based 3-spot couplers. A free space optics 6-spot coupler can also be implemented using a pentagonal pyramid with a central hole along the main axis of the pyramid for generating the center spot [127].

2) Laser-inscribed 3DW 3-spot coupler is much more compact than the free space solution and has less alignment requirements. 576Gb/s transmission of

MDM with 192Gb/s dual-polarization 8QAM over 480km FMF was demonstrated by employing the 3DW 3-spot coupler as a mode DEMUX.

Laser-inscribed 3DW technology is promising for mode (de)multiplexing and can enable the inscription of both coupled and uncoupled optical waveguides. 3DW based 6-mode coupler has been demonstrated with strongly coupled waveguides [136], which is also called as photonic lantern [55]. The next chapter will describe a photonic lantern-based mode coupler, which is a lossless mode multiplexing solution potentially.

Chapter 6 Photonic Lantern Mode Coupler

This chapter is based on the publication [25] carried out during the internship in Bell Labs¹⁴. This chapter describes photonic lantern based mode couplers, which potentially can realize lossless mode (de)multiplexing. Employing low-loss fiber-lanterns as mode couplers, 900km FDM transmission distance is achieved for the combined MDM and WDM transmission with a spectral efficiency of 3.0bit/s/Hz.

6.1 Photonic Lantern Schemes

Photonic lantern is an optical device which couples light from an MMF to SMFs [137]–[139]. In astronomy, photonic lanterns have been used to collect more light from the telescope with the large multi-mode facet, which can drastically enhance the light couple efficiency compared to the use of an SMF. In order to avoid the information loss, the number of SMFs need to be equal or more than the number of spatial modes guided in the MMF section. Moreover, an adiabatic tapering process is required to guarantee that no modes become evanescent cladding modes. In [55], photonic lanterns were introduced into the application of MDM, where N SMFs need to be positioned in the same arrangement as the spot coupler, and subsequently are adiabatically tapered down into a few-mode front end, guiding N spatial modes.

¹⁴ The measurements in this chapter were under the direct supervision of Dr. Roland Ryf and Dr. Nicolas K. Fontaine.

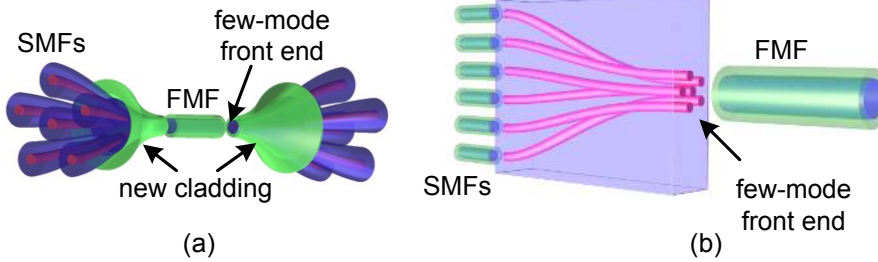


Figure 6-1 Schematics of photonic lantern: (a) fiber-based and (b) 3DW-based.

Two schemes were proposed to realize the photonic lantern mode coupler [140]. One is fully fiber-based as shown in Figure 6-1 (a), where multiple SMFs are surrounded by a low index capillary. After down-tapering, the cladding of SMFs become the new few-mode core and the capillary becomes the new few-mode cladding. The other method is based on femto-second laser inscription, as shown in Chapter 5. In contrast to the spot coupler with weakly-coupled waveguides, laser-inscribed 3DW lantern brings multiple single-mode waveguides very close together to create a strongly-coupled regime with super-modes, which can match the guided modes in an FMF, as depicted in Figure 6-1 (b).

6.2 Fiber Lantern

6.2.1 3-core fiber lantern

The 3-core fiber lantern¹⁵ [55] is fabricated by tapering 3 individual SMFs inserted in a low-refractive-index Fluorine-doped capillary, see Figure 6-2 (a). The structure is adiabatically tapered by passing the composite structure through a heating element while applying different feeding and pulling speeds to create the lantern profile. Figure 6-2 (b) gives the image of the taper section. The lantern is subsequently cleaved at the waist. In the taper section, the modes are initially guided by the original cores, but as the core diameter shrinks, the modes will start to strongly overlap and couple. In the final section of the lantern, the guidance of the core is negligible and the resulting modes are guided by the cladding of the original SMFs, whereas the low-index capillary plays the role of a cladding. The photonic lanterns are based on standard SMFs and the NA produced by the capillary is 3 times smaller than that of the FMF,

¹⁵ The photonic lanterns were fabricated by Dr. Sergio G. Leon-Saval, University of Sydney, Australia

therefore a double telecentric imaging system with a magnification of 2.7 was added between the fiber lantern and the FMF. The fiber lanterns have been fully characterized using swept-laser interferometry [141], and independent power transmission measurements indicating a CIL < 2 dB, and an MDL < 1 dB for both lanterns used in the transmitter and receiver side, respectively. Also the measured both CIL and MDL as a function of the wavelength across a 110 nm scanning range showing a negligible wavelength dependence and good performance across the whole wavelength range (from 1510 nm to 1620 nm).

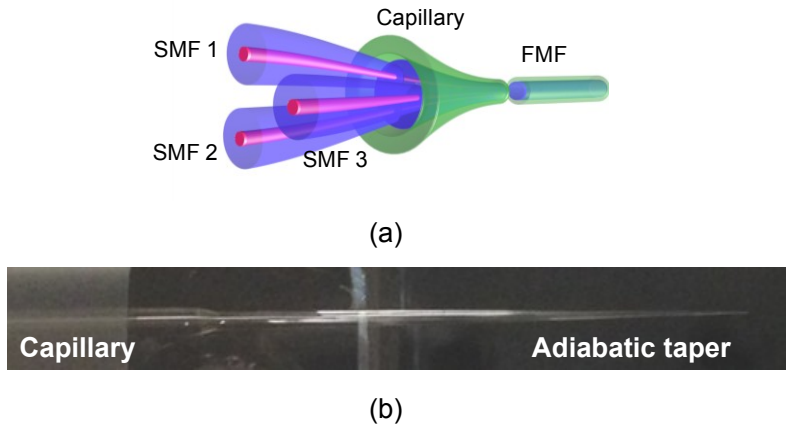


Figure 6-2 (a) 3-core fiber lantern and (b) image of the taper section.

6.2.2 Transmission results

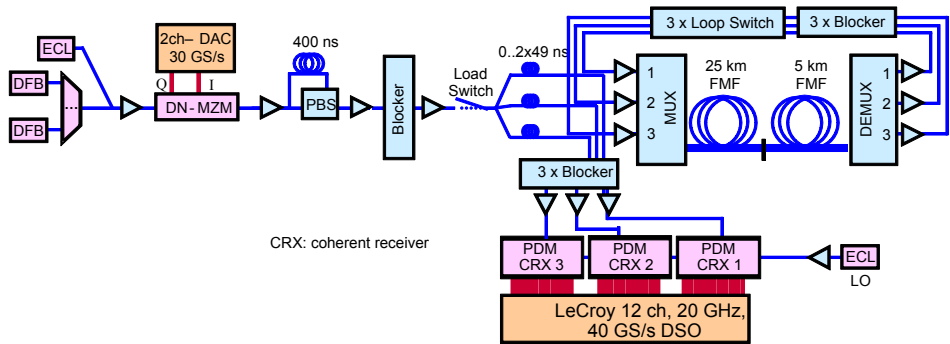


Figure 6-3 Experimental setup.

The MIMO transmission measurement is performed using the setup shown in Figure 6-3. The 32 wavelength channels on a 100-GHz grid are generated by modulating 32 DFBs using a double-nested LiNbO₃ modulator (DN-MZM), driven by a two-channel DAC operated at 30 GS/s. The electrical signals from

the DAC are pre-emphasized to compensate for the roll-off of the DN-MZM and produce a 30-GBaud QPSK signal. Two independent De Bruijn bit sequences (DBBS) of length 2^{15} are used for the I and Q components of the QPSK signal, respectively. An ECL with a linewidth of 100kHz is used for the CUT, and a second ECL is used as a LO in intradyne configuration. After traversing a PDM stage, that adds an orthogonally polarized copy of the signal delayed by 400-ns, the PDM QPSK signal is divided into 3 paths with a relative delay of 49 ns and 98 ns, respectively. The three delayed copies are then fed into a 3-fold recirculating loop. Three LiNbO₃ switches are used to control the loading and the closing of the loop. The loop consists of a fiber lantern pair connected to the 30-km DGD-compensated FMF span, and 3 two-stage single-mode EDFAs, where a multichannel blocker is inserted between amplification stages in order to spectrally equalize the power in the loop. The relative length of the loop is accurately tuned to within < 100 ps using fiber delays. The signals are extracted from the loop using 50:50 couplers, filtered with a multichannel blocker, amplified by EDFAs, and captured by three PDM coherent receivers. The 12 electrical signals from the coherent receivers are captured by a modular digital storage oscilloscope (LeCroy LabMaster 9zi) operating at 40 GS/s with a bandwidth of 20 GHz.

The waveforms captured by the digital storage oscilloscope are processed off-line using the frequency-domain MIMO DSP algorithm described in [142], where up to 900 equalizer taps were optimized using DA-LMS to assure convergence of the equalizer and the CMA was used during error counting. The resulting BER as a function of the wavelength are shown in Figure 6-4 (a) for a distance of 900 km and an input power of -5dBm per mode-, wavelength-, and polarization. Figure 6-4 (a) also shows the optical spectrum after 900 km transmission. After 900km transmission, the BER for all wavelength channels is below 2×10^{-2} , which can be compensated with a state-of-the-art FEC with a 20% overhead. The WDM channels are spread across a bandwidth of 3.2THz, confirming the broadband operation of the fiber lanterns. Figure 6-4 (b) shows the result of a single channel experiment at 1550.1nm wavelength for an input power of -3dBm per mode and polarization. Longer distances are reached in the case of single wavelength operation, where a BER $< 2 \times 10^{-2}$ was observed up to 1500km, which to our knowledge is the longest SDM transmission distance reported in FMFs. The reported results are for optimum launch powers, obtained by measuring the BER for different power levels. The impulse responses are shown in Figure 6-4 (c) for different transmission distances showing a slow transition between the DGD compensated impulse response of the single span (30km) into a bell-shaped profile starting from 200 km, which then grows in temporal width, following the square root of the transmission distance. The MDL of the total transmission matrix is also analyzed showing a

very small initial system MDL of around 1.5 dB for the first 300 km and afterward increasing linearly with around 0.5 dB every 100 km, which is very similar to the MDL observed for spot based coupler in [130].

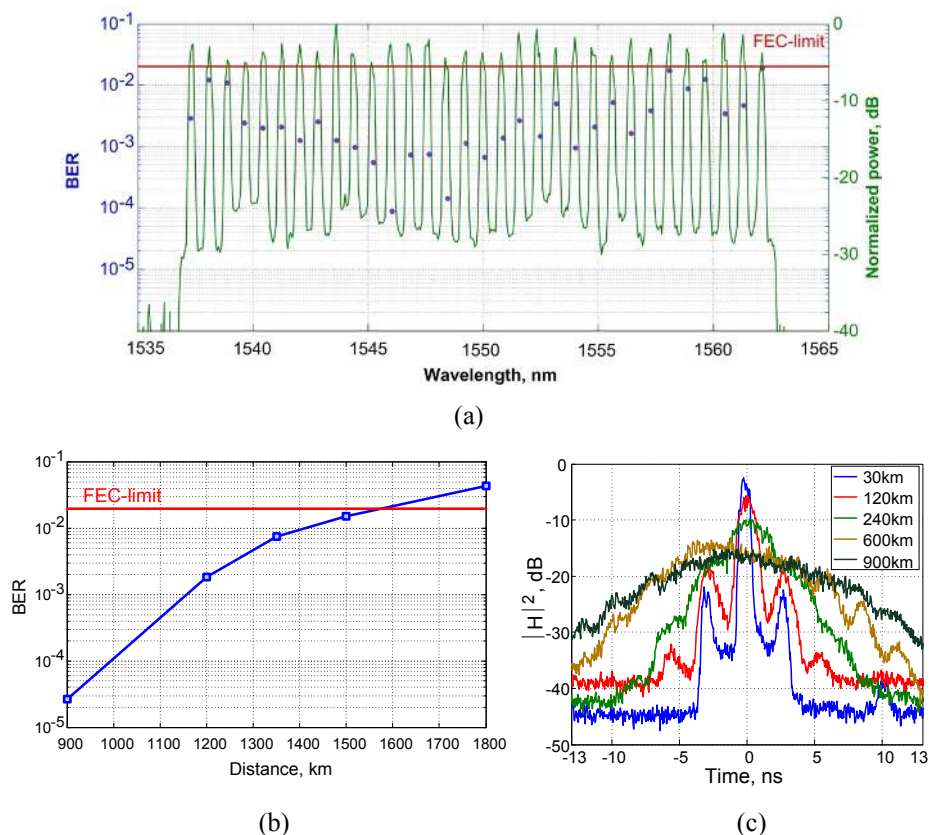


Figure 6-4 (a) BER and optical spectrum for all 32 WDM channels after 900 km transmission; (b) BER for single channel transmission as a function of the distance and (c) impulse responses calculated for 30, 120, 240, 600 and 900km distance.

6.3 Summary

In this chapter, a fiber-lantern was demonstrated as a low-loss 3-mode coupler with a CIL < 2 dB, and an MDL < 1 dB. There are two main achievements for the fiber-lantern based 3-mode FMF transmission: 1) a 900km FMF distance is achieved for the combined MDM and WDM transmission with a spectral efficiency of 3.0bit/s/Hz and 2) a record of 1500km FMF distance is achieved for MDM transmission with a single wavelength.

The CIL of the fiber-lantern is 2dB smaller than the value obtained for spot-based mode couplers [52], [53] and theoretically photonic-lantern based mode couplers can be lossless as analyzed in the introduction chapter.

By choosing the correct geometry of the SMFs and capillary, and related refractive indices, it is possible to produce fiber-lanterns that can be directly spliced to FMFs.

Chapter 7 Conclusions and Outlook

7.1 Conclusions

The main objective of this thesis is to analyze, design and implement novel mode or mode group multiplexing devices for realizing mode division multiplexing (MDM) and mode group division multiplexing (MGDM) transmission over few-mode fiber (FMF) and multi-mode fiber (MMF). For MGDM over MMF, aiming at short-reach applications, offset launch was demonstrated for exciting different mode groups and 30Gb/s 3×3 MGDM transmission was verified over a 20m graded-index (GI)-MMF.

In order to extend the transmission distance, selective mode excitation based solutions were exploited to excite pure fiber modes in FMF or MMF. A compact mode demultiplexer (DEMUX) based on a single multi-mode phase mask (MMPM) was demonstrated for separating different spatial modes, which avoids the use of beam splitters for the traditional bulky phase-plate based mode coupler. To avoid the large footprint of the bulky optics, a photonic integrated SOI mode coupler was researched. It was for the first time that 3-mode MDM/WDM transmission over FMF was demonstrated by employing a photonic integrated mode MUX. However, the scalability of the MMPM-based mode DEMUX and the photonic integrated mode coupler to a larger number of modes is limited due to the increasing coupler insertion loss (CIL) and design complexity.

Compared to selective mode excitation solutions, spot-based mode couplers are scalable to a larger number of modes. Free space and laser-inscribed 3DW based spot couplers were both explored. 7.68Tb/s MDM/WDM transmission was demonstrated over a 120km FMF based on the free space prism-based spot couplers, which has a 2dB MDL and 3dB CIL. 576Gb/s MDM transmission (single wavelength) over 480km FMF was demonstrated by employing the 3DW spot coupler, which gives an MDL of 3dB and a CIL of 6dB with imaging optics.

A theoretically lossless photonic lantern based mode coupler was discussed in the last part of the thesis, where 3-mode fiber-lanterns were exploited. Employing the fabricated fiber-lanterns, 1500km MDM-only and 900km MDM/WDM transmission was achieved which demonstrates that photonic lantern can be a promising mode coupler technology.

The evaluations for these exploited solutions with respect to key parameters are presented below.

MDL and CIL

The performance difference with respect to MDL and CIL can be seen from the transmission results with different mode multiplexing solutions employed. The 1500km MDM transmission distance record was achieved by fiber-lantern based MDM link as presented in chapter 6. The highest spectral efficiency 32bit/s/Hz for MDM system was also realized by employing laser-inscribed 3DW photonic lanterns, which support 6 spatial modes [16]. Theoretically, as analyzed in [55], photonic lanterns with a proper core arrangement can have negligible mode dependent loss (MDL) and CIL as the super-modes approximate the spatial modes. Therefore, based on these experimental demonstrations and theoretical analysis, a photonic lantern is more advantageous to achieve lower MDL and CIL.

Scalability

As discussed in the introduction, a mode coupling solution with a good scalability means the solution is able to achieve a low MDL and CIL as supporting a large number of mode channels. Therefore, a photonic lantern based mode coupler is still the most promising solution, especially compared to the phase-plate based mode coupler, which uses the lossy beam splitters.

Integration and packaging

Integration and packaging are essential to minimize the footprint and could provide repeatability and reliability in manufacturing. Photonic integrated and laser-inscribed 3D-waveguide (3DW) mode couplers are advantageous with respect to integration and packaging. InP- or SOI-based MDM compatible transceivers are able to lower the cost per device through high-density photonic integration of multiple transmitters and receivers required to support multiple modes. 3DW technology [143], which enables waveguide fabrication in 3D has received an increasing interest due to its promising achievements in spatial division multiplexing (SDM) applications. Besides the state-of-the-art 3DW based MDM and multi-core fiber (MCF) couplers, other optical components

such as optical splitters and AWG are being researched recently using 3D technology [144]. Therefore, 3DW technology is potentially a new photonic integration platform, which demonstrated capability for hybrid integration with silica-based planar lightwave circuits (PLCs) [145].

Mode extinction ratio

It has been discussed that mode coupling is inevitable for a practical fiber link due to fiber imperfections and splice issues so that a mode extinction ratio is less important than MDL and CIL. However, high mode extinction ratio, which can be achieved by selective mode excitation, is still useful for some MDM fiber/device characterizations as well as short-distance transmission. For instance, selective mode excitation is generally used for measuring the DGD of FMFs and the mode dependent gain of few-mode EDFAs.[22], [146]. It is meaningless to discuss the achievable mode extinction ratio for spot-based couplers and non mode-selective photonic lanterns as presented in Chapter 6 since they are not designed to excite pure fiber modes. However, theoretically high mode extinction ratio can also be achieved by the mode-selective photonic lanterns as proposed in [147]–[150], which are still being researched.

7.2 Outlook

State-of-the-art combined MDM and WDM transmission has been achieved by employing different mode couplers. These experiments substantiate the viability of MDM to overcome the capacity bottleneck of SMF-based optical networks. For future practical long-haul transmission applications, further research efforts are recommended for the following:

- 1) It is interesting to exploit photonic integrated MDM compatible transceivers with low chip-to-FMF coupling loss. Loss optimization for vertical emitters such as the compact SOI-based grating coupler and InP-based 45° vertical mirror is crucial.

- 2) A spliceable fiber lantern is also a promising research topic based on the impressive results which have been achieved by fiber lanterns. It is also worthwhile to explore photonic lanterns, which can support a larger number of modes (i.e. >10 spatial modes).

- 3) It will be interesting if conventional 50 μm MMF can support MDM/WDM transmission with full use of the guided modes, especially after robust 23Tb/s 6-mode MDM over 17km MMF was demonstrated [33]. For the 50 μm GI-MMF, >150 times capacity increase can be achieved if all mode channels are actively in use. In order to support long-haul transmission, MMF with low DGD and optimization in DSP requires investigation.

4) Due to the fact that optical fiber is not lossless, few-mode or multi-mode amplifiers such as the EDFA [22] and Raman amplifier [46] will become more critical to support long-haul MDM/WDM transmission. It is important to investigate solutions which are able to offer scalable MDM amplification with low mode dependent gain.

References

- [1] R. Essiambre, "Impact of fiber parameters on nonlinear fiber capacity," in *Optical Fiber Communication Conference and Exposition (OFC/NFOEC), 2011 and the National Fiber Optic Engineers Conference*, 2011, pp. 1–3.
- [2] L. E. Nelson, X. Zhou, B. Zhu, M. F. Yan, P. W. Wisk, and P. D. Magill, "All-Raman-Amplified, 73 nm Seamless Band Transmission of 9 Tb/s Over 6000 km of Fiber," *IEEE Photonics Technol. Lett.*, vol. 26, no. 3, pp. 242–245, Feb. 2014.
- [3] R.-J. Essiambre, G. Kramer, P. J. Winzer, G. J. Foschini, and B. Goebel, "Capacity Limits of Optical Fiber Networks," *J. Light. Technol.*, vol. 28, no. 4, pp. 662–701, Feb. 2010.
- [4] A. Mecozzi and R.-J. Essiambre, "Nonlinear Shannon Limit in Pseudolinear Coherent Systems," *J. Light. Technol.*, vol. 30, no. 12, pp. 2011–2024, Jun. 2012.
- [5] X. Chen and W. Shieh, "Closed-form expressions for nonlinear transmission performance of densely spaced coherent optical OFDM systems," *Opt. Express*, vol. 18, no. 18, pp. 19039–19054, Aug. 2010.
- [6] R. W. Tkach, "Scaling optical communications for the next decade and beyond," *Bell Labs Tech. J.*, vol. 14, no. 4, pp. 3–9, Feb. 2010.
- [7] D. J. Richardson, J. M. Fini, and L. E. Nelson, "Space-division multiplexing in optical fibres," *Nat. Photonics*, vol. 7, no. 5, pp. 354–362, May 2013.
- [8] A. D. Ellis, "The nonlinear Shannon limit and the need for new fibres," 2012, vol. 8434, p. 84340H–84340H–10.
- [9] P. J. Winzer and G. J. Foschini, "MIMO capacities and outage probabilities in spatially multiplexed optical transport systems," *Opt. Express*, vol. 19, no. 17, pp. 16680–16696, 2011.
- [10] R.-J. Essiambre and R. W. Tkach, "Capacity Trends and Limits of Optical Communication Networks," *Proc. IEEE*, vol. 100, no. 5, pp. 1035–1055, May 2012.
- [11] A. Chralyvy, "Plenary paper: The coming capacity crunch," in *35th European Conference on Optical Communication, 2009. ECOC '09*, 2009, pp. 1–1.
- [12] "ModeGap," *Multi-mode capacity enhancement with PBG fiber*. [Online]. Available: <http://modegap.eu>.
- [13] P. J. Winzer and G. J. Foschini, "Mode division multiplexed

- transmission systems,” in *Optical Fiber Communication Conference*, 2014, p. Th1J.1.
- [14] P. J. Winzer, “Energy-Efficient Optical Transport Capacity Scaling Through Spatial Multiplexing,” *IEEE Photonics Technol. Lett.*, vol. 23, no. 13, pp. 851–853, Jul. 2011.
- [15] Cen Xia, R. Amezcua-Correa, Neng Bai, E. Antonio-Lopez, D. M. Arrijoja, A. Schulzgen, M. Richardson, J. Liñares, C. Montero, E. Mateo, Xiang Zhou, and Guifang Li, “Hole-Assisted Few-Mode Multicore Fiber for High-Density Space-Division Multiplexing,” *IEEE Photonics Technol. Lett.*, vol. 24, no. 21, pp. 1914–1917, Nov. 2012.
- [16] R. Ryf, S. Randel, N. K. Fontaine, M. Montoliu, E. Burrows, S. Chandrasekhar, A. H. Gnauck, C. Xie, R.-J. Essiambre, and P. Winzer, “32-bit/s/Hz Spectral Efficiency WDM Transmission over 177-km Few-Mode Fiber,” in *Optical Fiber Communication Conference*, 2013.
- [17] H. Takahashi, T. Tsuritani, E. L. T. de Gabory, T. Ito, W. R. Peng, K. Igarashi, K. Takeshima, Y. Kawaguchi, I. Morita, Y. Tsuchida, Y. Mimura, K. Maeda, T. Saito, K. Watanabe, K. Imamura, R. Sugizaki, and M. Suzuki, “First demonstration of MC-EDFA-repeated SDM transmission of 40 x 128-Gbit/s PDM-QPSK signals per core over 6,160-km 7-core MCF,” *Opt. Express*, vol. 21, no. 1, pp. 789–795, Jan. 2013.
- [18] M. D. Feuer, L. E. Nelson, K. S. Abedin, X. Zhou, T. F. Taunay, J. F. Fini, B. Zhu, R. Isaac, R. Harel, G. Cohen, and D. M. Marom, “ROADM System for Space Division Multiplexing with Spatial Superchannels,” in *Optical Fiber Communication Conference/National Fiber Optic Engineers Conference 2013*, 2013, p. PDP5B.8.
- [19] K. Igarashi, T. Tsuritani, I. Morita, Y. Tsuchida, K. Maeda, M. Tadakuma, T. Saito, K. Watanabe, K. Imamura, R. Sugizaki, and M. Suzuki, “1.03-Exabit/skm Super-Nyquist-WDM transmission over 7,326-km seven-core fiber,” in *39th European Conference and Exhibition on Optical Communication (ECOC 2013)*, 2013, pp. 1–3.
- [20] V. A. J. M. Sleiffer, Y. Jung, V. Veljanovski, R. G. H. van Uden, M. Kuschnerov, H. Chen, B. Inan, L. G. Nielsen, Y. Sun, D. J. Richardson, S. U. Alam, F. Poletti, J. K. Sahu, A. Dhar, A. M. J. Koonen, B. Corbett, R. Winfield, A. D. Ellis, and H. de Waardt, “73.7 Tb/s (96 x 3 x 256-Gb/s) mode-division-multiplexed DP-16QAM transmission with inline MM-EDFA,” *Opt. Express*, vol. 20, no. 26, pp. B428–B438, Dec. 2012.
- [21] Q. Kang, E. L. Lim, Y. Jung, F. Poletti, S. Alam, and D. J. Richardson, “Design of Four-Mode Erbium Doped Fiber Amplifier with Low Differential Modal Gain for Modal Division Multiplexed

- Transmissions,” in *Optical Fiber Communication Conference/National Fiber Optic Engineers Conference 2013*, 2013, p. OTu3G.3.
- [22] Y. Jung, S. Alam, Z. Li, A. Dhar, D. Giles, I. P. Giles, J. K. Sahu, F. Poletti, L. Grüner-Nielsen, and D. J. Richardson, “First demonstration and detailed characterization of a multimode amplifier for space division multiplexed transmission systems,” *Opt. Express*, vol. 19, no. 26, pp. B952–B957, Dec. 2011.
- [23] E. Ip, M.-J. Li, Y.-K. Huang, A. Tanaka, E. Mateo, W. Wood, J. Hu, Y. Yano, and K. Koreshkov, “146λx6x19-Gbaud Wavelength-and Mode-Division Multiplexed Transmission over 10x50-km Spans of Few-Mode Fiber with a Gain-Equalized Few-Mode EDFA,” in *National Fiber Optic Engineers Conference*, 2013.
- [24] V. A. J. M. Sleiffer, Y. Jung, M. Kuschnerov, S. U. Alam, D. J. Richardson, L. Grüner-Nielsen, Y. Sun, and H. de Waardt, “Optical chopper-based re-circulating loop for few-mode fiber transmission,” *Opt. Lett.*, vol. 39, no. 5, pp. 1181–1184, Mar. 2014.
- [25] R. Ryf, N. K. Fontaine, M. Montoliu, S. Randel, B. Ercan, H. Chen, S. Chandrasekhar, A. Gnauck, S. G. Leon-Saval, J. Bland-Hawthorn, J. R. Salazar Gil, Y. Sun, and R. Lingle, “Photonic-Lantern-Based Mode Multiplexers for Few-Mode-Fiber Transmission,” in *Optical Fiber Communication Conference*, 2014, p. W4J.2.
- [26] T. Kobayashi, H. Takara, A. Sano, T. Mizuno, H. Kawakami, Y. Miyamoto, K. Hiraga, Y. Abe, H. Ono, M. Wada, Y. Sasaki, I. Ishida, K. Takenaga, S. Matsuo, K. Saitoh, M. Yamada, H. Masuda, and T. Morioka, “2 #x00D7; 344 Tb/s propagation-direction interleaved transmission over 1500-km MCF enhanced by multicarrier full electric-field digital back-propagation,” in *39th European Conference and Exhibition on Optical Communication (ECOC 2013)*, 2013, pp. 1–3.
- [27] Y. Abe, K. Shikama, S. Yanagi, and T. Takahashi, “Low-loss Physical-contact-type Fan-out Device for 12-core Multicore Fiber,” 2013.
- [28] S. Chandrasekhar, A. H. Gnauck, X. Liu, P. J. Winzer, Y. Pan, E. C. Burrows, T. F. Taunay, B. Zhu, M. Fishteyn, M. F. Yan, J. M. Fini, E. M. Monberg, and F. V. Dimarcello, “WDM/SDM transmission of 10 x 128-Gb/s PDM-QPSK over 2688-km 7-core fiber with a per-fiber net aggregate spectral-efficiency distance product of 40,320 km·b/s/Hz,” *Opt. Express*, vol. 20, no. 2, pp. 706–711, Jan. 2012.
- [29] R. Ryf, R.-J. Essiambre, A. H. Gnauck, S. Randel, M. A. Mestre, C. Schmidt, P. J. Winzer, R. Delbue, P. Pupalaiakis, and A. Sureka, “Space-division multiplexed transmission over 4200-km 3-core microstructured fiber,” in *Optical Fiber Communication Conference*

- and Exposition (OFC/NFOEC), 2012 and the National Fiber Optic Engineers Conference, 2012, pp. 1–3.
- [30] J. Li, E. Tipsuwannakul, T. Eriksson, M. Karlsson, and P. A. Andrekson, “Approaching Nyquist Limit in WDM Systems by Low-Complexity Receiver-Side Duobinary Shaping,” *J. Light. Technol.*, vol. 30, no. 11, pp. 1664–1676, Jun. 2012.
- [31] J. Zhang, J. Yu, and N. Chi, “Generation and transmission of 512-Gb/s quad-carrier digital super-Nyquist spectral shaped signal,” *Opt. Express*, vol. 21, no. 25, pp. 31212–31217, Dec. 2013.
- [32] T. Mizuno, T. Kobayashi, H. Takara, A. Sano, H. Kawakami, T. Nakagawa, Y. Miyamoto, Y. Abe, T. Goh, M. Oguma, and T. Morioka, “12-core x 3-mode Dense Space Division Multiplexed Transmission over 40 km Employing Multi-carrier Signals with Parallel MIMO Equalization,” in *Optical Fiber Communication Conference*, 2014, p. Th5B.2.
- [33] R. Ryf, N. K. Fontaine, H. Chen, B. Guan, S. Randel, N. Sauer, S. J. B. Yoo, A. M. J. Koonen, R. Delbue, P. Pupalais, A. Sureka, R. Shubochkin, Y. Sun, and R. Lingle, “23 Tbit/s Transmission over 17-km Conventional 50- μ m Graded-Index Multimode Fiber,” in *Optical Fiber Communication Conference*, 2014, p. Th5B.1.
- [34] S. Berdagué and P. Facq, “Mode division multiplexing in optical fibers,” *Appl. Opt.*, vol. 21, no. 11, pp. 1950–1955, Jun. 1982.
- [35] H. R. Stuart, “Dispersive Multiplexing in Multimode Optical Fiber,” *Science*, vol. 289, no. 5477, pp. 281–283, Jul. 2000.
- [36] G. J. Foschini, “Layered space-time architecture for wireless communication in a fading environment when using multi-element antennas,” *Bell Labs Tech. J.*, vol. 1, no. 2, pp. 41–59, Jun. 1996.
- [37] G. J. Foschini and M. J. Gans, “On Limits of Wireless Communications in a Fading Environment when Using Multiple Antennas,” *Wirel. Pers. Commun.*, vol. 6, no. 3, pp. 311–335, Mar. 1998.
- [38] T. Koonen, H. van den Boom, I. Tafur Monroy, and G.-D. Khoe, “High capacity multi-service in-house networks using mode group diversity multiplexing,” in *Optical Fiber Communication Conference*, 2004, p. FG4.
- [39] M. De Boer, C. P. Tsekrekos, A. Martinez, H. Kurniawan, J. W. M. Bergmans, A. M. J. Koonen, H. P. A. Van den Boom, and F. M. J. Willems, “A first demonstrator for a mode group diversity multiplexing communication system,” in *Optical Fibre Communications and Electronic Signal Processing, 2005. The IEE Seminar on (Ref. No. 2005-11310)*, 2005, pp. 0_46–16/5.

- [40] C. P. Tsekrekos, M. De Boer, A. Martinez, F. M. J. Willems, and A. M. J. Koonen, "Demonstration of a Transparent 2-Input 2-Output Mode Group Diversity Multiplexing Link," in *European Conference on Optical Communications, 2006. ECOC 2006*, 2006, pp. 1–2.
- [41] S. Schollmann, S. Soneff, and W. Rosenkranz, "10.7 Gb/s Over 300 m GI-MMF Using a 2 × 2 MIMO System Based on Mode Group Diversity Multiplexing," in *Conference on Optical Fiber Communication and the National Fiber Optic Engineers Conference, 2007. OFC/NFOEC 2007*, 2007, pp. 1–3.
- [42] A. Tarighat, R. C. J. Hsu, A. Shah, A. H. Sayed, and B. Jalali, "Fundamentals and challenges of optical multiple-input multiple-output multimode fiber links [Topics in Optical Communications]," *IEEE Commun. Mag.*, vol. 45, no. 5, pp. 57–63, May 2007.
- [43] W. Van Etten and J. Van der Plaats, *Principles of optical fibre communications*. Prentice Hall International, 1990.
- [44] K. Okamoto, *Fundamentals of optical waveguides*. San Diego: Academic Press, 2000.
- [45] L. Tong, J. Lou, and E. Mazur, "Single-mode guiding properties of subwavelength-diameter silica and silicon wire waveguides," *Opt. Express*, vol. 12, no. 6, pp. 1025–1035, Mar. 2004.
- [46] R. Ryf, R. Essiambre, J. Von Hoyningen-Huene, and P. J. Winzer, "Analysis of mode-dependent gain in Raman amplified few-mode fiber," in *Optical Fiber Communication Conference and Exposition (OFC/NFOEC), 2012 and the National Fiber Optic Engineers Conference, 2012*, pp. 1–3.
- [47] R. Ryf, S. Randel, A. H. Gnauck, C. Bolle, A. Sierra, S. Mumtaz, M. Esmaeelpour, E. C. Burrows, R. Essiambre, P. J. Winzer, D. W. Peckham, A. H. McCurdy, and R. Lingle, "Mode-Division Multiplexing Over 96 km of Few-Mode Fiber Using Coherent 6 × 6 MIMO Processing," *J. Light. Technol.*, vol. 30, no. 4, pp. 521–531, 2012.
- [48] A. Li, A. A. Amin, X. Chen, S. Chen, G. Gao, and W. Shieh, "Reception of Dual-Spatial-Mode CO-OFDM Signal Over a Two-Mode Fiber," *J. Light. Technol.*, vol. 30, no. 4, pp. 634–640, Feb. 2012.
- [49] A. M. J. Koonen, H. Chen, H. P. A. Van den Boom, and O. Raz, "Silicon Photonic Integrated Mode Multiplexer and Demultiplexer," *IEEE Photonics Technol. Lett.*, vol. 24, no. 21, pp. 1961–1964, 2012.
- [50] H. Chen, S. Zou, and A. M. J. Chen, "Statistical Analysis of the Performance of Cyclic-prefixed and Zero-padded OFDM over Multimode Fibers," in *Asia Communications and Photonics*

- Conference*, 2013, p. AW4G.5.
- [51] H. Chen and T. Koonen, "Single Multi-mode Mask for Multi-channel Mode Division Demultiplexing," in *Optical Fiber Communication Conference/National Fiber Optic Engineers Conference 2013*, 2013, p. OT1B.4.
 - [52] R. Ryf, M. A. Mestre, A. Gnauck, S. Randel, C. Schmidt, R. Essiambre, P. Winzer, R. Delbue, P. Pupalaiakis, and A. Sureka, "Low-loss mode coupler for mode-multiplexed transmission in few-mode fiber," in *National Fiber Optic Engineers Conference*, 2012.
 - [53] H. Chen, V. Sleiffer, F. Huijskens, R. van Uden, C. Okonkwo, P. Leoni, M. Kuschnerov, L. Gruner-Nielsen, Y. Sun, H. de Waardt, and T. Koonen, "Employing Prism-Based Three-Spot Mode Couplers for High Capacity MDM/WDM Transmission," *IEEE Photonics Technol. Lett.*, vol. 25, no. 24, pp. 2474–2477, 2013.
 - [54] H. Chen and T. Koonen, "Scalable multi-segment Phase Mask for spatial power splitting and mode division demultiplexing," in *39th European Conference and Exhibition on Optical Communication (ECOC 2013)*, 2013, pp. 1–3.
 - [55] N. K. Fontaine, R. Ryf, J. Bland-Hawthorn, and S. G. Leon-Saval, "Geometric requirements for photonic lanterns in space division multiplexing," *Opt. Express*, vol. 20, no. 24, pp. 27123–27132, 2012.
 - [56] V. A. J. M. Sleiffer, H. Chen, Y. Jung, M. Kuschnerov, D. J. Richardson, S. U. Alam, Y. Sun, L. Gruner-Nielsen, N. Pavarelli, B. Snyder, P. O'Brien, A. D. Ellis, A. M. J. Koonen, and H. de Waardt, "480 km transmission of MDM 576-Gb/s 8QAM using a few-mode re-circulating loop," in *2013 IEEE Photonics Conference (IPC)*, 2013, pp. 1–2.
 - [57] R. Ryf, N. K. Fontaine, and R.-J. Essiambre, "Spot-based mode coupler for mode-multiplexed transmission in few-mode fiber," in *Photonics Society Summer Topical Meeting Series, 2012 IEEE*, 2012, pp. 199–200.
 - [58] C. Koebele, M. Salsi, L. Milord, R. Ryf, C. Bolle, P. Sillard, S. Bigo, and G. Charlet, "40km transmission of five mode division multiplexed data streams at 100Gb/s with low MIMO-DSP complexity," in *2011 37th European Conference and Exhibition on Optical Communication (ECOC)*, 2011, pp. 1–3.
 - [59] H. Chen, V. Sleiffer, B. Snyder, M. Kuschnerov, R. van Uden, Y. Jung, C. M. Okonkwo, O. Raz, P. O'Brien, H. de Waardt, and T. Koonen, "Demonstration of a Photonic Integrated Mode Coupler With MDM and WDM Transmission," *IEEE Photonics Technol. Lett.*, vol. 25, no. 21, pp. 2039–2042, 2013.

- [60] K.-P. Ho and J. M. Kahn, "Mode Coupling and its Impact on Spatially Multiplexed Systems," in *Optical Fiber Telecommunications*, Elsevier, 2013, pp. 491–568.
- [61] J. M. Kahn, K.-P. Ho, and M. Bagher Shemirani, "Mode coupling effects in multi-mode fibers," in *Optical Fiber Communication Conference*, 2012, p. OW3D-3.
- [62] S. Warm and K. Petermann, "Capacity increase in spliced mode-multiplexed transmission systems by using mode mixers," in *2012 IEEE Photonics Society Summer Topical Meeting Series*, 2012, pp. 201–202.
- [63] A. Goldsmith, *Wireless Communications*. Cambridge University Press, 2005.
- [64] J. Wang, J.-Y. Yang, I. M. Fazal, N. Ahmed, Y. Yan, H. Huang, Y. Ren, Y. Yue, S. Dolinar, M. Tur, and A. E. Willner, "Terabit free-space data transmission employing orbital angular momentum multiplexing," *Nat. Photonics*, vol. 6, no. 7, pp. 488–496, Jun. 2012.
- [65] B. Guan, R. P. Scott, N. K. Fontaine, T. Su, C. Ferrari, M. Cappuzzo, F. Klemens, B. Keller, M. Earnshaw, and S. J. Yoo, "Integrated Optical Orbital Angular Momentum Multiplexing Device using 3-D Waveguides and a Silica PLC," in *CLEO: Science and Innovations*, 2013.
- [66] N. K. Fontaine, R. Ryf, S. G. Leon-Saval, and J. Bland-Hawthorn, "Evaluation of photonic lanterns for lossless mode-multiplexing," in *European Conference and Exhibition on Optical Communication*, 2012.
- [67] M. Sakakura, T. Sawano, Y. Shimotsuma, K. Miura, and K. Hirao, "Fabrication of three-dimensional 1×4 splitter waveguides inside a glass substrate with spatially phase modulated laser beam," *Opt. Express*, vol. 18, no. 12, pp. 12136–12143, 2010.
- [68] M. Kuschnerov, F. N. Hauske, K. Piyawanno, B. Spinnler, A. Napoli, and B. Lankl, "Adaptive chromatic dispersion equalization for non-dispersion managed coherent systems," in *Optical Fiber Communication Conference*, 2009.
- [69] A. Viterbi, "Nonlinear estimation of PSK-modulated carrier phase with application to burst digital transmission," *IEEE Trans. Inf. Theory*, vol. 29, no. 4, pp. 543–551, 1983.
- [70] R. G. H. van Uden, C. M. Okonkwo, V. A. J. M. Sleiffer, M. Kuschnerov, H. de Waardt, and A. M. J. Koonen, "Single DPLL Joint Carrier Phase Compensation for Few-Mode Fiber Transmission," *IEEE Photonics Technol. Lett.*, vol. 25, no. 14, pp. 1381–1384, Jul. 2013.

- [71] M. S. Faruk and K. Kikuchi, "Adaptive frequency-domain equalization in digital coherent optical receivers," *Opt. Express*, vol. 19, no. 13, pp. 12789–12798, Jun. 2011.
- [72] N. Bai and G. Li, "Adaptive Frequency-Domain Equalization for Mode-Division Multiplexed Transmission," *IEEE Photonics Technol. Lett.*, vol. 24, no. 21, pp. 1918–1921, 2012.
- [73] S. Randel, P. J. Winzer, M. Montoliu, and R. Ryf, "Complexity analysis of adaptive frequency-domain equalization for MIMO-SDM transmission," in *Optical Communication (ECOC 2013), 39th European Conference and Exhibition on*, 2013, pp. 1–3.
- [74] H. S. Chen, H. P. A. van den Boom, and A. M. J. Koonen, "30-Gb/s 3×3 Optical Mode Group-Division-Multiplexing System With Optimized Joint Detection," *IEEE Photonics Technol. Lett.*, vol. 23, pp. 1283–1285, Sep. 2011.
- [75] H. Chen, B. H.P.A. van den, and T. Koonen, "30Gbit/s 3×3 Optical Mode Group Division Multiplexing System with Mode-Selective Spatial Filtering," in *Optical Fiber Communication Conference/National Fiber Optic Engineers Conference 2011*, 2011, p. OWB1.
- [76] H. Chen, T. Koonen, R. van Uden, H. van den Boom, and O. Raz, "Integrated Mode Group Division Multiplexer and Demultiplexer Based on 2-Dimensional Vertical Grating Couplers," in *European Conference and Exhibition on Optical Communication*, 2012, p. Th.1.B.2.
- [77] L. Raddatz, I. H. White, D. G. Cunningham, and M. C. Nowell, "An experimental and theoretical study of the offset launch technique for the enhancement of the bandwidth of multimode fiber links," *J. Light. Technol.*, vol. 16, no. 3, pp. 324–331, 1998.
- [78] D. H. Sim, Y. Takushima, and Y. C. Chung, "High-Speed Multimode Fiber Transmission by Using Mode-Field Matched Center-Launching Technique," *J. Light. Technol.*, vol. 27, no. 8, pp. 1018–1026, Apr. 2009.
- [79] L. Geng, C. H. Kwok, S. H. Lee, J. D. Ingham, R. V. Penty, I. H. White, and D. G. Cunningham, "Efficient line launch for bandwidth improvement of 10 Gbit/s multimode fibre links using elliptical Gaussian beam," in *Optical Communication (ECOC), 2010 36th European Conference and Exhibition on*, 2010, pp. 1–3.
- [80] L. Geng, S. H. Lee, K. A. William, R. V. Penty, I. H. White, and D. G. Cunningham, "Symmetrical 2-D hermite-gaussian square launch for high bit rate transmission in multimode fiber links," in *Optical Fiber Communication Conference and Exposition (OFC/NFOEC)*,

- 2011 and the National Fiber Optic Engineers Conference, 2011, pp. 1–3.
- [81] C. H. Kwok, R. V. Penty, I. H. White, and D. G. Cunningham, “Novel passive launch scheme for ultimate bandwidth improvement of graded-index multimode fibers,” in *Optical Fiber Communication (OFC), collocated National Fiber Optic Engineers Conference, 2010 Conference on (OFC/NFOEC)*, 2010, pp. 1–3.
- [82] P. S. Chow, J. M. Cioffi, and J. A. C. Bingham, “A practical discrete multitone transceiver loading algorithm for data transmission over spectrally shaped channels,” *IEEE Trans. Commun.*, vol. 43, no. 234, pp. 773–775, 1995.
- [83] S. C. Jeffrey Lee, F. Breyer, S. Randel, H. van den Boom, and A. M. Koonen, “High-speed transmission over multimode fiber using discrete multitone modulation [Invited],” *J. Opt. Netw.*, vol. 7, no. 2, pp. 183–196, 2008.
- [84] D. Visani, C. M. Okonkwo, S. Loquai, H. Yang, Y. Shi, H. P. van den Boom, T. Ditewig, G. Tartarini, B. Schmauss, and S. Randel, “Record 5.3 Gbit/s transmission over 50m 1mm core diameter graded-index plastic optical fiber,” in *Optical Fiber Communication Conference*, 2010.
- [85] Z. Wang and G. B. Giannakis, “Wireless multicarrier communications,” *IEEE Signal Process. Mag.*, vol. 17, no. 3, pp. 29–48, May 2000.
- [86] H. Chen, A. M. J. Koonen, and S. Zou, “Statistical Analysis of the Performance of Cyclic-prefixed and Zero-padded OFDM over Multimode Fibers,” in *Asia Communications and Photonics Conference*, 2013, p. AW4G.5.
- [87] P. Medina, V. Almenar, and J. L. Corral, “Evaluation of optical ZP-OFDM transmission performance in multimode fiber links,” *Opt. Express*, vol. 22, no. 1, p. 1008, Jan. 2014.
- [88] H. R. Stuart, “Dispersive Multiplexing in Multimode Optical Fiber,” *Science*, vol. 289, no. 5477, pp. 281–283, Jul. 2000.
- [89] T. Koonen, H. van den Boom, I. T. Monroy, and G.-D. Khoe, “High capacity multiservice in-house networks using mode group diversity multiplexing,” in *Optical Fiber Communication Conference, 2004. OFC 2004*, 2004, vol. 2, p. 3 pp. vol.2–.
- [90] “Mode group diversity multiplexing in multimode fiber transmission systems.” [Online]. Available: <http://www.tue.nl/en/publication/ep/p/d/ep-uid/214803/>. [Accessed: 16-Feb-2014].
- [91] C. P. Tsekrekos and A. M. J. Koonen, “Mitigation of Impairments in

- MGDM Transmission With Mode-Selective Spatial Filtering,” *IEEE Photonics Technol. Lett.*, vol. 20, no. 13, pp. 1112–1114, 2008.
- [92] C. P. Tsekrekos and A. M. J. Koonen, “Mode-selective spatial filtering for increased robustness in a mode group diversity multiplexing link,” *Opt. Lett.*, vol. 32, no. 9, pp. 1041–1043, May 2007.
- [93] K. M. Patel and S. E. Ralph, “Multimode fiber link equalization by mode filtering via a multisegment photodetector,” in *Microwave Symposium Digest, 2003 IEEE MTT-S International*, 2003, vol. 2, pp. 1343–1346 vol.2.
- [94] K. M. Patel, “Spatially Resolved Equalization: A New Concept in Intermodal Dispersion Compensation for Multimode Fiber,” 2004.
- [95] A. Koonen, “Bit-error-rate degradation in a multimode fiber optic transmission link due to modal noise,” *Sel. Areas Commun. IEEE J. On*, vol. 4, no. 9, pp. 1515–1522, 1986.
- [96] J. Carpenter and T. D. Wilkinson, “All Optical Mode-Multiplexing Using Holography and Multimode Fiber Couplers,” *J. Light. Technol.*, vol. 30, no. 12, pp. 1978–1984, Jun. 2012.
- [97] C. R. Doerr, “Proposed Architecture for MIMO Optical Demultiplexing Using Photonic Integration,” *IEEE Photonics Technol. Lett.*, vol. 23, no. 21, pp. 1573–1575, Nov. 2011.
- [98] H.-S. Chen, P. A. van den Boom, and A. M. J. Koonen, “WDM 2 x 2 mode group division multiplexing system and investigation of polarisation division multiplexing,” *Electron. Lett.*, vol. 47, no. 23, pp. 1289–1290, 2011.
- [99] H. Takara, A. Sano, T. Kobayashi, H. Kubota, H. Kawakami, A. Matsuura, Y. Miyamoto, Y. Abe, H. Ono, and K. Shikama, “1.01-Pb/s (12 SDM/222 WDM/456 Gb/s) crosstalk-managed transmission with 91.4-b/s/Hz aggregate spectral efficiency,” in *European Conference and Exhibition on Optical Communication*, 2012.
- [100] S. Matsuo, Y. Sasaki, I. Ishida, K. Takenaga, K. Saitoh, and M. Koshiba, “Recent Progress in Multi core and Few mode Fiber,” in *Optical Fiber Communication Conference/National Fiber Optic Engineers Conference 2013*, 2013, p. OM3I.3.
- [101] B. Zhu, T. F. Taunay, M. F. Yan, J. M. Fini, M. Fishteyn, E. M. Monberg, and F. V. Dimarcello, “Seven-core multicore fiber transmissions for passive optical network,” *Opt. Express*, vol. 18, no. 11, pp. 11117–11122, May 2010.
- [102] K. Igarashi, K. Takeshima, T. Tsuritani, H. Takahashi, S. Sumita, I. Morita, Y. Tsuchida, M. Tadakuma, K. Maeda, T. Saito, K. Watanabe, K. Imamura, R. Sugizaki, and M. Suzuki, “110.9-Tbit/s

- SDM transmission over 6,370 km using a full C-band seven-core EDFA,” *Opt. Express*, vol. 21, no. 15, pp. 18053–18060, Jul. 2013.
- [103] J. Carpenter, B. C. Thomsen, and T. D. Wilkinson, “Degenerate Mode-Group Division Multiplexing,” 2012.
- [104] J. Carpenter, B. Thomsen, and T. D. Wilkinson, “2x56-Gb/s Mode-Division Multiplexed Transmission Over 2km of OM2 Multimode Fibre Without MIMO Equalization,” in *European Conference and Exhibition on Optical Communication*, 2012.
- [105] S. Randel, R. Ryf, A. Sierra, P. J. Winzer, A. H. Gnauck, C. A. Bolle, R.-J. Essiambre, D. W. Peckham, A. McCurdy, and R. Lingle, “6x56-Gb/s mode-division multiplexed transmission over 33-km few-mode fiber enabled by 6x6 MIMO equalization,” *Opt. Express*, vol. 19, no. 17, pp. 16697–16707, 2011.
- [106] C. Koebele, M. Salsi, D. Sperti, P. Tran, P. Brindel, H. Mardoyan, S. Bigo, A. Boutin, F. Verluise, P. Sillard, M. Astruc, L. Provost, F. Cerou, and G. Charlet, “Two mode transmission at 2x100Gb/s, over 40km-long prototype few-mode fiber, using LCOS-based programmable mode multiplexer and demultiplexer,” *Opt. Express*, vol. 19, no. 17, pp. 16593–16600, Aug. 2011.
- [107] J. Carpenter and T. D. Wilkinson, “Characterization of multimode fiber by selective mode excitation,” *J. Light. Technol.*, vol. 30, no. 10, pp. 1386–1392, 2012.
- [108] J. von Hoyningen-Huene, R. Ryf, and P. Winzer, “LCoS-based mode shaper for few-mode fiber,” *Opt. Express*, vol. 21, no. 15, pp. 18097–18110, Jul. 2013.
- [109] G. J. Swanson, “Binary optics technology: theoretical limits on the diffraction efficiency of multilevel diffractive optical elements,” DTIC Document, 1991.
- [110] E. Neiss, M. Flury, L. Mager, J.-L. Rehspringer, A. Fort, P. Montgomery, P. Gérard, J. Fontaine, and S. Robert, “Multi-level diffractive optical elements produced by excimer laser ablation of sol-gel,” *Opt. Express*, vol. 16, no. 18, pp. 14044–14056, Sep. 2008.
- [111] H. S. Chen and A. M. J. Koonen, “LP01 and LP11 mode division multiplexing link with mode crossbar switch,” *Electron. Lett.*, vol. 48, no. 19, pp. 1222–1223, 2012.
- [112] A. Albores-Mejia, F. Gomez-Agis, H. J. S. Dorren, X. J. M. Leijtens, T. de Vries, Y.-S. Oei, M. J. R. Heck, R. Notzel, D. J. Robbins, M. K. Smit, and K. A. Williams, “Monolithic Multistage Optoelectronic Switch Circuit Routing 160 Gb/s Line-Rate Data,” *J. Light. Technol.*, vol. 28, no. 20, pp. 2984–2992, Oct. 2010.
- [113] P. J. Winzer, A. H. Gnauck, A. Konczykowska, F. Jorge, and J.-Y.

- Dupuy, "Penalties from in-band crosstalk for advanced optical modulation formats," in *2011 37th European Conference and Exhibition on Optical Communication (ECOC)*, 2011, pp. 1–3.
- [114] P. J. Winzer, "Spatial multiplexing: The next frontier in network capacity scaling," in *39th European Conference and Exhibition on Optical Communication (ECOC 2013)*, 2013, pp. 1–4.
- [115] S. Warm and K. Petermann, "Splice loss requirements in multi-mode fiber mode-division-multiplex transmission links," *Opt. Express*, vol. 21, no. 1, pp. 519–532, Jan. 2013.
- [116] C. R. Doerr and T. F. Taunay, "Silicon Photonics Core-, Wavelength-, and Polarization-Diversity Receiver," *IEEE Photonics Technol. Lett.*, vol. 23, no. 9, pp. 597–599, May 2011.
- [117] C. R. Doerr, N. Fontaine, M. Hirano, T. Sasaki, L. Buhl, and P. Winzer, "Silicon photonic integrated circuit for coupling to a ring-core multimode fiber for space-division multiplexing," in *European Conference and Exposition on Optical Communications*, 2011.
- [118] N. K. Fontaine, C. R. Doerr, M. A. Mestre, R. Ryf, P. Winzer, L. Buhl, Y. Sun, X. Jiang, and R. Lingle, "Space-division multiplexing and all-optical MIMO demultiplexing using a photonic integrated circuit," in *Optical Fiber Communication Conference*, 2012.
- [119] X. Chen, C. Li, and H. K. Tsang, "Two dimensional silicon waveguide chirped grating couplers for vertical optical fibers," *Opt. Commun.*, vol. 283, no. 10, pp. 2146–2149, May 2010.
- [120] V. A. J. M. Sleiffer, M. Kushnerov, R. G. H. van Uden, and H. de Waardt, "Differential Phase Frame Synchronization for Coherent Transponders," *IEEE Photonics Technol. Lett.*, vol. 25, no. 21, pp. 2137–2140, Nov. 2013.
- [121] F. Poletti, N. V. Wheeler, M. N. Petrovich, N. Baddela, E. Numkam Fokoua, J. R. Hayes, D. R. Gray, Z. Li, R. Slavík, and D. J. Richardson, "Towards high-capacity fibre-optic communications at the speed of light in vacuum," *Nat. Photonics*, vol. 7, no. 4, pp. 279–284, Mar. 2013.
- [122] Y. Jung, V. Sleiffer, N. Baddela, M. Petrovich, J. R. Hayes, N. Wheeler, D. Gray, E. R. Numkam Fokoua, J. Wooler, N. Wong, F. Parmigiani, S.-U. Alam, J. Surof, M. Kushnerov, V. Veljanovski, de, Hugo Waardt, F. Poletti, and D. J. Richardson, "First Demonstration of a Broadband 37-cell Hollow Core Photonic Bandgap Fiber and Its Application to High Capacity Mode Division Multiplexing," in *Optical Fiber Communication Conference/National Fiber Optic Engineers Conference 2013*, 2013, p. PDP5A.3.
- [123] J. W. Nicholson, A. D. Yablon, J. M. Fini, and M. D. Mermelstein,

- “Measuring the Modal Content of Large-Mode-Area Fibers,” *IEEE J. Sel. Top. Quantum Electron.*, vol. 15, no. 1, pp. 61–70, 2009.
- [124] L. A. Johansson, S. Estrella, J. Thomas, S. Kumar, M. Mashanovitch, and J. S. Barton, “Integrated Indium Phosphide Coherent Optical Receivers and Transmitters,” 2012.
- [125] B. Snyder and P. O’Brien, “Packaging Process for Grating-Coupled Silicon Photonic Waveguides Using Angle-Polished Fibers,” *IEEE Trans. Compon. Packag. Manuf. Technol.*, vol. 3, no. 6, pp. 954–959, 2013.
- [126] D. D’Agostino, E. Kleijn, R. Santos, H. P. M. M. Ambrosius, and M. K. Smit, “A dense spot size converter array fabricated in a generic process on InP,” 2013, vol. 8767, p. 87670Q–87670Q–11.
- [127] R. Ryf, N. K. Fontaine, and R.-J. Essiambre, “Spot-Based Mode Couplers for Mode-Multiplexed Transmission in Few-Mode Fiber,” *IEEE Photonics Technol. Lett.*, vol. 24, no. 21, pp. 1973–1976, 2012.
- [128] H. Chen, V. Sleiffer, R. van Uden, C. Okonkwo, M. Kuschnerov, F. Huijskens, L. Gruner-Nielsen, Y. Sun, H. de Waardt, and T. Koonen, “3 MDM amp;#x00D7;8 WDM amp;#x00D7;320-Gb/s DP-32QAM transmission over a 120km few-mode fiber span employing 3-spot mode couplers,” in *OptoElectronics and Communications Conference held jointly with 2013 International Conference on Photonics in Switching (OECC/PS), 2013 18th*, 2013, pp. 1–2.
- [129] R. Ryf, S. Randel, M. A. Mestre, C. Schmidt, A. H. Gnauck, R.-J. Essiambre, P. Winzer, R. Delbue, P. Pupalaiskis, and A. Sureka, “209-km single-span mode-and wavelength-multiplexed transmission over hybrid few-mode fiber,” in *European Conference and Exhibition on Optical Communication*, 2012.
- [130] R. Ryf, M. A. Mestre, S. Randel, X. Palou, A. H. Gnauck, R. Delbue, P. Pupalaiskis, A. Sureka, Y. Sun, and X. Jiang, “Combined SDM and WDM transmission over 700-km Few-Mode Fiber,” in *Optical Fiber Communication Conference*, 2013.
- [131] L. Gruner-Nielsen, Y. Sun, J. W. Nicholson, D. Jakobsen, R. Lingle, and B. Palsdottir, “Few Mode Transmission Fiber with low DGD, low Mode Coupling and low Loss,” in *National Fiber Optic Engineers Conference*, 2012, p. PDP5A.1.
- [132] V. A. J. M. Sleiffer, Y. Jung, N. K. Baddela, J. Surof, M. Kuschnerov, V. Veljanovski, J. R. Hayes, N. V. Wheeler, E. R. N. Fokoua, J. P. Wooler, D. R. Gray, N. H.-L. Wong, F. R. Parmigiani, S.-U. Alam, M. N. Petrovich, F. Poletti, D. J. Richardson, and H. de Waardt, “High Capacity Mode-Division Multiplexed Optical Transmission in a Novel 37-cell Hollow-Core Photonic Bandgap

- Fiber,” *J. Light. Technol.*, vol. 32, no. 4, pp. 854–863, Feb. 2014.
- [133] P. Leoni, V. Sleiffer, S. Calabrò, M. Kuschnerov, S. L. Jansen, B. Spinnler, and B. Lankl, “On the Performance of a Soft Decision FEC Scheme Operating in Highly Non-Linear Regime,” in *Advanced Photonics Congress*, 2012, p. SpTu3A.6.
- [134] A. A. Said, M. Dugan, P. Bado, Y. Bellouard, A. Scott, and J., Jose R. Mabesa, “Manufacturing by laser direct-write of three-dimensional devices containing optical and microfluidic networks,” 2004, vol. 5339, pp. 194–204.
- [135] Y. Bellouard, A. Said, M. Dugan, and P. Bado, “Monolithic three-dimensional integration of micro-fluidic channels and optical waveguides in fused silica,” in *MATERIALS RESEARCH SOCIETY SYMPOSIUM PROCEEDINGS*, 2004, vol. 782, pp. 63–68.
- [136] R. Ryf, N. K. Fontaine, M. A. Mestre, S. Randel, X. Palou, C. Bolle, A. H. Gnauck, S. Chandrasekhar, X. Liu, and B. Guan, “12 x 12 MIMO Transmission over 130-km Few-Mode Fiber,” in *Frontiers in Optics*, 2012.
- [137] S. G. Leon-Saval, T. A. Birks, J. Bland-Hawthorn, and M. Englund, “Multimode fiber devices with single-mode performance,” *Opt. Lett.*, vol. 30, no. 19, pp. 2545–2547, 2005.
- [138] D. Noordegraaf, P. M. Skovgaard, M. D. Nielsen, and J. Bland-Hawthorn, “Efficient multi-mode to single-mode coupling in a photonic lantern,” *Opt Express*, vol. 17, no. 3, pp. 1988–1994, 2009.
- [139] S. G. Leon-Saval, A. Argyros, and J. Bland-Hawthorn, “Photonic lanterns: a study of light propagation in multimode to single-mode converters,” *Opt Express*, vol. 18, no. 8, pp. 8430–8439, 2010.
- [140] N. K. Fontaine, “Photonic lantern spatial multiplexers in space-division multiplexing,” in *2013 IEEE Photonics Society Summer Topical Meeting Series*, 2013, pp. 97–98.
- [141] N. K. Fontaine, R. Ryf, M. A. Mestre, B. Guan, X. Palou, S. Randel, Y. Sun, L. Gruner-Nielsen, R. V. Jensen, and R. Lingle, “Characterization of Space-Division Multiplexing Systems using a Swept-Wavelength Interferometer,” in *Optical Fiber Communication Conference*, 2013.
- [142] S. Randel, M. A. Mestre, R. Ryf, and P. Winzer, “Digital signal processing in spatially-multiplexed coherent communication,” in *European Conference and Exhibition on Optical Communication*, 2012.
- [143] K. M. Davis, K. Miura, N. Sugimoto, and K. Hirao, “Writing waveguides in glass with a femtosecond laser,” *Opt. Lett.*, vol. 21, no. 21, pp. 1729–1731, Nov. 1996.

- [144] N. Psaila, “Couplers for Multicore Fibers and 3D Waveguide Technology,” in *Optical Fiber Communication Conference*, 2014, p. M3K.3.
- [145] B. Guan, R. P. Scott, C. Qin, N. K. Fontaine, T. Su, C. Ferrari, M. Cappuzzo, F. Klemens, B. Keller, M. Earnshaw, and S. J. B. Yoo, “Free-space coherent optical communication with orbital angular momentum multiplexing/demultiplexing using a hybrid 3D photonic integrated circuit,” *Opt. Express*, vol. 22, no. 1, p. 145, Dec. 2013.
- [146] Y. Jung, S. Alam, Z. Li, A. Dhar, D. Giles, I. Giles, J. Sahu, F. Poletti, and D. Richardson, “Detailed study of modal gain in a multimode EDFA supporting LP01 and LP11 mode group amplification,” in *Optical Fiber Communication Conference*, 2012, p. OM3C.4.
- [147] N. K. Fontaine, S. G. Leon-Saval, R. Ryf, J. S. Gil, B. Ercan, and J. Bland-Hawthorn, “Mode selective dissimilar fiber photonic-lantern spatial multiplexers for few-mode fiber,” in *Proceedings of European Conference on Optical Communication*, 2013.
- [148] S. Yerolatsitis and T. A. Birks, “Tapered mode multiplexer based on standard single-mode fibre,” in *Proceedings of European Conference on Optical Communication*, 2013.
- [149] S. Yerolatsitis, I. Gris-Sánchez, and T. A. Birks, “Adiabatically-tapered fiber mode multiplexers,” *Opt. Express*, vol. 22, no. 1, pp. 608–617, Jan. 2014.
- [150] S. G. Leon-Saval, N. K. Fontaine, J. R. Salazar-Gil, B. Ercan, R. Ryf, and J. Bland-Hawthorn, “Mode-selective photonic lanterns for space-division multiplexing,” *Opt. Express*, vol. 22, no. 1, pp. 1036–1044, Jan. 2014.

Acronyms

2D	2-dimensional
3DW	3-dimensional Waveguide
AR	Anti-reflection
BER	Bit Error Rate
CD	Chromatic Dispersion
CE	Coupling Efficiency
CFO	Carrier Frequency Offset
CMA	Constant Modulus Algorithm
CPE	Carrier Phase Estimation
CUT	Channel Under Test
DA	Data-aided
DAC	Digital-to-Analog Convertor
DD	Decision-directed
DEMUX	Demultiplexer
DFB	Distributed Feedback Laser
DGD	Differential Group Delay
DOE	Diffractive Optical Element
DQPSK	Differential Quadrature Phase Shift Keying
DSP	Digital Signal Processing
ECL	External Cavity Laser
EDFA	Erbium Doped Fiber Amplifier
EO	Eye Opening
EPS	Endless Phase Shifter

FDE	Frequency Domain Equalizer
FEC	Forward Error Correction
FIB	Focused Ion Beam
FIR	Finite Impulse Response
FMF	Few-mode Fiber
GI	Graded Index
HC	Hollow Core
InP	Indium Phosphide
LMS	Least Mean Square
LO	Local Oscillator
MCF	Multi-core Fiber
MDM	Mode Division Multiplexing
MFD	Mode Field Diameter
MGDM	Mode Group Division Multiplexing
MMF	Multi-mode Fiber
MPI	Multi-path Interference
MUX	Multiplexer
MZM	Mach-Zehnder Modulator
NA	Numerical Aperture
NFD	Near Field Pattern
OAM	Orbital Angular Momentum
OEO	Optical-electronic-optical
OSNR	Optical Signal Noise Ratio
PBC	Polarization Beam Combiner
PBGF	Photonic Bandgap Fiber
PBS	Polarization Beam Splitter
PC	Polarization Controller

PD	Photodiode
PDM	Polarization Division Multiplexing
PLC	Planar Lightwave Circuit
PRBS	Pseudo-random Binary Sequence
QAM	Quadrature Amplitude Modulation
QPSK	Quadrature Phase Shift Keying
ROADM	Reconfigurable Optical Add/drop Multiplexer
RF	Radio Frequency
SDM	Spatial Division Multiplexing
SEM	Scanning Electron Microscope
SI	Step-index
SMF	Single-mode Fiber
SNR	Signal-noise-ratio
SOP	State of Polarization
SOI	Silicon-on-Insulator
SSC	Spot Size Convertor
SVD	Singular Value Decomposition
TC	Tunable Coupler
TIR	Total Internal Reflection
VCSEL	Vertical Cavity Surface Emitting Laser
WDM	Wavelength Division Multiplexing
WSS	Wavelength Selective Switch
ZF	Zero Forcing

Acknowledgments

I would like to appreciate my promoter Prof. Ton Koonen for offering me this Ph.D position as part of the EU FP7 MODE-GAP project. Under this research collaborative project, I had the chance to contact with many advanced technologies and work with many brilliant but modest people.

I am grateful to Henrie van den Boom for his kind helps and supervisions, especially at the beginning of my Ph.D period when I was struggling to understand the “complicated” multi-mode world. I appreciate the valuable advices from Dr. Oded Raz and Prof. Kevin Williams for photonic integration. I am grateful to Vincent Sleiffer. Without his help and instructions, it would have been impossible to the large capacity combined MDM/WMD transmission demonstrations in the thesis. I also appreciate the time and efforts which Roy van Uden and Dr. Chigo Okonkwo have put for the transmission measurements. I want to thank Frans Huiskens, Dr. Eduward Tangdiongga, Dr. Huug de Waardt and Prof. Harm Dorren for their helps. During the Ph.D period, I had the pleasure of sharing the office with Dr. Nicola Calabretta, Dr. Aaron Albores-Mejia, Dr. Nikolaos Sotiropoulos, Diptanil Debbarma and Gonzalo Guelbenzu de Villota, who gave me a lot of suggestions and helps. Moreover, I appreciate Abhinav, Bo, Cac, Davide, Fausto, George, Hejie, Joanne, Johan, Jun, Karen, Patty, Piet, Pinxiang, Prasanna, Prometheus, Qing, Rongguo, Shihuan, Solomon, Stefano, Vlado, Wang, Yan, Zizheng and other colleagues in Electro-Optical Commutation (ECO) group in Eindhoven for the helps and happy talks.

I want to thank other colleagues in Eindhoven: Dr. Beatriz Barcones Campo, Dr. Erwin Bente, Dr. Jos van der Tol, Dr. Xaveer Leijtens, Barry, Domenico, Dzmityr, Tjibbe, Yuqing, Jing, Longfei, Rui and Srivathsa for their kind helps and discussions.

I would like to appreciate my friends and MODE-GAP colleagues: Dr. Brad Snyder, Dr. Nicola Pavarelli, Dr. Hua Yang, Dr. Peter O'Brien and Nan Ye in Cork, Ireland, Dr. Maxim Kuschnerov, Yingkan Chen, Paolo Leoni, Beril Inan, Adriana Lobato, Talha Rahman, Dr. Antonio Napoli and Johannes Rabe in

Munich, Germany and Dr Yongmin Jung, Zhihong Li and Eric Numkam Fokoua in Southampton, UK, for their helps and discussions.

I would like to thank Dr. Bob Tkach for giving the internship chance in Bell labs, Crawford Hill in my last Ph.D year. I appreciate the daily supervision from Dr. Roland Ryf and Dr. Nicolas Fontaine during the internship. I am also grateful to Binbin Guan, Dr. David Neilson, Dr. René-Jean Essiambre, Greg Raybon, Dr. Po Dong, Dr. Chongjin Xie, Dr. Sebastian Randel, Dr. Peter Winzer, Dr. Liming Zhang, Dr. Xiang Liu for their helps and discussions.

I would like to thank the committee members for reviewing my thesis and providing the valuable comments and suggestions. Moreover, I really appreciate Dr. Nicolas Fontaine's instructions, valuable discussions, helps and contributions to this thesis. Although he is not in the official list of the committee members, in my mind, he is the "ninth" committee member, who provides a continuous support.

Finally, I would like to thank my parents, my uncle and my grandmother for their unconditional love and encouragement.

List of Publications

All publications are ranked chronologically.

Journals:

- [1] R. van Uden, C. Okonkwo, H. Chen, H. de Waardt, and A. Koonen, "28GBaud 32QAM FMF Transmission with Low Complexity Phase Estimators and Single DPLL," *IEEE Photonics Technol. Lett.*, vol. Early Access Online, 2014.
- [2] H. Chen, V. Sleiffer, B. Snyder, M. Kuschnerov, R. van Uden, Y. Jung, C. M. Okonkwo, O. Raz, P. O'Brien, H. de Waardt, and T. Koonen, "Demonstration of a Photonic Integrated Mode Coupler With MDM and WDM Transmission," *IEEE Photonics Technol. Lett.*, vol. 25, no. 21, pp. 2039–2042, 2013.
- [3] H. Chen, V. Sleiffer, F. Huijskens, R. van Uden, C. Okonkwo, P. Leoni, M. Kuschnerov, L. Gruner-Nielsen, Y. Sun, H. de Waardt, and T. Koonen, "Employing Prism-Based Three-Spot Mode Couplers for High Capacity MDM/WDM Transmission," *IEEE Photonics Technol. Lett.*, vol. 25, no. 24, pp. 2474–2477, 2013.
- [4] V. A. J. M. Sleiffer, H. Chen, Y. Jung, P. Leoni, M. Kuschnerov, A. Simperler, H. Fabian, H. Schuh, F. Kub, D. J. Richardson, S. U. Alam, L. Grüner-Nielsen, Y. Sun, A. M. J. Koonen, and H. de Waardt, "Field demonstration of mode-division multiplexing upgrade scenarios on commercial networks," *Opt. Express*, vol. 21, no. 25, p. 31036, Dec. 2013.
- [5] B. Yang, X. Jin, H. Chi, X. Zhang, S. Zheng, S. Zou, H. Chen, E. Tangdiongga, and T. Koonen, "Optically Tunable Frequency-Doubling Brillouin Optoelectronic Oscillator With Carrier Phase-Shifted Double Sideband Modulation," *IEEE Photonics Technol. Lett.*, vol. 24, no. 12, pp. 1051–1053, 2012.
- [6] A. M. J. Koonen, H. Chen, H. P. A. Van den Boom, and O. Raz, "Silicon Photonic Integrated Mode Multiplexer and Demultiplexer," *IEEE Photonics Technol. Lett.*, vol. 24, no. 21, pp. 1961–1964, 2012.

- [7] H. Chen, H. P. A. Van den Boom, E. Tangdiongga, and T. Koonen, "30-Gb/s Bidirectional Transparent Optical Transmission With an MMF Access and an Indoor Optical Wireless Link," *IEEE Photonics Technol. Lett.*, vol. 24, no. 7, pp. 572–574, 2012.
- [8] H. Chen and A. M. J. Koonen, "LP01 and LP11 mode division multiplexing link with mode crossbar switch," *Electron. Lett.*, vol. 48, no. 19, pp. 1222–1223, 2012.
- [9] H. Chen, P. A. van den Boom, and A. M. J. Koonen, "WDM 2 x 2 mode group division multiplexing system and investigation of polarisation division multiplexing," *Electron. Lett.*, vol. 47, no. 23, pp. 1289–1290, 2011.
- [10] H. Chen, H. P. A. van den Boom, and A. M. J. Koonen, "30-Gb/s 3×3 Optical Mode Group-Division-Multiplexing System With Optimized Joint Detection," *IEEE Photonics Technol. Lett.*, vol. 23, pp. 1283–1285, Sep. 2011.

Conferences:

- [1] R. Ryf, N. K. Fontaine, H. Chen, B. Guan, S. Randel, N. Sauer, S. J. B. Yoo, A. M. J. Koonen, R. Delbue, P. Pupalakis, A. Sureka, R. Shubochkin, Y. Sun, and R. Lingle, "23 Tbit/s Transmission over 17-km Conventional 50- μ m Graded-Index Multimode Fiber," in *Optical Fiber Communication Conference*, 2014, p. Th5B.1. (**post-deadline paper**)
- [2] N. K. Fontaine, B. Guan, R. Ryf, H. Chen, A. M. J. Koonen, S. J. B. Yoo, K. S. Abedin, J. M. Fini, T. Taunay and D. T. Neilson, "Programmable Gain Equalizer for Multicore Fiber Amplifiers," in *Optical Fiber Communication Conference*, 2014, p. Th5C.5. (**post-deadline paper**)
- [3] J. (Shihuan) Zou, H. Chen, F. Huijskens, Z. Cao, E. Tangdiongga, and T. Koonen, "Demonstration of Fully Functional MIMO Wireless LAN Transmission over GI-MMF for In-building Networks," in *Optical Fiber Communication Conference/National Fiber Optic Engineers Conference 2013*, 2013, p. JTh2A.08.
- [4] R. G. H. van Uden, C. M. Okonkwo, H. Chen, F. M. Huijskens, B. Corbett, R. Winfield, H. de Waardt, and A. M. J. Koonen, "2.576 Tb/s ($23 \times 2 \times 56$ Gb/s) mode division multiplexed 4PAM over 11.8 km differential mode delay uncompensated few-mode fiber using direct detection," in *Optical Communication (ECOC 2013), 39th European Conference and Exhibition on*, 2013, pp. 1–3.

- [5] van Uden Roy, C. Okonkwo, V. Sleiffer, H. Chen, M. Kuschnerov, de, Hugo Waardt, and T. Koonen, "Employing a Single DPLL for Joint Carrier Phase Estimation in Few-Mode Fiber Transmission," in *Optical Fiber Communication Conference/National Fiber Optic Engineers Conference 2013*, 2013, p. OM2C.1.
- [6] H. Chen, R. van Uden, C. Okonkwo, B. Snyder, O. Raz, P. O'Brien, H. van den Boom, H. de Waardt, and T. Koonen, "Employing an integrated mode multiplexer on Silicon-on-Insulator for Few-mode Fiber transmission," in *39th European Conference and Exhibition on Optical Communication (ECOC 2013)*, 2013, pp. 1–3.
- [7] H. Chen, V. Sleiffer, R. van Uden, C. Okonkwo, M. Kuschnerov, F. Huijskens, L. Gruner-Nielsen, Y. Sun, H. de Waardt, and T. Koonen, "3 MDM amp;#x00D7;8 WDM amp;#x00D7;320-Gb/s DP-32QAM transmission over a 120km few-mode fiber span employing 3-spot mode couplers," in *OptoElectronics and Communications Conference held jointly with 2013 International Conference on Photonics in Switching (OECC/PS), 2013 18th*, 2013, pp. 1–2. (**post-deadline paper**)
- [8] H. Chen, V. Sleiffer, B. Snyder, M. Kuschnerov, R. van Uden, Y. Jung, C. Okonkwo, O. Raz, P. O'Brien, H. de Waardt, and T. Koonen, "Demonstration of a photonic integrated mode coupler with 3.072Tb/s MDM and WDM transmission over few-mode fiber," in *OptoElectronics and Communications Conference held jointly with 2013 International Conference on Photonics in Switching (OECC/PS), 2013 18th*, 2013, pp. 1–2. (**post-deadline paper**)
- [9] H. Chen and T. Koonen, "Single Multi-mode Mask for Multi-channel Mode Division Demultiplexing," in *Optical Fiber Communication Conference/National Fiber Optic Engineers Conference 2013*, 2013, p. OTh1B.4.
- [10] H. Chen and T. Koonen, "Scalable multi-segment Phase Mask for spatial power splitting and mode division demultiplexing," in *39th European Conference and Exhibition on Optical Communication (ECOC 2013)*, 2013, pp. 1–3.
- [11] V. A. J. M. Sleiffer, H. Chen, Y. Jung, M. Kuschnerov, D. J. Richardson, S. U. Alam, Y. Sun, L. Gruner-Nielsen, N. Pavarelli, B. Snyder, P. O'Brien, A. D. Ellis, A. M. J. Koonen, and H. de Waardt, "480 km transmission of MDM 576-Gb/s 8QAM using a few-mode re-circulating loop," in *2013 IEEE Photonics Conference (IPC)*, 2013, pp. 1–2. (**post-deadline paper**)
- [12] B. Yang, S. Zou, E. Tangdiongga, X. Jin, Z. Cao, C. Okonkwo, H.

- Chen, and T. Koonen, "A Lightwave Centralized and Dispersion Immune Bidirectional mm-Wave over Fiber Scheme for Access Networks," in *European Conference and Exhibition on Optical Communication*, 2012, p. P6.07.
- [13] V. Sleiffer, Y. Jung, V. Veljanovski, R. van Uden, M. Kushnerov, Q. Kang, L. Grüner-Nielsen, Y. Sun, D. Richardson, S. Alam, F. Poletti, J. Sahu, A. Dhar, H. Chen, B. Inan, T. Koonen, B. Corbett, R. Winfield, A. Ellis, and H. De Waardt, "73.7 Tb/s (96X3x256-Gb/s) mode-division-multiplexed DP-16QAM transmission with inline MM-EDFA," in *European Conference and Exhibition on Optical Communication*, 2012, p. Th.3.C.4. (**post-deadline paper**)
- [14] V. Sleiffer, Y. Jung, B. Inan, H. Chen, R. van Uden, M. Kushnerov, D. van den Borne, S. Jansen, V. Veljanovski, T. Koonen, D. Richardson, S. Alam, F. Poletti, J. Sahu, A. Dhar, B. Corbett, R. Winfield, A. Ellis, and H. De Waardt, "Mode-division-multiplexed 3x112-Gb/s DP-QPSK transmission over 80 km few-mode fiber with inline MM-EDFA and Blind DSP," in *European Conference and Exhibition on Optical Communication*, 2012, p. Tu.1.C.2.
- [15] A. M. J. Koonen, H. Chen, H. P. A. van den Boom, and O. Raz, "Silicon photonic integrated mode multiplexer," in *Photonics Society Summer Topical Meeting Series, 2012 IEEE*, 2012, pp. 240–241.
- [16] H. Chen, T. Koonen, R. van Uden, H. van den Boom, and O. Raz, "Integrated Mode Group Division Multiplexer and Demultiplexer Based on 2-Dimensional Vertical Grating Couplers," in *European Conference and Exhibition on Optical Communication*, 2012, p. Th.1.B.2.
- [17] H. Chen, T. Koonen, B. Snyder, X. Chen, and G. T. Reed, "Packaged Mode Multiplexer based on Silicon Photonics," in *Asia Communications and Photonics Conference*, 2012, p. ATh2B.4.
- [18] H. Chen, A. M. J. Koonen, B. Corbett, R. Winfield, and H. P. A. Van den Boom, "20Gbit/s two LP₁₁ modes transmission over 10km two-moded fiber without crosstalk compensation," in *Opto-Electronics and Communications Conference (OECC), 2012 17th*, 2012, pp. 749–750.
- [19] H. Chen, H. van den Boom, L. Grüner-Nielsen, and T. Koonen, "Wavelength and Polarization Division Multiplexing using the LP₁₁ Mode in a Two-mode Fiber for Mode Division Multiplexing," in *Optical Transmission Systems, Subsystems, and Technologies*, 2011, vol. 8309, p. 830909.

- [20] H. Chen, B. H.P.A. van den, and T. Koonen, “30Gbit/s 3×3 Optical Mode Group Division Multiplexing System with Mode-Selective Spatial Filtering,” in *Optical Fiber Communication Conference/National Fiber Optic Engineers Conference 2011*, 2011, p. OWB1.
- [21] S. T. Abraha, N.-C. Tran, C. Okonkwo, H. Chen, E. Tangdiongga, and T. Koonen, “Service Multicasting by All-Optical Routing of 1 Gb/s IR UWB for In-Building Networks,” in *Optical Fiber Communication Conference/National Fiber Optic Engineers Conference 2011*, 2011, p. JWA068.
- [22] H. Chen, H. P. A. Van Den Boom, and A. M. J. Koonen, “Optical mode group division multiplexing (MGDM) system over graded index-multimode fiber,” in *Asia Communications and Photonics Conference and Exhibition*, 2010, p. 79880N.

Patents:

- [1] H. Chen and A. M. J. Koonen, “Multi-segment Phase Mask (MSPM) for Spatial Power Splitting and Mode Division Demultiplexing,” US Provisional Patent Application No. TUE-140/PROV, 2013.
- [2] A. M. J. Koonen, O. Raz and H. Chen, “Photonic integrated circuit for excitation/detection of multiple fiber modes,” US Provisional Patent Application No. TUE-109/PROV, 2011.

Curriculum Vitae

Haoshuo Chen was born in Shanghai, China, on September 24, 1984. He received both his B.S. and M.S. degrees in communication and information engineering in 2007 and 2009 from Shanghai University, China. The topic of his master thesis was “Bi-directional millimeter-wave over fiber system based on optical frequency multiplication and Brillouin amplification”. From July 2009 to April 2010, he was working as a network engineer at China Mobile in Shanghai, China.

In May 2010, he started working as a PhD student in the Electro-Optical Communication group (ECO), department of Electrical Engineering, Eindhoven University of Technology, under the supervision of Professor A.M.J. Koonen. His research work was done as part of the EU FP7 MODE-GAP project, which develops few-mode fibers, long haul transmission and associated technologies to enhance the overall capacity of optical networks. From September 2013 to March 2014, he was an intern at Bell Laboratories, Holmdel, New Jersey where he researched novel mode multiplexers and optical switches.

His main research topics are mode division multiplexing, photonic integration, digital signal processing and optical switch. He received the best student award in Asia Communications and Photonics Conference (ACP), 2012. He has also served as a peer-reviewer for IEEE Photonics Technology Letters, OSA Optics Express, Optics Letters and Applied Optics.

